E&G

Quaternary Science Journal

Eiszeitalter und Gegenwart

DEUQUA
DEUTSCHE QUARTÄRVEREINIGUNG

E&G Quaternary Science Journal

Copernicus Publications
The Innovative Open Access Publisher

Image credit:
Middle Waimakariri River Valley, eastern-central Southern Alps, New Zealand. The image depicts a view from Late Glacial (17.5 ka ago) terminal moraines near the confluence of Poulter River (inner "Poulter moraine") downvalley towards the entry of Waimakariri Gorge and Puketeraki Range (far distance). Different levels of lower (young fluvial) and upper (old glaciofluvial) terraces are visible especially on the true right. Stefan Winkler, 2018, all rights reserved.

Open Access

E&G Quaternary Science Journal

Editorial

Editorial *E&G Quaternary Science Journal*, Vol. 67 (2018)

Christopher Lüthgens[1] **and Margot Böse**[2]

[1]University of Natural Resources and Life Sciences (BOKU), Institute of Applied Geology,
Peter-Jordan-Str. 82, 1190 Vienna, Austria
[2]Freie Universität Berlin, Institute of Geographical Sciences, Physical Geography, Malteserstr. 74–100,
12249 Berlin, Germany

With the finalisation of volume 67 of *E&G Quaternary Science Journal* (*EGQSJ*), it seems fitting to have a short look back at the past 1.5 years, which may have marked one of the most eventful periods in the history of *Eiszeitalter und Gegenwart – Quaternary Science Journal* and its transformation to *EGQSJ*, but even more importantly to have a glance at the future development of the journal. The transfer of *EGQSJ* to Copernicus Publications in late 2017 paved the way for a successful relaunch, which was celebrated at 2018's EGU (European Geosciences Union) conference in Vienna, Austria, and attracted interested parties from various fields of geoscientific research. The relaunch was also highly supported by the Quaternary and geomorphological research community during last year's Central European Conference on Geomorphology and Quaternary Sciences held in Giessen, Germany. In August 2018, *EGQSJ* was accepted into the Directory of Open Access Journals (DOAJ) and thus received the DOAJ Seal, which recognises journals that adhere to an exceptionally high level of publishing standards and best practice. This was an important milestone because a growing number of funding agencies require the DOAJ Seal as a prerequisite for applying for funding which is exclusively dedicated to supporting the open access publication of scientific results. Backed up by the unprecedented publication infrastructure in the history of the journal provided by Copernicus Publications, a significant increase in submissions of all manuscript types eligible for publication in *EGQSJ* – full research papers, express reports, and

thesis abstracts – was recorded. Some of these submissions could already be published in Vol. 67, highlighting our efforts in minimising turnaround times from submission to publication, notwithstanding the strict application of our peer review system, the latter also being responsible for a recent increase of the rejection rate.

Vol. 67 also includes an innovation with regard to the treatment of special issues. Two special issues were initiated in 2018, both resulting from the initiative and effort of teams of guest editors promoting *EGQSJ* at different conferences. The first special issue *Geoarchaeology and past human–environment interactions* is edited by Hans von Suchodoletz, Stefanie Berg, Lukas Werther, Christoph Zielhofer, and Eileen Eckmeier, and the second special issue *Connecting disciplines – Quaternary archives and geomorphological processes in a changing environment* is edited by Johanna Lomax, Thomas Kolb, and Markus Fuchs. Papers submitted to these and all upcoming special issues undergo the same review process as those submitted to regular issues of *EGQSJ*. In contrast to traditional special issues, each article, once accepted, is immediately published online in the regular *EGQSJ* volume, but will clearly be assigned to a special issue. Publications as contributions to special issues will also be included in the regular printed version of *EGQSJ*. In addition, a compilation of all papers of a certain special issue will be available online via a dedicated section of the *EGQSJ* website. This reduces the turnaround times for publication of special issues, and at the same time enables DEUQUA (Ger-

man Quaternary Association) to offer the coverage of the article processing charges for papers to be published not only in the regular series, but also in *EGQSJ* special issues.

At the last DEUQUA general meeting in Giessen in September 2018, Christopher Lüthgens was elected new chief editor for *EGQSJ*, and will take over the respective duties from Margot Böse from Vol. 68 onwards. Building on the solid foundation of *EGQSJ* established during the last year, the new editorial team consisting of more than 30 Quaternary scientists is looking forward to facing the challenge of helping *EGQSJ* become an indispensable journal for the publication of Quaternary-related research in central Europe (and beyond). To fulfil that aim in the near future, we rely on you, the members of the Quaternary research community, to support *EGQSJ* by promoting the journal, and last but not least, by submitting your high-quality manuscripts to *EGQSJ*. You are also cordially invited to join DEUQUA as the parent organisation of *EGQSJ*, and support the journal and benefit from all other activities of the association.

Open Access

E&G Quaternary Science Journal

Express report

Middle to Late Holocene mobilization of DOC-bound Pb and Y in the Magellanic moorlands (53° S) as a function of sea spray fertilization, climate variations and volcanic fallout? A preliminary report

Björn Klaes[1], **Rolf Kilian**[1], **Gerhard Wörner**[2], **Sören Thiele-Bruhn**[3], and **Helge W. Arz**[4]

[1]Department of Geology, University of Trier, Campus II, Geozentrum, Behringstraße 21, 54296 Trier, Germany
[2]Geochemistry Division, University of Göttingen, Goldschmidtstraße 1, 37077 Göttingen, Germany
[3]Soil Science Department, University of Trier, Campus II, Geozentrum, Behringstraße 21, 54296 Trier, Germany
[4]Department of Marine Geology, IOW Warnemünde, Seestraße 15, 18119 Rostock, Germany

1   Introduction

In the course of previously reconstructed paleoclimate, the yttrium (Y) content of the MA1 stalagmite from the Marcelo Arévalo (MA) cave at 53° S has been used as proxy for rainfall intensity-related transport of siliciclastic detritus onto the speleothem (Schimpf et al., 2011). Due to the fact that later works (e.g., Hartland et al., 2012; Birkel et al., 2017) highlight organic complexation as the dominant transport pathway of Y and other hardly soluble trace elements in DOC-rich waters, a reconsideration of the MA1 stalagmite's Y record was necessary, including an investigation on local soil formation as well as rock weathering.

In southernmost Patagonia, the Magellanic moorlands cover an extended area at the windward side of the Andes (Kilian et al., 2006; Whittle and Gallego-Sala, 2016), but pedogenetic processes of the dominantly occurring soil types in this region (Podsols and Histosols) are still poorly studied (Casanova et al., 2013). Such peatlands are one of the world's most important terrestrial carbon sinks, but they also release large amounts of dissolved organic carbon (DOC)

into nearby aquatic systems (Birkel et al., 2017). Besides particulate organic carbon (POC), this flux may contribute to an organic carbon burial in fjord sediments from southernmost Patagonia that is up to hundred times higher than the global ocean average (Smith et al., 2015). DOC releases from peatland ecosystems are mainly controlled by rainfall intensity, water table fluctuations, temperature, soil pH and peat accumulation–degradation cycles (e.g., Broder et al., 2015; Birkel et al., 2017). Here, the transport of typically more insoluble trace elements, such as lead (Pb) and yttrium, is strongly linked to the solute export of carbon (Birkel et al., 2017). Due to the fact that complexation of Pb and Y in soil solutions and surface and drip waters is more susceptible to organic substances than to pedogenic (hydr)oxides, they represent suitable proxies to determine paleo-fluxes of DOC in the course of speleothem trace element analysis (e.g., Hartland et al., 2012).

Sea spray has been considered as the most important nutrient source for ombrotrophic peatlands in westerly dominated coastal mountain belts, such as the superhumid southernmost Andes (Kilian et al., 2013; Whittle and Gallego-Sala, 2016),

in particular during periods with an increasing strength of the southern westerly wind belt (SWW; Lamy et al., 2010). It has a significant control on peat accumulation and decomposition rates as well as on the hydrochemistry of surface waters and chemical leaching of soils and bedrock (e.g., Kilian et al., 2013; Broder et al., 2015): sea-salt aerosols introduce various basic ions, micro-nutrients and sulfate into terrestrial ecosystems. Moreover, they are suggested to be the major contributor to the natural deposition of selenium (Se) at coastal sites (Wen and Carignan, 2009). For that reason, Se concentrations in a stalagmite from the southernmost Andes have been previously used as a valuable paleoenvironmental proxy for sea spray deposition to the Magellanic moorlands (Kilian et al., 2013), especially since Se pollution by regional anthropogenic sources (e.g., industry, Wen and Carignan, 2009) is limited in such a remote study area. In soils characterized by high OC contents and acidic pore water, e.g., in peat soils, Se mobilization/immobilization is rather controlled by plant uptake and the adsorption onto organic substances than by adsorption onto Fe/Al (hydr)oxides (Li et al., 2017). Nevertheless, a certain amount of Se remains dissolved in soil solutions of acid environments (Li et al., 2017).

Previous investigations in the study area highlighted that regional climate variations (wind velocities, precipitation and temperature) during distinct Holocene phases are closely related to changes in SWW intensities (Lamy et al., 2010). Furthermore, large centennial to millennium-scale modifications of aquatic as well as terrestrial ecosystems of the superhumid southernmost Andes have been interpreted as a consequence of (1) climate variations (e.g., the global cooling-phenomena during the Little Ice Age, LIA; Schimpf et al., 2011; Kilian et al., 2013) and (2) local tephra fallout, in particular after the Plinian 4.15 kyr cal BP Mt. Burney eruption (Kilian et al., 2006).

Here we present first insights into Middle to Late Holocene peat formation–degradation cycles in the Magellanic moorlands as revealed by a revaluation of trace element concentrations detected in the MA1 stalagmite, based on newly gathered Pb, Y and Se data from the MA cave's host rocks as well as distinguished soil horizons and weathered parent rocks from its peat-vegetated catchment.

2   Setting

The MA cave from where the stalagmite MA1 has been recovered is located in the core zone of the SWW in the western Strait of Magellan (52°41.7′ S, 73°23.3′ W; Schimpf et al., 2011; Fig. 1a). It was formed by fjord coastal erosion in a fracture zone at 20 m a.s.l. during a period with more elevated coastlines. Next to the site, the automatic weather station Arévalo (Fig. 1b) recorded during the last decade an annual precipitation of up to 4500 mm a^{-1} and mean temperatures at 5.3 °C (Schimpf et al., 2011, and unpublished data). The small catchment (ca. 25 m × 25 m at 80 m a.s.l.) is

situated on top of a relatively flat ridge (Fig. 1b), which is characterized by peat vegetation and bare rock surfaces. It is connected by drainage pathways along the fracture zone with the interior of the cave.

The cave's walls and rock lithology of the catchment are composed of granitoid rocks and mylonitic orthogneiss which are cross-cut by some mafic dykes. The soils of the peat catchment (Histic Podsols, termed according to FAO, 2015) reach a solum thickness of 50 cm on average and have a sandy loam texture. Its pore water is characterized by a distinct acidity (pH between 3.9 and 5.7). Within the four soil profiles, a spodic horizon underlies the histic epipedon (ombrotrophic peat). An up to 10 cm thick tephra layer of the Mt. Burney volcano (4.15 kyr cal BP; Kilian et al., 2013) is embedded in the stagnic subsoils. The sampling position of the MA1 stalagmite inside the cave and other details of the site are described in detail by Schimpf et al. (2011).

3   Methods

A representative sampling from soil horizons and rock lithologies in and around the cave and its catchment was conducted during the austral winter expedition with RV *Gran Campo II* in 2015. Samples include the distinguished horizons of four peat soil profiles from the catchment, weathered rock fragments obtained from the lowermost peat soil horizons, and unweathered rocks derived from the cave's walls. Representative samples were prepared, e.g., by crushing and milling, at the Geology Department of the University of Trier. Trace element analysis (Pb, Y and Se) of pulverized bulk samples was realized with ICP-MS (Perkin Elmer DRC II Q-ICP-MS) at the Geochemistry Division of the University of Göttingen after using a ultra-pure HF/HClO$_4$-HF/HNO$_3$ mixture in a pressurized Teflon apparatus (Picotrace®) for acid digestion. The international standard JA-2 was applied to calibrate these ICP-MS measurements. The pH values of soil horizons were detected in CaCl$_2$ solution using a digital pH meter at the University of Trier (Soil Science Department). Detailed information concerning previously obtained ICP-MS/OES measurements of drilled samples along the growth axis of the MA1 stalagmite as well as U/Th dating and the age–depth model has been presented in Schimpf et al. (2011). Already published trace element concentrations of the MA1 speleothem used here are Y, Se and U (Schimpf et al., 2011; Kilian et al., 2013).

4   Results and discussion

As shown in Fig. 2a and b the majority of upper soil horizons from the MA catchment, including the histic epipedons (H) and the spodic mineral horizons (B), show up to 2 times higher Se concentrations than underlying unaltered parent rocks (between 16 and 23 ppm). This indicates that leaching of selenium from such rock sources was limited during soil
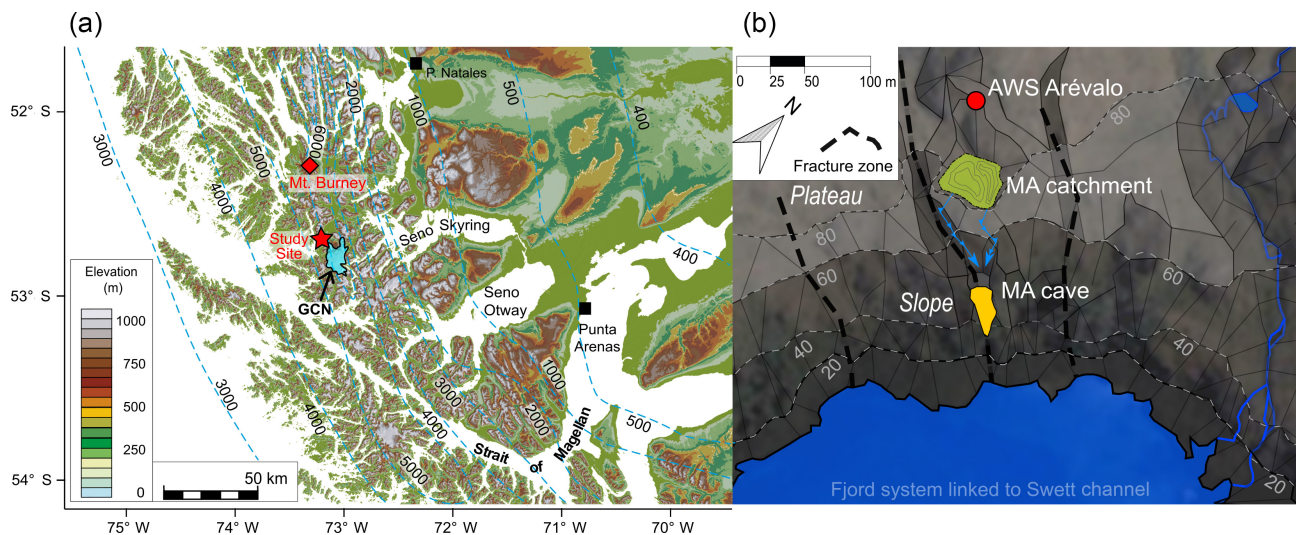
Figure 1. (a) The southernmost Patagonian Andes with the study site in the northwest of the Gran Campo Nevado ice field (GCN), the location of the Mt. Burney volcano and isolines for annual precipitation (Lamy et al., 2010). **(b)** The MA cave system and the associated catchment in a small bay of a fjord arm connected to the Strait of Magellan with the drainage pathways (blue arrows) and the automatic weather station (AWS) Arévalo.

formation. The significant top-to-bottom difference of Se enrichment in soils and its decoupling from lithogenic Se budgets suggests that the deposition by sea-salt aerosols to the ombrotrophic peat of the H horizon represent an important Se source (Wen and Carignan, 2009; Broder et al., 2015), especially during frequent storm events with strong westerly winds (Lamy et al., 2010; Schimpf et al., 2011). However, the fixation of Se to organic materials and its uptake by peat vegetation seem to be an important process here, which also controls the Se retention in comparable soil types (Li et al., 2017, Fig. 2a, b and d).

The high Se contents (20 ppm) detected in tephra are most likely to be explained by illuviation of Se complexed to soil organic matter (Li et al., 2017) due to prevailing podsolization processes (Vermeire et al., 2016). The vesicular structure of pumice particles promotes the accumulation of plant residuals (e.g., Hughes et al., 2013), in particular as Se in bulk samples of tephra-containing subsoils is reduced (Fig. 2a, b).

In contrast to Se, the trace elements Pb and Y are mainly of a lithogenic origin and leached from source rocks (granites and granodiorite, mylonitic orthogneiss and mafic dykes; see Fig. 2a–c) as a consequence of strong mineral dissolution under acid conditions, which is a common characteristic of podsolic soils (Vermeire et al., 2016). Due to distinct host minerals (e.g., allanites for Y and certain heavy minerals for Pb; unpublished data), leaching intensities of both more lithogenic trace elements are not equal (Fig. 2a–c): in the case of Y, strongly decreased concentrations in weathered rock samples may indicate such a pronounced feedback to meteoric weathering (up to ~ 15 ppm loss in gneisses, Fig. 2b). Furthermore, mafic dykes could represent a potential source for Y release. With regard to Pb, greater leaching

tendencies can be assumed for gneisses, whereas weathered and unweathered samples of granitoid rocks exhibit a diffuse loss–gain pattern. Mafic dykes seem to be of minor importance for Pb leaching compared to that of Y (Fig. 2a, b).

However, despite a possible slightly different behavior during chemical weathering in source rocks, Pb and Y show a very high correlation ($R^2 = 0.89$ for all investigated soil horizons and $R^2 = 0.65$ for the narrow grouped field excluding the subsoil horizon that shows elevated Y and Pb contents; Fig. 2c) with respect to their concentrations in soil horizons and tephra, which separates pedogenic processes triggered by a high OC availability from weathering of parent rocks. Both show a loss of up to ~ 20 ppm compared to lithogenic sources. According to, for example, Hartland et al. (2012), Vermeire et al. (2016) and Birkel et al. (2017), the particular and uniform behavior of Pb and Y is controlled by a similar binding affinity to organic substances (preferred), e.g., DOC, and the formation of mineral–organic complexes with Fe/Al hydroxides (subordinate); see Fig. 2d. Consequently, it can be argued that they share the same transport mechanism in DOC-rich drainage and drip waters during their transport from the MA catchment to the MA1 speleothem. This transport mechanism and eluviation is further accelerated by the extraordinarily high precipitation. Thus, Pb and Y can be used as proxies for tracing past DOC fluxes onto the MA1 stalagmite which depend on the past climate, environmental changes and its influences on the peat ecosystem in the MA catchment as described for comparable hydrological environments (e.g., Hartland et al., 2012). The high Y content of the MA1 stalagmite (1 to 16 ppm) is most likely strongly controlled by DOC flux and only to a minor extent by the
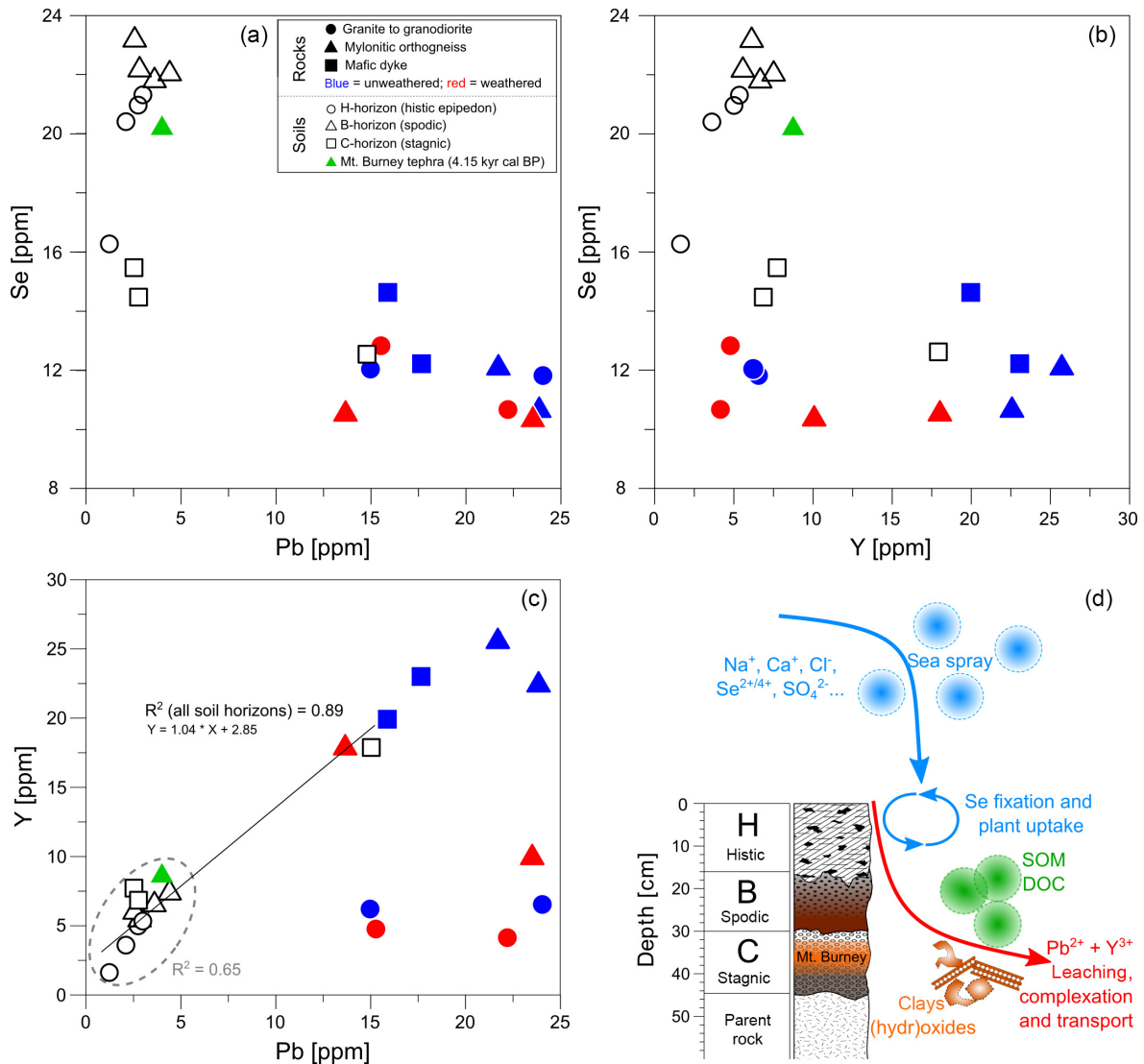
Figure 2. Selenium, yttrium and lead concentrations detected in representative samples of the three different lithological features as well as of the distinguished soil horizons and Mt. Burney tephra deposits from four peat soil profiles (Histic Podsols) of the MA catchment (**a, b, c**). For the interpretation of the shown correlation coefficients shown in panel (**c**), the reader is referred to the text. (**d**) The processual linkage of sea spray deposition and related fixation of selenium in ombrotrophic peat is displayed schematically in combination with leaching/transport of lead and yttrium due to podsolization (according to Wen and Carignan, 2009; Broder et al., 2015; Vermeire et al., 2016; and Li et al., 2017).

incorporation of detrital minerals in the stalagmite's laminae as previously suggested by Schimpf et al. (2011).

The MA1 stalagmite record presented in Fig. 3a shows that the concentrations of DOC-bound Pb and Y are highly correlated during the last four millennia since the 4.15 kyr cal BP Mt. Burney eruption ($R^2 = 0.91$; up to 16 ppm Y and up to 9 ppm Pb were measured). In particular, during an assumed warmer and more humid phase between 2.5 and 0.7 kyr BP (e.g., Lamy et al., 2010) with an estimated annual mean precipitation of up to 6500 mm a^{-1} for the cave site (Schimpf et al., 2011), the trace elements Pb and Y show generally increasing concentrations in the MA1 stalagmite, but also pronounced centennial-scale variations following a significant millennium-scale decline since the Mt. Burney tephra fallout (Kilian et al., 2006). At the beginning of the LIA (cooling of ~ 1.5 °C and reduced precipitation, e.g., Kilian and Lamy, 2012; Schimpf et al., 2011), the peak intensities of Pb and Y decrease abruptly and then persist with very low concentrations throughout this cold phase. Se shows peak intensities with periodicities of 500 years that coincide with phases of elevated global solar irradiance (Fig. 3b, c). This is consistent with findings of Lamy et al. (2010) and Kilian and Lamy (2012), who have argued that this wind-driven variability of sea spray input is closely linked to changes in

Figure 3. Middle to Late Holocene variations of element concentrations recorded by the MA1 stalagmite in combination with distinct climate phases (Lamy et al., 2010) and the 4.15 kyr cal BP Mt. Burney tephra fallout (Kilian et al., 2006). **(a)** Lead and yttrium (Schimpf et al., 2011) records as proxies for DOC-bound transport (e.g., Hartland et al., 2012). **(b)** Sea spray depositio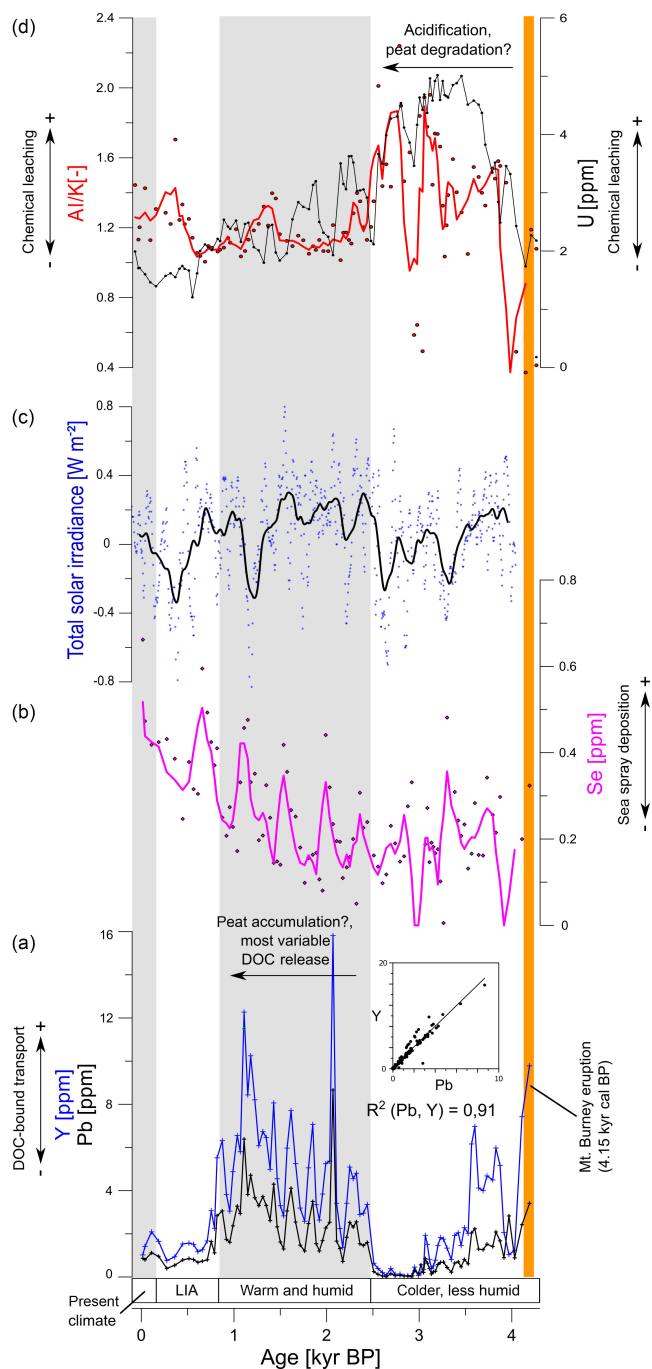n to the site as indicated by variations of selenium concentrations (Kilian et al., 2013). **(c)** ^{10}Be-based total solar irradiance (Fröhlich, 2009). **(d)** Intensity of chemical leaching depicted by uranium concentrations (Schimpf et al., 2011) and the Al / K ratio according to Miriyala et al. (2017).

SWW strength and associated stormy phases in the course of Late Holocene variations in the South Pacific Ocean climate system and sea surface temperatures.

Between 2.5 and 0.7 kyr BP the pattern of Pb, Y and Se in the MA1 stalagmite (Fig. 3a, b) indicates that in this period, renewed peat formation was stimulated by a slightly warmer and more humid climate (Lamy et al., 2010) combined with a higher nutrient availability due to sea spray fertilization (e.g., Broder et al., 2015). At that time, frequent storm events with intense precipitation (Schimpf et al., 2011) and subsequent water table fluctuations may have led to an increasing DOC release from terrestrial sites. Thus, it is also expected that the peat surface layer underwent pronounced changes during this climate period. Peat accumulation may have been significantly enhanced by sea-spray-induced buffering of soil pH (Kilian et al., 2013) in the MA catchment after the long-term acidification caused by the 4.15 kyr cal BP Mt. Burney tephra fallout (Kilian et al., 2006). Based on the uranium record (Schimpf et al., 2011) and the Al / K ratio (reflecting extreme chemical weathering, according to Miriyala et al., 2017) of the MA1 stalagmite (Fig. 3d), initial intensive alteration of the 10 cm thick tephra layer is assumed to proceed for more than 1000 years. The possible peat decomposition due to high tephra loading (e.g., Hughes et al., 2013) was likely accompanied by a decrease in DOC export (see Y and Pb, Fig. 3a). Furthermore, the observed variations in peat accumulation and/or degradation are well correlated with Late Holocene changes in peat forming plant species (e.g., *Astelia, Cyperaceae*) in several regional pollen records (Kilian et al., 2006; Lamy et al., 2010; Kilian and Lamy, 2012). However, the abrupt decline of DOC-bound trace element concentrations in the MA1 stalagmite indicates that distinct changes in the regional climate during the LIA seem to have a similar control on the peat ecosystem as the 4.15 kyr cal BP Mt. Burney eruption (Fig. 3a).

Our preliminary results indicate that Holocene soil formation of Histic Podsols in the Magellanic moorlands has been influenced by specific changes in hydrochemical conditions and sea-spray-derived nutrient supply with regard to SWW-related climate variations and high tephra loading. New insights into the leaching behavior of hardly soluble Y and Pb in these peaty soils and their application as paleoenvironmental proxies for DOC-bound transport can constrain peat accumulation and/or degradation in the MA1 stalagmite. Moreover, Y concentrations of MA1 may still reflect rainfall intensities since extreme high precipitation also leads to elevated DOC export rates from peatlands, especially during distinct Holocene storm periods (e.g., between 2.5 and 0.7 kyr BP).

5 Perspective

Since peatlands represent an important source of OC and trace element fluxes to nearby aquatic systems (e.g., Birkel et al., 2017), such as fjords in high latitudes globally (Smith et

al., 2015), the sensitivity of these highly vulnerable ecosystems (e.g., Whittle and Gallego-Sala, 2016) to exogenic forcing factors (e.g., climate impacts and volcanic fallout) should be investigated further in superhumid southernmost Patagonia. This includes the quantification of past and present organic fluxes from peatlands to estuarine environments in combination with its linkage to the cyclic behavior of element transport to understand the implications of these processes for the terrestrial nutrient supply to marine biochemical cycles in fjords (e.g., Ríos et al., 2016).

References

Birkel, C., Broder, T., and Biester, H.: Nonlinear and threshold-dominated runoff generation controls DOC export in a small peat catchment, J. Geophys. Res.-Biogeo., 122, 498–513, https://doi.org/10.1002/2016JG003621, 2017.

Broder, T., Blodau, C., Biester, H., and Knorr, K. H.: Sea spray, trace elements, and decomposition patterns as possible constraints on the evolution of CH_4 and CO_2 concentrations and isotopic signatures in oceanic ombrotrophic bogs, Biogeochemistry, 122, 327–342, https://doi.org/10.1007/s10533-014-0044-5, 2015.

Casanova, M., Salazar, O., Seguel, O., and Luzio, W.: The Soils of Chile, Springer World Soils Book Series, Dordrecht, the Netherlands, https://doi.org/10.1007/978-94-007-5949-7, 2013.

FAO: World reference base for soil resources 2014: International classification system for naming soils and creating legends for soil maps, World Soil Resources Reports, 106, Rome, Italy, 2015.

Fröhlich, C.: Evidence of a long-term trend in total solar irradiance, Astron. Astrophys., 501, L28–L30, https://doi.org/10.1051/0004-6361/200912318, 2009.

Hartland, A., Fairchild, I. J., Lead, J. R., Borsato, A., Baker, A., Frisia, S., and Baalousha, M.: From soil to cave: Transport of trace metals by natural organic matter in karst dripwaters, Chem. Geol., 304–305, 68–82, https://doi.org/10.1016/j.chemgeo.2012.01.032, 2012.

Hughes, P. D. M., Mallon, G., Brown, A., Essex, H. J., Stanford, J. D., and Hotes, S.: The impact of high tephra loading on late-Holocene carbon accumulation and vegetation succession in peatland ecosystems, Quaternary Sci. Rev., 67, 160–175, https://doi.org/10.1016/j.quascirev.2013.01.015, 2013.

Kilian, R. and Lamy, F.: A review of Glacial and Holocene paleoclimate records from southernmost Patagonia 1 (49-55° S), Quaternary Sci. Rev., 53, 1–23, https://doi.org/10.1016/j.quascirev.2012.07.017, 2012.

Kilian, R., Biester, H., Behrmann, J., Baeza, O., Fesq-Martin, M., Hohner, M., Schimpf, D., Friedmann, A., and Mangini, A.: Millennial-scale volcanic impact on a superhumid and pristine ecosystem, Geology, 34, 609–612, https://doi.org/10.1130/G22605.1, 2006.

Kilian, R., Lamy, F., and Arz, H.: Late Quaternary variations of the southern westerly wind belt and its influences on glacier extend, denudation as well as terrestrial and aquatic ecosystems within the southernmost Andes, German Journal of Geosciences, 164, 279–294, https://doi.org/10.1127/1860-1804/2013/0027, 2013.

Lamy, F., Kilian, R., Arz, H., Francois, J., Kaiser, J., Prange, M., and Steinke, T.: Holocene changes in the position and intensity of the southern westerly wind belt, Nat. Geosci., 3, 695–699, https://doi.org/10.1038/NGEO959, 2010.

Li, Z., Liang, D., Peng, Q., Cui, Z., Huang, J., and Lin, Z.: Interaction between selenium and soil organic matter and its impact on soil selenium bioavailability: A review, Geoderma, 295, 69–79, https://doi.org/10.1016/j.geoderma.2017.02.019, 2017.

Miriyala, P., Sukumaran, N. P., Nagender Nath, B., Ramamurty, P. B., Sijinkumar, A. V., Vijayagopal, B., Ramaswamy, V., and Sebastian, T.: Increased chemical weathering during the deglacial to mid-Holocene summer monsoon intensification, Nature Scientific Reports, 7, 44310, https://doi.org/10.1038/srep44310, 2017.

Ríos, F., Kilian, R., and Mutschke, E.: Chlorophyll-α thin layers in the Magellan fjord system: The role of the water column stratification, Cont. Shelf Res., 124, 1–12, https://doi.org/10.1016/j.csr.2016.04.011, 2016.

Schimpf, D., Kilian, R., Kronz, A., Simon, K., Spötl, C., Wörner, G., Deininger, M., and Mangini, A.: The significance of chemical, isotopic, and detrital components in three coeval stalagmites from the superhumid southernmost Andes (53° S) as high-resolution palaeo-climate proxies, Quaternary Sci. Rev., 30, 443–459, https://doi.org/10.1016/j.quascirev.2010.12.006, 2011.

Smith, R. W., Bianchi, T. S., Allison, M., Savage, C., and Galy, V.: High rates of organic carbon burial in fjord sediments globally, Nat. Geosci., 8, 450–454, https://doi.org/10.1038/ngeo2421, 2015.

Vermeire, M.-L., Cornu, S., Fekiacova, Z., Detienne, M., Delvaux, B., and Cornélis, J.-T.: Rare earth dynamics along pedogenesis in a chronosequence of podzolic soils, Chem. Geol., 446, 163–174, https://doi.org/10.1016/j.chemgeo.2016.06.008, 2016.

Wen, H. and Carignan, J.: Ocean to continent transfer of atmospheric Se as revealed by epiphytic lichens, Environ. Pollut., 157, 2790–2797, https://doi.org/10.1016/j.envpol.2009.04.021, 2009.

Whittle, A. and Gallego-Sala, A. V.: Vulnerability of the peatland carbon sink to sea level rise, Sci. Rep., 6, 28758, https://doi.org/10.1038/srep28758, 2016.

Open Access

E&G

Quaternary
Science
Journal

Research article

Capability of U–Pb dating of zircons from Quaternary tephra: Jemez Mountains, NM, and La Sal Mountains, UT, USA

Jana Krautz[1]**, Mandy Hofmann**[2]**, Andreas Gärtner**[2]**, Ulf Linnemann**[2]**, and Arno Kleber**[1]

[1]Institute of Geography, Technische Universität Dresden, Helmholtzstr. 10, 01690 Dresden, Germany
[2]Senckenberg Naturhistorische Sammlungen Dresden, Museum für Mineralogie und Geologie, Sektion Geochronologie, GeoPlasma Lab, Königsbrücker Landstraße 159, 01109 Dresden, Germany

Correspondence: Jana Krautz (jana.krautz@tu-dresden.de)

Abstract: Two Quaternary tephras derived from the Jemez Mountains, New Mexico – the Guaje and Tsankawi tephras – are difficult to distinguish due to their similar glass-shard chemical composition. Differences in bulk chemical composition are small as well. Here we examine the feasibility to assign an age to a distal tephra layer in the La Sal Mountains, Utah, by U–Pb dating of zircons and to correlate it with one of the two Jemez eruptions. We also dated original Jemez tephras for comparison. Even though the tephras are very young, we obtained reasonable age determinations using the youngest cluster of zircon grains overlapping in age at 2σ. Thereafter, the Guaje tephra is 1.513 ± 0.021 Myr old. The La Sal Mountains tephra is correlated with the Tsankawi tephra. Three samples yielded a common age range of 1.31–1.40 Myr. All ages are in slight disagreement with published age determinations obtained by ^{40}Ar / ^{39}Ar dating. These findings indicate that distal Jemez tephras can be distinguished by U–Pb dating. Furthermore, we encourage giving this method a try for age assignments even of Quaternary volcanic material.

Kurzfassung: Zwei quartäre Tephren aus den Jemez Mountains, New Mexico, – Guaje- und Tsankawi-Tephra – sind durch die ähnliche chemische Zusammensetzung ihrer Gläser nur schwer zu unterscheiden. Dies gilt auch, bis auf geringfügige Unterschiede, für die Totalanalyse. Wir haben die Möglichkeit untersucht, das Alter einer distalen Tephralage in den La Sal Mountains, Utah, zu bestimmen und einer der Tephren aus den Jemez Mountains zuzuordnen. Zur Vergleichbarkeit haben wir auch die Zirkone der Tephren aus den Jemez Mountains U–Pb datiert. Obwohl die Tephren alle sehr jung sind, haben wir reliable Alter durch das Cluster der jüngsten, im 2σ Fehler überlappenden Zirkone erhalten. Demzufolge ist die Guaje-Tephra 1.513 ± 0.021 Myr alt. Die Tephra aus den La Sal Mountains wurde mit der Tsankawi-Tephra korreliert: Drei Proben aus den Jemez Mountains ($1\times$) und den La Sal Mountains ($2\times$) ergaben eine Altersspanne von 1.31–1.40 Myr. Alle Alter weichen etwas von bereits publizierten ^{40}Ar / ^{39}Ar ab. Die Ergebnisse deuten darauf hin, dass die distalen Jemez-Tephren durch U–Pb Datierung unterschieden werden können. Wir wollen dazu ermutigen, diese Methode der Altersbestimmung auch für quartäres vulkanisches Material in Erwägung zu ziehen.

1   Introduction

Tephra is eruptive rock material deposited as airborne fallout often quite distant from its source volcano. Because of its chemical composition – usually obtained from glass shards – it often may be related to a particular volcanic eruption (Westgate et al., 1994). Therefore, tephrochronology has become an established method, using tephra intercalated between other deposits as a stratigraphic marker bed, provided the original eruption is well dated (Lowe, 2011).

There are a lot of reliable methods for dating Quaternary tephra (Dickinson and Gehrels, 2009). Most commonly the ^{40}Ar / ^{39}Ar method is applied using K-rich minerals (Lowe, 2011). This utilizes the fact that embedded argon completely leaves the mineral lattice by disturbances such as a volcanic eruption. After this the enrichment by radioactive decay of K re-starts, and thenceforward the accrued isotopes may be measured. So ages can be calculated via the half-life of the isotopes (Worsley, 1998).

A distal tephra layer discovered in the La Sal Mountains, Utah, was linked to the volcanic province of the Jemez Mountains, New Mexico, based on glass-shard chemistry. However, correlation with a particular eruption remained ambiguous (Kleber, 2013), because two tephras derived from there have closely similar chemical compositions (Slate et al., 2007) – one of the major threads of tephrochronology (Lowe, 2011). Zimmerer et al. (2016) state that both tephras are difficult to date by Ar–Ar dating, asking for elaborate sample preparation and calculation of the results. Though still not done very often on such young zircons (Lee, 2012), there have been a few successful applications of U–Pb dating of zircons to young material in recent years (e.g., Ito et al., 2016; Sakata et al., 2017). Zircons have the advantage of being outstandingly chemically and physically robust. They are unsusceptible to alteration and weathering even under extreme conditions (Wilson et al., 2008). Thus, we tried dating the tephra layer using zircon dating.

Here we demonstrate reasonable age determinations of zircons from the La Sal Mountains tephra layer and of the two suspect tephras in the Jemez Mountains. Through this, the Jemez tephra layers may be discriminated with high certainty. Furthermore, we encourage giving the U–Pb method – which is available in a variety of labs worldwide – a try for dating volcanic material of undisclosed age even if the assumed age is as young as 1 Myr, after having tested the total uranium contents.

2   Geological setting

2.1   Jemez Mountains, New Mexico

The Jemez Mountains (Fig. 1) are calderas of various volcanic eruptions, among which the Valles, Antonio, and Toledo calderas are still recognizable as concentric moun-

tain ranges. Their eruptive products, mainly basalt–andesite–dacite–rhyolite associations, range from about 15 Myr (mid-Miocene) to < 2 Myr (Pleistocene) (Kues et al., 2007). The Neogene and Quaternary formations are divided into three groups, named after Indian nations, from oldest to youngest: the Keres, the Polvadera, and the Tewa group (Bailey et al., 1969). We took our samples from the Tewa group. This comprises the Bandelier Tuff, which is mainly the result of two large ignimbrite- and caldera-forming eruptions. The lower Otowi (including the Guaje tephra) and the upper Tshirege (including the Tsankawi tephra) sequences were deposited approximately 1.6 and 1.2 Ma, respectively (Self et al., 1996; Slate et al., 2007). Today large parts of these ignimbrite and tephra sequences belong to the Bandelier National Monument.

The Jemez Mountains are known to be the source area of the La Sal Mountains tephra layer. We took samples approximately 8 km southeast of Los Alamos, New Mexico, from a slope along New Mexico State Road 502 (Guaje and Tsankawi tephras, located at 35°52′05″ N, 106°11′59″ W and at 35°52′05″ N, 106°12′00″ W, respectively). The site is depicted in Goff (2009) and in Fig. 2a.

2.2   La Sal Mountains, Utah

The chain of the La Sal Mountains lies at the eastern border of Utah (Fig. 1). Like the Jemez Mountains, it is part of the Colorado Plateau Province and together with Mount Peale (3877 m a.s.l.) is the highest peak of the plateau (Henning, 1975; Grahame and Sisk, 2002). The La Sal Mountains are remnants of laccoliths and mainly consist of granitoid rocks (Henning, 1975; Ross, 2006). The Precambrian basement is unconformably overlain by Paleozoic and Mesozoic sedimentary rocks, which were intruded by monzonite and diorite porphyry during the Paleogene (K–Ar ages are 25–28 Myr; Ross, 2006). The laccolithic structures preserve Mesozoic rocks at the mountain flanks, mainly clays and sandstones (Richmond, 1962; Henning, 1975). Within the adjacent Paradox Basin, the Mesozoic rock sequence is underlain by marine sediments, which include limestone, dolomite, slate, and a several-hundreds-of-meters-thick diapiric layer of salt and gypsum (Henning, 1975).

A distal tephra layer was found in the northwestern La Sal Mountains, Utah, USA (located 38°34′33″ N, 109°17′32″ W), approximately 20 km linear distance from Moab, Utah, at 2130 m a.s.l., on a 22° steep slope, exposed by a road cut of the Manti-La Sal Circuit (Kleber, 2013 and Fig. 2b). The tephra was identified by the US Geological Survey, Tephrochronology Laboratory, Menlo Park, CA, via the chemical composition of its glass shards. It was correlated with either the approximately 1.25 Myr old (Phillips et al., 2007) Tsankawi tephra or – because of the Fe contents somewhat more likely – the approximately 1.65 Myr old (Spell

Figure 1. Areas under study. Source of maps: Google Maps 2016 (http://maps.google.com).

and Harrison, 1993) Guaje tephra, both derived from the Jemez Mountains, New Mexico (Kleber, 2013).

3 Methods

We took two samples from the deposition area in the La Sal Mountains, UT, USA, and one from each original tephra layer, derived from the Toledo Caldera (Guaje tephra) and from the Valles Caldera (Tsankawi tephra). The latter two – taken from well-known tephra locations – were mainly measured to disclose whether the results of the U–Pb determinations are consistent with the aforementioned earlier ^{40}Ar / ^{39}Ar datings and may, thus, yield reliable ages of distal tephra layers.

We performed sample preparation for cathodoluminescence (CL) images, LA-ICP-MS (laser ablation with inductively coupled plasma mass spectrometry) U–Pb analyses, and age calculations at the Geochronology Department of Senckenberg Naturhistorische Sammlungen Dresden, Germany. Circa 1 kg of material was collected for each sample. After crushing in a jaw crusher, the samples were sieved for the fraction 36 to 400 µm. Density separation of this fraction was accomplished with LST (solution of lithium heteropolytungstates in water). We used a Frantz isodynamic separator for the magnetic separation of the extracted heavy minerals. Single zircon grains of all grain sizes, colors, and mor-

phological types were randomly picked under a binocular microscope and subsequently analyzed regarding their morphology based on backscatter electron (BSE) images of the unmounted zircon grain surfaces using a Zeiss EVO50SEM at 20 kV and a spot size of 300 nm. Then the grains were mounted in resin blocks and polished to approximately half their thickness, in order to expose their internal structure. We obtained CL images using a Zeiss EVO50SEM coupled to a CL detector system at 20 kV and a spot size of 500 nm. Zircons were analyzed for U, Th, and Pb isotopes by LA-ICP-MS, utilizing a Thermo Scientific ELEMENT 2 XR sector field ICP-MS coupled to a New Wave UP-193 excimer laser system with laser spot sizes of 20 to 35 µm. Fifteen seconds of background acquisition was followed by 25 s of data acquisition during each analysis. The signal was tuned for a maximum sensitivity for Pb and U, whereas oxide production (^{235}UO vs. ^{238}U) was kept well below 1 %. Raw data were corrected for background signal, common Pb, laser-induced elemental fractionation, instrumental mass discrimination, and time- and depth-dependent elemental fractionation of Pb / Th and Pb / U using an Excel$^{®}$ macro developed by Axel Gerdes (Geosciences Inst., Goethe University Frankfurt, Germany). Reported uncertainties were propagated by quadratic addition of the external reproducibility obtained from the standard zircon GJ-1 ($\sim$ 0.6 and 0.5–1 % for ^{207}Pb / ^{206}Pb and ^{206}Pb / ^{238}U, respectively) dur-
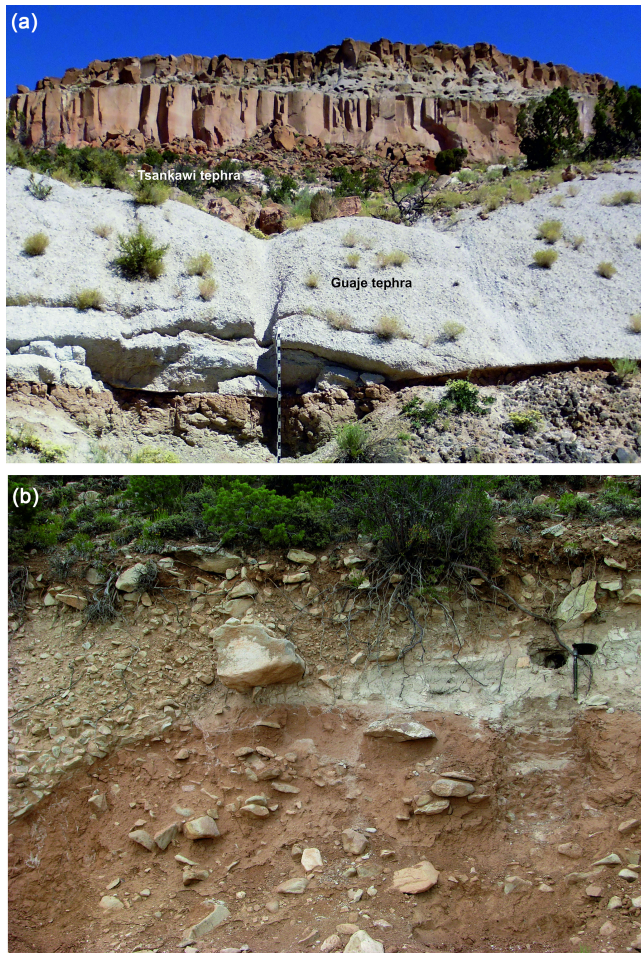
Figure 2. (a) Sampling sites of tephras in the Jemez Mountains. All visible rocks are volcanic in origin. Photo: Jana Krautz (22 August 2014). **(b)** Sampling site in the La Sal Mountains. The whitish tephra intercalates between periglacial cover beds and is to the left of the picture cut by a gully fill. Photo: Arno Kleber (27 July 2009). The sampling spot visible in the La Sal Mountains tephra was for radiofluorescence dating, not for the present dating.

Table 1. Electron microprobe analyses of glass shards from tephra layers. ±: standard deviation. Values are weight-percent oxide, re-calculated to be 100% fluid-free. Normalized data (raw data are available in Supplement).

source	phase	n	SiO_2	TiO_2	Al_2O_3	Fe_2O_3	MnO	MgO	CaO	Na_2O	K_2O	P_2O_5	Total
2014-NM-Gu	glass shards	31	77.12±0.84	0.05±0.02	12.29±0.31	1.42±0.07	0.09±0.02	0.02±0.04	0.26±0.03	3.84±0.28	4.90±0.31	0.01±0.01	100.00
2014-LSM-T	glass shards	22	77.44±0.73	0.08±0.02	12.24±0.10	1.50±0.14	0.07±0.02	0.03±0.01	0.29±0.03	4.03±0.18	4.30±0.25	0.01±0.01	99.99
2013-LSM-T	glass shards	44	77.41±0.74	0.09±0.03	12.21±0.12	1.47±0.16	0.07±0.02	0.03±0.01	0.28±0.02	3.92±0.24	4.51±0.23	0.01±0.01	100.00

ing individual analytical sessions and the within-run precision of each analysis. Concordia diagrams (2σ error ellipses) and concordia ages (95% confidence level) were created using Isoplot/Ex 2.49 (Ludwig, 2001). ^{207}Pb / ^{206}Pb ages were used for concordant analyses of zircons above 1.0 Ga, and ^{206}Pb / ^{238}U ages for younger ones. For ages younger than 10 Myr, we corrected for ^{230}Th disequilibrium using the formula of Simon et al. (2008).

Geochemical analyses of bulk samples were performed at Activation Laboratories Ltd. (Ancaster, Ontario, Canada) using their standard protocols RX4 for sample preparation and 4LITHO-Quant Major Elements Fusion ICP (WRA)/Trace Elements Fusion ICP-MS (WRA4B2) for the analyses as described on their website (ActLabs, 2014). The samples from the La Sal Mountains were contaminated with pedogenic

Figure 3. Ages of tephra layers as derived from the youngest cluster of grain ages overlapping at the 2σ level. **(a)** Guaje tephra, **(b)** Tsankawi tephra, **(c)** La Sal Mountains tephra sampled in 2013, **(d)** same but sampled in 2014.

carbonates, whereas the samples from the Jemez Mountains were not, or at least not to the same degree. Therefore, the major elements (and the total percentages) were re-calculated on a carbonate-free basis, i.e., without considering MgO, CaO, and loss on ignition (LOI), though the original values of these three measurements are given so that one could re-assemble all original quantities. In addition to the aforementioned samples, we analyzed a confirmed Guaje tephra sample provided by David B. Dethier (Slate et al., 2007).

Microprobe analyses were conducted aided by a CAMECA SX51 electron microprobe with five wavelength-dispersive spectrometers at the Earth Sciences Institute at Heidelberg University. The standard operating conditions were 15 kV accelerating voltage, 20 nA beam current, and a beam diameter of ca. 20 μm. Counting times during analyses were 10 s for Na and K; 20 s for Fe; 30 s for Mn and P; and 50 s for Si, Ti, Al, Mg, and Ca. Detection limits were 0.02 wt % for Si, Al, and Ca, 0.001 wt % for Ti and Mn, 0.08 wt % for Fe, and 0.09 wt % for K and Na. Calibration was performed using natural and synthetic oxide and silicate standards. Values given are weight-percent oxide, re-calculated to be 100 % fluid-free.

4 Results and discussion

The microprobe analyses of glass shards corroborate the great similarity of the Guaje and the La Sal Mountains tephras (Table 1; cf. Supplement for raw data). Even the differences in Fe contents, typically acknowledged as the only clue to distinguish Guaje from Tsankawi tephras (Andrei M. Sarna-Wojcicki, personal communication, 1990), are within the standard deviations of the analyses.

Table 2 shows that the major and especially the trace element concentrations from bulk samples of the La Sal Mountains tephra are very close to the Tsankawi tephra from the Jemez Mountains but somewhat dissimilar to the Guaje tephra sample as well as to the Guaje sample DN-97-117 submitted by David B. Dethier. This holds especially true for the elements shaded in yellow in Table 2, with the most remarkable being Cr, Rb, Nb, and Th. The differences in the Sr and Ba contents between the La Sal Mountains and Jemez Mountains samples may be explained by eolian contamination, as both elements are frequent components of eolian deposits (Jones, 1986). Similar differences in Tl contents may be due to different durations of sample materials being ex-

Table 2. Major and trace element concentrations of tephra samples. The table displays analyses from bulk samples. Major element percentages are calculated carbonate-free, i.e., without considering the columns in italic font. Trace elements which show remarkable differences between Guaje and Tsankawi tephras are identified in bold font. Source: Actlab report number A14-07544; report date: 24 October 2014.

Analyte symbol	SiO_2	Al_2O_3	Fe_2O_3	MnO	MgO	CaO	Na_2O	K_2O	TiO_2	P_2O_5	LOI	Total	Sc	Be	V	Cr	Co	Ni	Cu
Unit symbol	%	%	%	%	%	%	%	%	%	%	%	%	ppm	ppm	ppm	ppm	ppm	ppm	ppm
Detection limit	0.01	0.01	0.01	0.001	0.01	0.01	0.01	0.01	0.001	0.01	–	–	1	1	5	1	1	20	10
Analysis method	ICP	ICP	ICP	ICP	ICP	ICP	ICP	ICP	ICP	ICP	ICP	–	ICP	ICP	ICP	MS	MS	MS	MS
2013 LSM-T	75.53	12.92	2.79	0.07	0.22	*1.06*	3.43	4.42	0.13	0.03	*6.95*	99.33	2	5	8	1	1	<20	<10
2014 LSM-T	74.67	13.81	2.56	0.08	0.29	*2.48*	3.46	4.22	0.14	0.04	*8.07*	98.99	2	7	12	1	1	<20	<10
2014 NM-GU	76.56	12.65	2.47	0.09	0.39	*0.48*	3.14	4.84	0.06	<0.01	*6.84*	99.82	1	13	7	1	1	<20	20
DN-97-117	74.52	13.78	3.09	0.10	0.19	*0.47*	2.70	5.39	0.11	0.02	*5.9*	99.70	2	13	13	1	2	20	20
2014 NM-TS	76.12	11.77	2.54	0.07	0.08	*0.39*	4.00	4.26	0.09	<0.01	*0.78*	98.87	6	5	6	1	1	<20	20

Analyte symbol	Zn	Ga	Ge	As	Rb	Sr	Y	Zr	Nb	Mo	Ag	In	Sn	Sb	Cs	Ba	Bi	La	Ce
Unit symbol	ppm	ppm	ppm	ppm	ppm	ppm	ppm	ppm	ppm	ppm	ppm	ppm	ppm	ppm	ppm	ppm	ppm	ppm	ppm
Detection limit	30	1	1	5	2	2	2	4	1	2	0.5	0.2	1	0.5	0.5	3	0.4	0.1	0.1
Analysis method	MS	MS	MS	MS	ICP	ICP	ICP	ICP	MS	MS	MS	MS	MS	MS	MS	ICP	MS	MS	MS
2013 LSM-T	80	23	2	<5	**149**	90	244	244	**59**	6	0.9	<0.2	**5**	0.6	3.9	**216**	<0.4	**67.8**	**133**
2014 LSM-T	100	25	2	<5	**164**	151	76	272	**80**	6	1.1	<0.2	**6**	0.6	4.8	**411**	<0.4	**71.6**	**135**
2014 NM-GU	130	29	2	<5	**335**	17	93	245	**150**	8	0.8	<0.2	**11**	0.7	8.9	**39**	<0.4	**40.6**	**93.3**
DN-97-117	120	31	2	<5	**305**	29	92	243	**144**	8	0.8	<0.2	**10**	0.7	10.2	**125**	<0.4	**43.1**	**105**
2014 NM-TS	90	23	2	<5	**160**	23	59	200	**57**	2	0.7	<0.2	**3**	<0.5	2.9	**78**	<0.4	**58.6**	**116**

| Analyte symbol	Pr	Nd	Sm	Eu	Gd	Tb	Dy	Ho	Er	Tm	Yb	Lu	Hf	Ta	W	Tl	Pb	Th	U
Unit symbol	ppm	ppm	ppm	ppm	ppm	ppm	ppm	ppm	ppm	ppm	ppm	ppm	ppm	ppm	ppm	ppm	ppm	ppm	ppm
Detection limit	0.05	0.1	0.1	0.05	0.05	0.1	0.1	0.05	0.1	0.05	0.1	0.04	0.2	0.1	1	0.1	5	0.1	0.1
Analysis method	MS	MS	MS	MS	MS	MS	MS	MS	MS	MS	MS	MS	MS	MS	MS	MS	MS	MS	MS
2013 LSM-T	14	48.8	9.9	0.24	8.3	1.5	9	1.8	5.4	0.87	5.2	0.72	7.3	**4.7**	0.6	0.6	**28**	**19.9**	**5.6**
2014 LSM-T	15.2	56	12	0.55	10.5	1.9	12	2.4	7.1	1.2	7.5	1.12	9.3	**6.5**	0.7	0.7	**37**	**24.9**	**6.8**
2014 NM-GU	10.8	39.9	11.4	<0.05	10.9	2.1	13.7	2.9	8.5	1.45	9.3	1.3	10.9	**14**	6	0.9	**42**	**43.4**	**16**
DN-97-117	11.2	42	11.4	0.15	10.9	2	13.6	2.8	8.2	1.34	9.1	1.23	10.8	**13.4**	5	1	**44**	**43.4**	**13.9**
2014 NM-TS	12.6	44.1	9.8	0.13	8.6	1.5	9.7	1.9	5.6	0.92	5.7	0.8	6.7	**4.9**	3	0.2	**19**	**19.6**	**6.1**
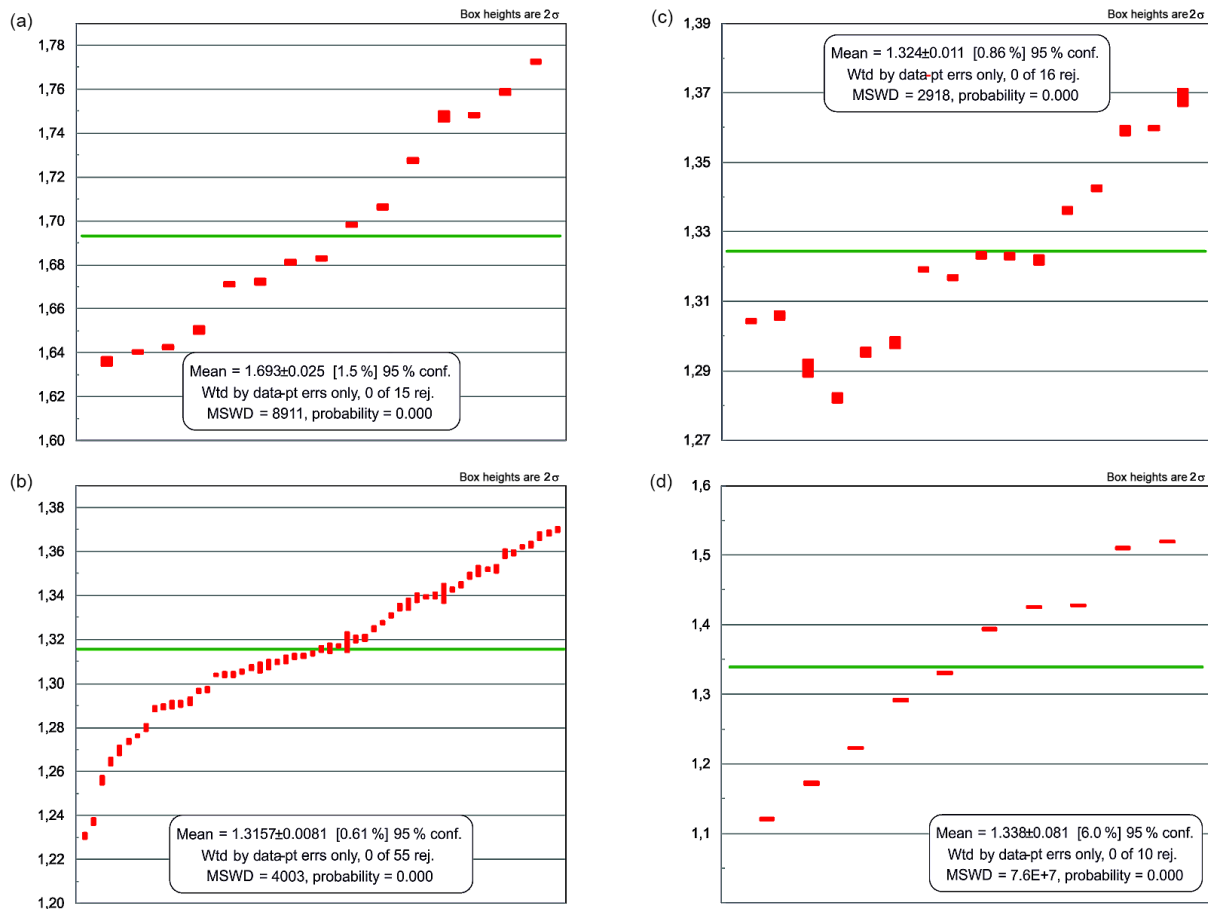
Figure 4. Weighted average ages of tephra layers to compare with the age displays. **(a)** Guaje tephra, **(b)** Tsankawi tephra, **(c)** La Sal Mountains tephra sampled in 2013, **(d)** same but sampled in 2014.

posed to oxidation. These findings render the La Sal Mountains tephra correlative to the Tsankawi rather than the Guaje tephra.

In all samples, primary uranium contents in zircons were sufficiently high to allow reliable age determinations. Given the apparently young ages of the tephras, ^{207}Pb could not be accumulated in quantities remarkably above the detection limit of the instrument due to the extremely long half-life of ^{235}U and/or insufficiently high U contents to produce enough Pb in such short intervals of time (compare young grains in the Supplement). Thus, we could use only the ^{206}Pb / ^{238}U for age estimations (cf. Gehrels, 2014). Therefore, ^{207}Pb / ^{235}U and ^{207}Pb / ^{206}Pb ratios for cross-validation are not available; the degree of concordance cannot be calculated for these young zircon grains, and those data are left blank (Supplement). Accordingly, the ages we report are regarded as model ages.

To establish the age of each tephra sample, we used the youngest cluster of zircon-derived U–Pb ages overlapping at 2σ. The mean age of the youngest cluster of grain ages that overlap in age at 2σ is regarded as the most conserva-

tive measure of age (Dickinson and Gehrels, 2009). These clusters may be seen as groups of analyses resulting in ages close together, thereby validating each other even without a reliable Pb–Pb age. Grains with younger ^{238}U / ^{206}Pb ages than the ones used for the calculation of the concordia ages (cf. Supplement) are not part of such a cluster in the concordia plot and, thus, cannot be cross-validated. Accordingly, they were not considered sufficiently reliable.

The grains used for age determination are accentuated in tables in the Supplement. The clusters are sufficiently large for the ages to be constrained to small confidence intervals (2σ); see also Figs. 3 and 4: we assigned an age of 1.513 ± 0.021 Myr to the Guaje tephra from the Jemez Mountains, which is somewhat younger than the published Ar–Ar-derived ages of 1.651 ± 0.011 Myr (Zimmerer et al., 2016) or 1.613 ± 0.011 Myr (Izett and Obradovich, 1994). The other three samples yielded ages incompatible with the Guaje tephra: the Tsankawi tephra from the Jemez Mountains was determined to be as old as 1.316 ± 0.012 Myr. The two samples from the La Sal Mountains yielded ages of 1.327 ± 0.017 Myr (sample from the year 2013) and
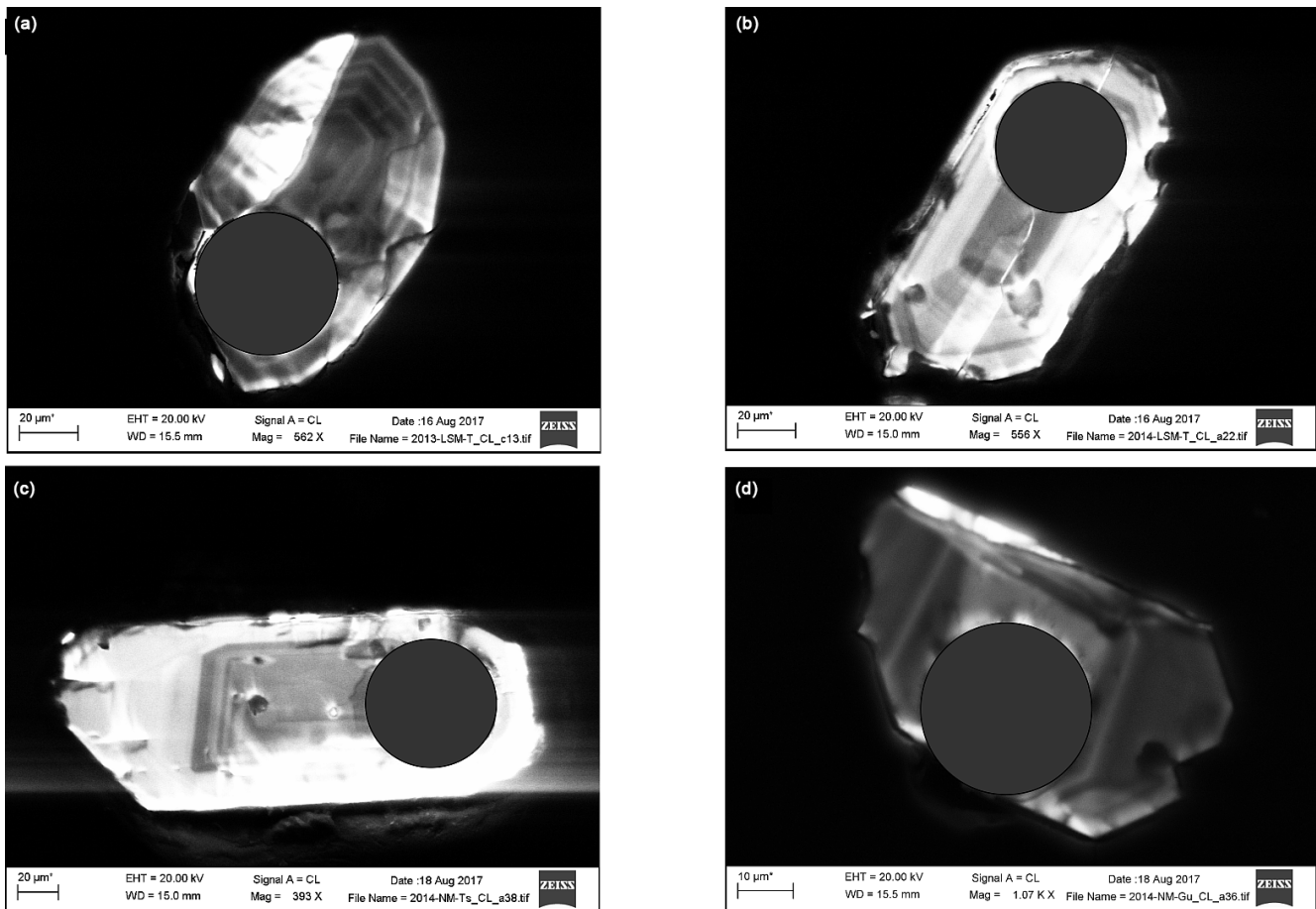
Figure 5. CL images of selected zircons which have been included in the age displays (including laser ablation mark). **(a)** La Sal Mountains tephra sampled in 2013: c13; **(b)** same but sampled in 2014: a22; **(c)** Tsankawi tephra: a38; **(d)** Guaje tephra: a36.

1.341 ± 0.059 Myr (2014 sample, which had the smallest number of zircon ages within the overlapping cluster). The confidence intervals of the latter three samples do all overlap within errors. Therefore, we correlate these tephra-layer samples with the same, the Tsankawi eruption. The common age range within 2σ of both samples is 1.31–1.40 Myr. We assume this is the most likely age array. Zoning of zircons indicates steady growth. If there is a core depicted in the CL images, the measuring spot may not be located at a core's edge (Fig. 5).

The ages derived via Ar–Ar dating are 1.264 ± 0.010 Myr (Phillips et al., 2007; recalculated by Zimmerer et al., 2016) and 1.223 ± 0.018 Myr (Izett and Obradovich, 1994); i.e., they are slightly younger than ours. Though being very close to each other, the U–Pb ages are slightly older. The common notion is that Ar–Ar ages approximate the eruption ages and U–Pb ages indicate the (earlier) time of crystal closure (Simon et al., 2008). However, this does not work for the Guaje tephra. Zimmerer et al. (2016) observed similar differences between ^{40}Ar / ^{39}Ar and uranium-series (U / Th) ages for other tephras of the Jemez Mountains. They explain their findings with a complicated crystallization history of the magma, leading to disequilibrium between the uranium isotopes in the melt. Another explanation could be that the zircon crystal lattices of the Guaje tephra were not completely closed during eruption, as our sample was taken close to an underlying mafic lava bed which still could have been hot enough to achieve this effect. Or there still are problems with the Ar–Ar dating of some Jemez tephras not yet understood.

Older zircons (cf. Supplement for raw data) are assumed to be inherited from rocks melted during magma rise, with those zircons being their most temperature-resistant components.

5   Conclusions

Our findings demonstrate that U–Pb dating of zircons from Quaternary volcanic material may result in valuable age determination. U–Pb dating of zircons seems to allow – at least combined with bulk geochemical analyses – confident distinction between the two tephras derived from the Jemez Mountains, which are too similar to be clearly kept apart by glass-shard chemistry alone. This approach avoids the

complications accompanying the Ar–Ar dating of Bandelier tephras (Phillips et al., 2007; Zimmerer et al., 2016).

We recommend considering U–Pb dating as a possible approach to identifying rather young tephras or to distinguish such tephras, as in our study. However, before application, we recommend measuring total uranium contents in zircon minerals, which might indicate whether this dating method will be applicable.

In Quaternary research, dating of zircons as young as 1 Myr may well become a tool for better defining age models of sedimentary archives – such as loesses, cover beds, or paleosols – with interbedded or admixed tephra layers.

References

Actlabs: Geochemistry/Assay Overview, available at: http://www.actlabs.com/Page.Aspx?Menu=64&App=210&Cat1=499&Tp=2&Lk=No, last access: 22 December 2014.

Bailey, R. A., Smith, R. L., and Ross, C. S.: Stratigraphic nomenclature of volcanic rocks in the Jemez Mountains, New Mexico, Geological Survey Bulletin, 1274-P, U.S. Government Printing Office, Washington, USA, 1969.

Dickinson, W. R. and Gehrels, G. E.: Use of U-Pb Ages of detrital zircons to infer maximum depositional ages of strata. A test against a Colorado Plateau Mesozoic database, Earth Planet. Sc. Lett., 288, 115–125, https://doi.org/10.1016/J.Epsl.2009.09.013, 2009.

Gehrels, G. E.: Detrital zircon U-Pb geochronology applied to tectonics, Annu. Rev. Earth Pl. Sc., 42, 127–149, https://doi.org/10.1146/Annurev-Earth-050212-124012, 2014.

Goff, F.: Valles Caldera. A geologic history, University of New Mexico Press, Albuquerque, USA, 2009.

Grahame, J. D. and Sisk, T. D.: La Sal Mountains, Utah, available at: https://web.archive.org/web/20060208054415/http://www.cpluhna.nau.edu/index.htm (last access: 10 December 2014), 2002.

Henning, I.: Die La Sal Mountains, Utah. Ein Beitrag zur Geoökologie der Colorado-Plateau-Provinz und zur vergleichenden Hochgebirgsgeographie, Akademie der Wissenschaften und der Literatur, Mainz, Germany, 88 pp., 1975.

Ito, H., Nanayama, F., and Nakazato, H.: Zircon U-Pb dating using LA-ICP-MS. Quaternary tephras in Boso Peninsula, Japan, Quat. Geochronol., 40, 12–22, https://doi.org/10.1016/j.quageo.2016.07.002, 2016.

Izett, G. A. and Obradovich, J. D.: ^{40}Ar$/^{39}$Ar age constraints for the Jaramillo Normal subchron and the Matuyama-Brunhes geomagnetic boundary, J. Geophys. Res., 99, 2925–2934, https://doi.org/10.1029/93JB03085, 1994.

Jones, R. L.: Barium in Illinois surface soils, Soil Sci. Soc. Am. J., 50, 1085–1087, 1986.

Kleber, A.: Heavy-mineral analysis as a tool in tephrochronology, with an example from the La Sal Mountains, Utah, USA, Geologos, 19, 87–94, https://doi.org/10.2478/logos-2013-0006, 2013.

Kues, B. S., Kelley, S. A., and Lueth, V. W. (Eds.): Geology of the Jemez region II. New Mexico Geological Society 58th Annual Field Conference, New Mexico Geological Society, 19–22 September 2007, Socorro, NM, USA, 499 pp., 2007.

Lee, M. S. (Ed.): Mass Spectrometry Handbook, John Wiley and Sons, Inc, Hoboken, NJ, USA, 2012.

Lowe, D. J.: Tephrochronology and its application: a review, Quat. Geochronol., 6, 107–153, https://doi.org/10.1016/J.Quageo.2010.08.003, 2011.

Ludwig, R. K.: User manual for Isoplot. Ex Rev. 2.49, Berkeley Geochronology Center Special Publication, 1a, 1–58, https://doi.org/10.1016/S1471-3918(01)80062-9, 2001.

Phillips, E. H., Goff, F., Kyle, P. R., Mcintosh, W. C., Dunbar, N. W., and Gardner, J. N.: The ^{40}Ar$/^{39}$Ar age constraints on the duration of resurgence at the Valles Caldera, New Mexico, J. Geophys. Res., 112, 2925–2934, https://doi.org/10.1029/2006JB004511, 2007.

Richmond, G. M.: Quaternary stratigraphy of the La Sal Mountains, Geological Survey, Professional Paper 450-D, United States Government Printing Office, Washington, USA, 1962.

Ross, M. L.: Preliminary geologic map of the Warner Lake Quadrangle, Grand County, Utah, Utah Department of Natural Resources, Salt Lake City, USA, 18 pp., 2006.

Sakata, S., Hirakawa, S., Iwano, H., Danhara, T., Guillong, M., and Hirata, T.: A new approach for constraining the magnitude of initial disequilibrium in Quaternary zircons by coupled uranium and thorium decay series dating, Quat. Geochronol., 38, 1–12, https://doi.org/10.1016/j.quageo.2016.11.002, 2017.

Self, S., Heiken, G., Sykes, M. L., Wohletz, K., Fisher, R. V., and Dethier, D. P. (Eds.): Field excursions to the Jemez Mountains, New Mexico, New Mexico Bureau of Mines and Mineral Resources, Socorro, NM, USA, 1996.

Simon, J. I., Renne, P. R., and Mundil, R.: Implications of pre-eruptive magmatic histories of zircons for U-Pb geochronology of silicic extrusions, Earth Planet. Sc. Lett., 266, 182–194, https://doi.org/10.1016/j.epsl.2007.11.014, 2008.

Slate, J. L., Sarna-Wojcicki, A. M., Wan, E., Dethier, D. P., Wahl, D. B., and Lavine, A.: A chronostratigraphic reference set of tephra

layers from the Jemez Mountains volcanic source, New Mexico, in: Geology of the Jemez region II. New Mexico Geological Society 58th Annual Field Conference, New Mexico Geological Society, edited by: Kues, B. S., Kelley, S. A., and Lueth, V. W., 19–22 September 2007, Socorro, NM, USA, 239–247, 2007.

Spell, T. L. and Harrison, T. M.: ^{40}Ar / ^{39}Ar geochronology of post-Valles Caldera rhyolites, Jemez volcanic field, New Mexico, J. Geophys. Res., 98, 8031–8051, https://doi.org/10.1029/92JB01786, 1993.

Westgate, J. A., Perkins, W. T., Fuge, R., Pearce, N., and Wintle, A. G.: Trace-element analysis of volcanic glass shards by laser ablation inductively coupled plasma mass spectrometry. Application to tephrochronological studies, Appl. Geochem., 9, 323–335, https://doi.org/10.1016/0883-2927(94)90042-6, 1994.

Wilson, C. J. N., Charlier, B. L. A., Fagan, C. J., Spinks, K. D., Gravley, D. M., Simmons, S. F., and Browne, P. R. L.: U–Pb dating of zircon in hydrothermally altered rocks as a correlation tool: application to the Mangakino geothermal field, New Zealand, J. Volcanol. Geoth. Res., 176, 191–198, 2008.

Worsley, P.: Altersbestimmung, in: Geomorphologie. Ein Methodenhandbuch für Studium und Praxis, edited by: Goudie, A., Springer, Berlin, Germany, 447–558, 1998.

Zimmerer, M. J., Lafferty, J., and Coble, M. A.: The eruptive and magmatic history of the youngest pulse of volcanism at the Valles Caldera. Implications for successfully dating Late Quaternary eruptions, J. Volcanol. Geoth. Res., 310, 50–57, https://doi.org/10.1016/J.Jvolgeores.2015.11.021, 2016.

E&G Quaternary Science Journal

Express report

Reconsidering the origin of the Sedrun fans (Graubünden, Switzerland)

Catharina Dieleman[1]**, Susan Ivy-Ochs**[2]**, Kristina Hippe**[2]**, Olivia Kronig**[2]**, Florian Kober**[3]**, and Marcus Christl**[2]

[1]Institute of Geology, ETH Zurich, 8093 Zurich, Switzerland
[2]Laboratory of Ion Beam Physics, ETH Zurich, 8092 Zurich, Switzerland
[3]NAGRA, Hardstrasse 73, 5430 Wettingen, Switzerland

1 Introduction

Four alluvial fans, Pulanera, L'Ondadusa, Drun and Bugnei, located near the town of Sedrun in the upper Vorderrhein Valley (Fig. 1), are striking in that they have a common aggradation surface ($\sim 1°$ slope oriented along the main valley axis) and distinct coterminous cut-off toes. Similar coalesced fans with marked incised toes occur just downstream at Disentis (Fig. 2a). These geomorphological characteristics suggest that the fans built up for a limited period of time and then were abruptly incised by the Vorderrhein River. Switching between aggradation, fan abandonment and channel entrenchment can be a response to (1) variation in discharge due to climate changes or extreme precipitation events, (2) decreases in sediment supply reflecting waning (e.g. paraglacial) sediment availability, (3) tectonic uplift, or (4) changes in base level (Harvey et al., 2005; Hornung et al., 2010, and references therein). Inside a mountain range, change in local base level can be caused by large-scale downstream blockage by a glacier, a landslide or a man-made dam (Korup and Tweed, 2007).

Previous work in the study area was focused on the bedrock (Huber, 1948), especially for characterization of the NEAT Gotthard basis tunnel site below Sedrun (Schneider, 1992, and references therein). In the northern tributary valleys (Val Giuv, Val Mila, Val Strem; Fig. 2a) Aar granite

dominates, while strongly sheared metamorphic rocks of the Tavetscher Zwischenmassif underlie the Vorderrhein Valley itself. Along the trough shoulder, especially at Cuolm da Vi (Fig. 2a), active deep-seated slope degradation is present as evidenced by abundant trenches and uphill facing scarps (Amann et al., 2006).

The aim of this study is to determine what caused this abrupt and apparently brief period of fan aggradation in the upper Vorderrhein. Previous researchers have interpreted the Sedrun and Disentis fans as kame terraces (Scapozza, 2012) or as Lateglacial outwash fans (Hantke, 1983). For the latter to be true the valley fill at Sedrun would have to be dominated by tributary valley sediment rather than Vorderrhein fluvial sediments. Both of these hypotheses require that the fans formed between about 17 and 11.7 kyr ago.

2 Methods

To decipher the evolution of the upper Vorderrhein region and the origin of the Sedrun fans, we did detailed geomorphologic mapping supported by ArcGIS landscape analysis, as well as cosmogenic ^{10}Be exposure dating of boulders on moraines at the mouths of the three tributary valleys. No boulders suitable for exposure dating were found on any of the fan surfaces. Debris-flow sediments of the fans bury several of these moraines; thus the moraine dates pro-
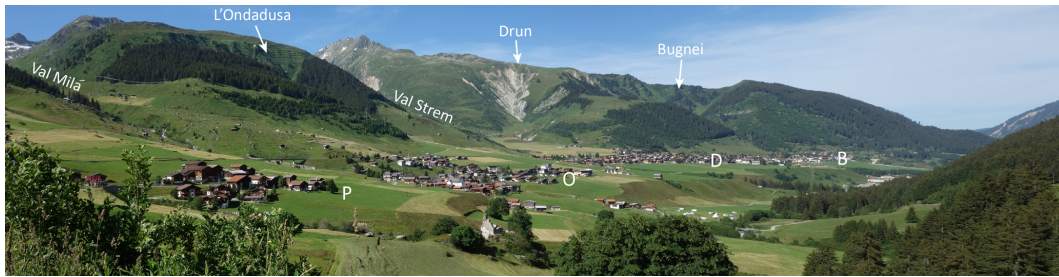
Figure 1. Panorama photograph (looking E) showing the coalesced-fan surface and the distinct cut-off toes of the fans in the upper Vorderrhein area near Sedrun. Fans and associated catchments are labelled P, Pulanera; O, L'Ondadusa; D, Drun; and B, Bugnei.
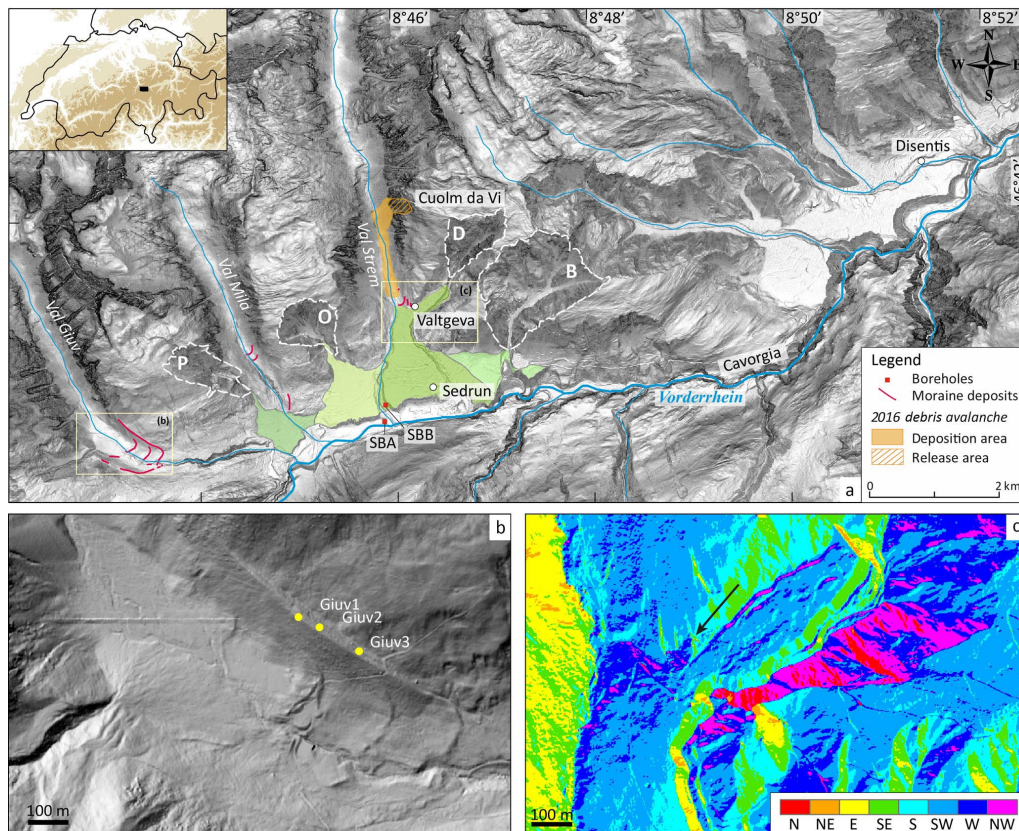
Figure 2. (a) Slope map based on 2 ± 0.5 m resolution DEM (swissAlti3D, swisstopo JA100120) of the oversize fans near Sedrun and Disentis. Catchments (encircled with dashed line) connected to the Sedrun fans are labelled P, Pulanera; O, L'Ondadusa; D, Drun; and B, Bugnei. The 14 March 2016 debris avalanche release and deposit area are shown. Squares indicate locations of Fig. 2b and c. **(b)** Close-up of the moraines in Val Giuv with ^{10}Be-dated boulder locations (dates shown in Fig. 4). **(c)** Close-up of the aspect map of the upper Drun fan. Note morphology of debris-flow levees on upper fan surface; arrow points to left-lateral moraines of the Val Strem paleoglacier that are partly buried by the upper Drun fan sediment.

vide maximum ages for aggradation of the fans. Sampling, sample preparation and age calculations for ^{10}Be exposure dating followed established procedures (Ivy-Ochs and Kober, 2008). Based on the mapped lateral and frontal moraines, paleoglaciers were reconstructed and the associated equilibrium line altitudes (ELAs) were calculated using the ArcGIS GlaRe tool (Pellitero et al., 2015, 2016). Knowledge of the ELA depression with respect to the Little Ice Age ELA is an-

other means of estimating the timing of the glacier advance and associated moraine construction. We reconstructed the sedimentary fill of the upper Vorderrhein Valley based on our own outcrop descriptions combined with the information gleaned from the published NEAT core logs (Schneider, 1992).

Figure 3. (a) Sediment of the upper Drun fan exposed in the Drun stream incision just south of Valtgeva (location shown in Fig. 2a). The outcrop is dominated by debris-flow deposits made up of crudely bedded, angular to subangular gneiss and schist cobbles and boulders (in part imbricated) in a silty, sandy matrix. Close to the top of the section, ~ 0.75 m of interbedded laminated sands is visible, which is in turn overlain by another block layer. **(b)** View up into Val Giuv along the dated inner left-lateral moraine. Boulder Giuv1 is in the right foreground (age $10\,880 \pm 430$ years).

3   Geomorphology of the upper Vorderrhein Valley

3.1   Fan morphology and valley fill

The four fans studied here have a common, coalesced aggradation surface (~ 1380 m a.s.l.) that once must have extended all the way across the valley to the southern slope. Although the Pulanera fan is located at the mouth of Val Mila, the fan emanates from the small erosional-collapse catchment named Val Pulanera (Fig. 2a). At the toe of the Pulanera fan, incision by the Vorderrhein created a sequence of nine terraces. Riser height of the oldest terrace is 20 m. The most recent terrace is 1 m above today's active channel. Just to the west at Val Giuv numerous lateral and frontal moraines mark past glacier positions (Fig. 2b), but there is very little outwash downstream of the moraines and no fan, and the Giuv stream enters a bedrock canyon before joining the Vorderrhein. The lower part of the canyon is filled with and draped by sediment of the neighbouring Pulanera fan. The L'Ondadusa fan is built up of material from the small catchment L'Ondadusa, which lies between Val Mila and Val Strem. Both the Pulanera and L'Ondadusa fans are largely inactive with little material being delivered to the fan today. Only tiny streams, which lack incised channels, traverse the two fans. The erosion escarpment along the Vorderrhein is about 50 m at L'Ondadusa and 70 m at the toe of the Drun fan. The Strem torrent, which separates the L'Ondadusa and Drun fans (Fig. 2a), has incised about 30 m into the topographically contiguous fan surface.

The Drun fan, which lies at the mouth of Val Strem, consists of a lower main fan and an upper fan to the northeast. Surface morphology shows that the fan itself does not emanate from Val Strem, but instead the upper fan sediment is sourced in the Drun catchment (Fig. 2c). The fan is a ski area and both the lower and upper fans were cleaned of large boulders. The upper Drun fan bears scattered boulders (< 0.5 m in height) and faint levees of abandoned channels. Outcrops of the upper fan deposit

along the incised Drun channel (~ 35 m) near Valtgeva reveal several-metre-thick, matrix-supported block layers with infrequent interbedded laminated sands (Fig. 3a). The former are dominated by angular to subangular schist and gneiss blocks in a matrix of silty sand. The Drun catchment lies at the foot of the Cuolm da Vi, the site of active gravitational collapse and toppling with reported movement rates of some tens of centimetres per year (Amann et al., 2006). Several-metre-thick debris-flow deposits within the channel itself attest to recent deposition by the Drun torrent. Left lateral moraines present in Val Strem at Valtgeva are partially buried by the debris-flow sediments of the upper Drun fan (Fig. 2c). The most upvalley moraine was buried in part by the 14 March 2016 Val Strem debris avalanche (Fig. 2a). During this event the western flank of Cuolm da Vi collapsed and $\sim 200\,000$ m^3 of rock debris mixed with snow detached and ran up tens of metres on the opposite valley slope to eventually form a ~ 1 km debris tongue (https://www.nzz.ch/panorama/ungluecksfaelle-und-verbrechen/felssturz-in-sedrun-geroell-verschuettet-wasser–und-stromversorgung-1.18712845, last access: 17 January 2018).

Two of the NEAT cores (Schneider, 1992) were taken close to the middle of the valley (locations shown in Fig. 2a). Examination of the published core log data allowed us a glimpse into the valley fill beneath the L'Ondadusa and Drun fans. Core SBA at 1342 m a.s.l. (2701381/1170326) lies in the Vorderrhein channel, while core SBB at 1358 m a.s.l. (2701314/1170165) lies in the Strem channel ~ 240 m north of the Vorderrhein. Both cores traversed bedrock (Schneider, 1992), in SBA at 55 m depth (1288 m a.s.l.) and in SBB at 89 m depth (1269 m a.s.l.). This reach of the Vorderrhein Valley is overdeepened as shown by the top bedrock surface at 1269 m a.s.l. (core SBB), which is tens of metres lower than the bedrock threshold in the canyon near Bugnei at 1340 m a.s.l. The first 5–10 m of sediment on top of bedrock was interpreted by Schneider (1992) as sub-

Table 1. Sample information, measured ^{10}Be concentrations and calculated surface exposure ages; all errors are 1σ.

Sample ID	Latitude	Longitude	Elevation (m a.s.l.)	Sample thickness (cm)	Topographic shielding factor	^{10}Be concentration (10^4 at g^{-1})[a]	Exposure age[b]
Mila1	46.6835	8.7412	1672	2.0	0.966	15.36 ± 0.67	$10\,120 \pm 440$
Mila2	46.6782	8.7472	1532	2.3	0.985	18.64 ± 0.93	$13\,430 \pm 670$
Mila3	46.6790	8.7509	1512	2.4	0.987	18.62 ± 0.79	$13\,600 \pm 580$
Giuv1	46.6741	8.7209	1841	4.0	0.979	18.64 ± 0.73	$10\,880 \pm 430$
Giuv2	46.6738	8.7213	1831	3.5	0.980	33.45 ± 1.43	$19\,610 \pm 840$
Giuv3	46.6734	8.7227	1795	2.5	0.982	20.31 ± 0.76	$12\,070 \pm 450$

[a] Analyses were normalized to the ETH AMS (accelerator mass spectrometry) standard S2007N (Christl et al., 2013). [b] Calculated with the online calculator of Balco et al. (2008) using the northeast North America calibration data set, a rock density of 2.65 g cm^{-3}, and no erosion. Errors include the statistical uncertainties of the AMS measurement and the error on the subtracted blank ($3.5 \pm 2.5 \times 10^{-15}$).

glacial till (overconsolidated diamicton). This is overlain by glaciofluvial gravels, rare interbedded glacigenic sediments ("tills") and lake sediments. The glaciofluvial deposits contain a broad spectrum of lithologies attesting to both local and Vorderrhein contributions. Starting at an elevation of about 1300 m a.s.l., Vorderrhein gravels with well-rounded clasts begin to dominate both cores. Schneider (1992) interpreted this as signalling the onset of the Holocene. No ^{14}C dates are reported for any of the NEAT cores in the valley. In core SBB, the presence of clean, well-sorted and at times crossbedded sands between elevations of 1330 and 1340 m a.s.l. was interpreted to indicate the presence of a lake (Schneider, 1992). Starting at elevation 1350 m a.s.l. and continuing to the top of core SBB poorly sorted, locally sourced debris-flow sediments with subangular gneiss blocks ranging up to 1 m^3 in diameter were logged. The elevation of the (abandoned) Drun fan surface just adjacent to core SBB is at 1385–1390 m a.s.l., allowing 35–40 m of debris-flow sediments, which comprise the fan topography visible today.

Topographically, the abandoned Drun fan surface continues to the east to coalesce with the Bugnei fan, where the Vorderrhein has incised more than 120 m at the fan toe. Fan outcrops along the northern canyon wall indicate the presence of a pre-existing canyon that was filled by Bugnei debris. The canyon is contiguous with the Cavorgia bedrock canyon that separates the Sedrun fan surface from the Disentis fan surface (Fig. 2a). The rather uniform 7° radial angle of the Bugnei fan surface on both the west and east side underscores the idea that during fan aggradation the (former) Cavorgia canyon must have been already completely filled up.

3.2   Moraines and paleoglacier reconstruction

Results of ^{10}Be exposure dating of moraine boulders are given in Table 1 and shown in Fig. 4. In Val Giuv, the prominent left-lateral moraine (Fig. 2b) is an accretionary moraine with the outermost left-lateral moraine (age $12\,070 \pm 450$ years, Giuv3) having been partially buried by the larger more prominent inner left-lateral moraine (age

$10\,880 \pm 430$ years, Giuv1, Fig. 3b). The apparently too old age of Giuv2 $19\,610 \pm 840$ years (also on outermost moraine) reflects cosmogenic nuclide inheritance and is not discussed further. Sub-parallel latero-frontal moraines at the mouth of Val Mila indicate that, $13\,430 \pm 670$ years ago (Mila2), the local glacier had just reached the main valley. The upvalley left-lateral moraine records stabilization of the glacier at a recessional position $10\,120 \pm 440$ years ago (Mila1). From a boulder on the left flank of the Vorderrhein Valley an age of $13\,600 \pm 580$ years (Mila3) was obtained. This gives a minimum age for the timing of an ice-free main valley. Pollen data indicate ice-free conditions around Sedrun by the beginning of the Bølling interstadial (ca. 14.6 kyr ago; Burga, 1987).

Comparison of the ELAs of the paleoglaciers provides an independent means of assessing contemporaneity of moraine formation in the three tributary valleys. Determined ELAs for the reconstructed paleoglaciers are 2300, 2230, and 2240 m a.s.l. (accumulation area ratio, AAR) for Val Giuv, Mila and Strem, respectively (Fig. 4). All three valleys hosted glaciers during the Little Ice Age. ELA depressions with respect to the Little Ice Age ELAs, which were 2700, 2570 and 2650 m a.s.l. (Maisch, 1992), are 400, 340 and 410 m, respectively. ELA depression during the Egesen stadial across the Alps varies between 250 and 350 m (Ivy-Ochs, 2015, and references therein). Both the ^{10}Be ages and ELA depressions support the hypothesis that the studied moraines record advance of Val Giuv, Mila, and Strem glaciers during the Egesen stadial, which was between about 13 and 11.5 kyr ago (Ivy-Ochs, 2015).

4   Discussion and conclusions

The dated left-lateral moraine at the mouth of Val Mila (Mila2) is buried along its downstream end by fan sediments sourced in the small basin Val Pulanera. In Val Strem three left-lateral moraines are partially buried by the Drun upper fan deposits (Fig. 2c). Although those moraines are undated, the similarity of the paleoglacier ELAs and ΔELAs
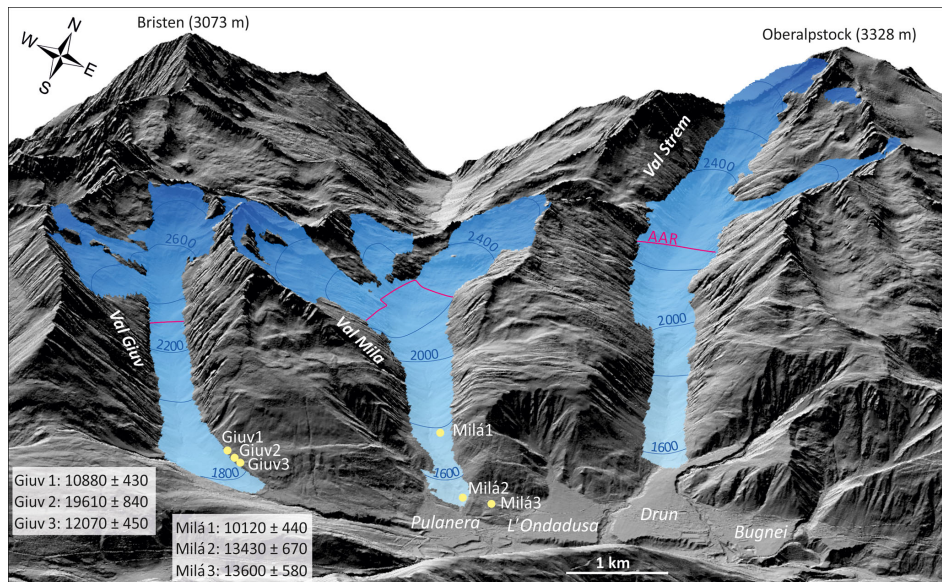
Figure 4. Reconstructed paleoglaciers in the three tributary valleys. Pink lines show the AAR ELAs calculated with the ArcGIS tool GlaRe (Pellitero et al., 2015, 2016). Yellow dots indicate the locations of [10]Be-dated boulders. The corresponding [10]Be ages and their uncertainties are given. The coherence of the ELAs and ΔELAs with respect to the Little Ice Age ELAs (see text) in concert with the [10]Be ages suggest that these glaciers advanced during the Alpine Lateglacial Egesen stadial.

with respect to Little Ice Age ELAs point to contemporaneity of moraine formation with the dated moraines in Val Giuv (12.9–10.9 kyr ago). As the footprint of the paleoglacier snout associated with the dated moraines (Fig. 4) was downstream of the Drun–Strem confluence, debris-flow activity post-dates the Egesen stadial. Similarly, the core data show that only the top 35–40 m of valley fill is actually debris-flow sediments; most is fluvial and glaciofluvial deposits of the Vorderrhein River, which accumulated in the overdeepening upstream of Bugnei. In sum, our data indicate that fan sediments built up after the end of the Lateglacial and that aggradation only took place for a few tens to at most hundreds of years (deposit thickness 30–40 m), when one considers that tens of metres of debris-flow sediment can accumulate in a single event (Harvey et al., 2005).

If the fans did not build up due to evacuation of Lateglacial glacial deposits from the tributary valleys, then why did they aggrade and why did aggradation stop and give way to toe incision so abruptly? We propose that the build-up of the Sedrun and Disentis fans was related to the damming of the Vorderrhein River by the Flims landslide. The Flims landslide (volume 9–12 km^3) has been dated to 9400 cal yr BP with radiocarbon (Deplazes et al., 2007) and 8900 ± 700 years with cosmogenic [10]Be and [36]Cl (Ivy-Ochs et al., 2009). The Vorderrhein was completely blocked by a more than 600 m-thick landslide dam and a lake, Ilanzersee, formed upstream (Wassmer et al., 2004; von Poschinger, 2005). This would have led to marked upstream aggradation for as long as the lake existed. Interestingly, in 1882 Heim mentioned that the Flims landslide-dammed lake had an im-

pact on the landscape all the way up to Disentis, without giving details (Heim, 1882). The highest elevation of the lake is difficult to assess, especially as it may not have been at that elevation for very long. Wassmer et al. (2004) suggest a lake level of 1150 m a.s.l. but geomorphological evidence shows that a lake that high would have overflowed the landslide at numerous locations (cf. von Poschinger, 2005). It seems that the lake could have attained a level of around 940 m a.s.l. without overflowing (Fig. 5). Von Poschinger (2005) estimated a highest level of 936 m a.s.l. and a level that was held for fairly long at about 830 m a.s.l. As soon as the lake had filled with water (taking many years, disregarding seepage), a new higher local base level for all torrents upstream of the lake was established. The marked flattening of the river gradient and reduction in stream power led to immediate and rapid aggradation upstream. First to aggrade were the fans near Disentis whose fan toes were closest to the western end of the lake. At present, there is no evidence that the Disentis fans were deltas. As these fans grew they blocked the Cavorgia canyon (Fig. 2). Vorderrhein sediment choked the canyon and the Bugnei fan began to build up. This led to formation of accommodation space around Sedrun. As shown by the core data, first a lake formed west of Bugnei (recorded by sand layers between 1330 and 1340 m a.s.l. in core SBB), then the three fans, Pulanera, L'Ondadusa and Drun, aggraded and coalesced to form a continuous surface with an elevation of about 1380 m a.s.l. Ilanzersee never filled completely with sediment but emptied (likely stepwise) due to breaches in the landslide deposit where the present Vorderrhein channel is. The uniformity of the marked cut-off toes of the Disentis and
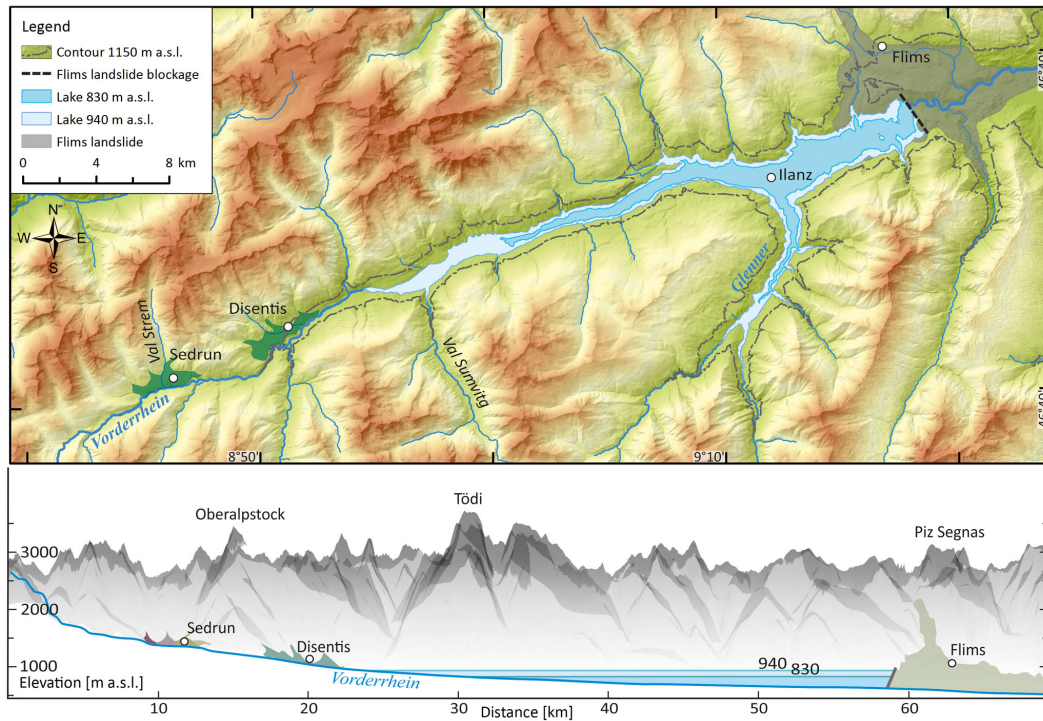
Figure 5. Coloured elevation overlain on hillshade map of the area between Disentis and Flims (swisstopo JA100120). The dark grey area represents the Flims landslide deposits. The black thick dashed line indicates the location of the blockage of the Vorderrhein River by the landslide dam (von Poschinger, 2005). The proposed Ilanzersee shoreline at an elevation of 1150 m a.s.l. (Wassmer et al., 2004) is outlined in grey dots. This reconstruction shows that a lake with surface at 1150 m a.s.l would have overflowed the landslide dam at several points both north and south of the location of the blockage and subsequent final breach. The white and light blue areas show extents of Ilanzersee with shorelines of 940 and 830 m a.s.l., respectively, as proposed by von Poschinger (2005). Lower panel: longitudinal ESE–WNW profile along the Vorderrhein River down to the Flims landslide deposits. The two lake levels, 940 and 830 m a.s.l., are shown. In the background the mountain peaks to the north are illustrated. Vertical exaggeration 2.5×.

Sedrun fans suggests coherent response to an abrupt downstream change in base level, which we suggest was the draining of Ilanzersee. As the lake level decreased suddenly, the Vorderrhein was able to clear out the Cavorgia canyon (there is no evidence for formation of a new bedrock canyon epigenetically), base level dropped and fan aggradation ceased. The fan toes were incised. The associated knickpoint is now located near the outlet of the Drun torrent just west of the Bugnei fan, as attested by the bedrock outcrops in the channel at elevation 1340 m a.s.l. This is also the approximate elevation of the present floodplain upstream of this point. The broad floodplain (200 m wide) and the nine cut terraces reflect meandering of the Vorderrhein near Pulanera and point to the river being in a stable state at present along this reach.

References

Amann, F., Donatsch, G., Bonanomi, Y., and Moser, M.: Kinematik und Bewegungsmechanismus der tiefgründigen Instabilität Cuolm Da Vi (Graubünden, Schweiz), Bulletin für angewandte Geologie, 11, 117–131, 2006.

Balco, G., Stone, J. O., Lifton, N. A., and Dunai, T. J.: A complete and easily accessible means of calculating surface exposure ages or erosion rates from [10]Be and

[26]Al measurements, Quaternary Geochronology, 3, 174–195, https://doi.org/10.1016/j.quageo.2007.12.001, 2008.

Burga, C. A.: Das alpine Spät- und Postglazial in Graubünden aufgrund geomorphologischer und pollenanalytischer Untersuchungen, Vierteljahresschrift der Naturforschenden Gesellschaft in Zürich, 132, 26–44, 1987.

Christl, M., Vockenhuber, C., Kubik, P. W., Wacker, L., Lachner, J., Alfimov, V., and Synal, H.-A.: The ETH Zurich AMS facilities: Performance parameters and reference materials, Nucl. Instrum. Meth. B, 294, 29–38, https://doi.org/10.1016/j.nimb.2012.03.004, 2013.

Deplazes, G., Anselmetti, F. S., and Hajdas, I.: Lake sediments deposited on the Flims rockslide mass: the key to date the largest mass movement of the Alps, Terra Nova, 19, 252–258, https://doi.org/10.1111/j.1365-3121.2007.00743.x, 2007.

Hantke, R.: Eiszeitalter: Die jüngste Erdgeschichte der Alpen und ihrer Nachbargebiete, Ott, Thun, Switzerland, 1983.

Harvey, A. M. Mather, A. E., and Stokes, M.: Alluvial Fans: Geomorphology, Sedimentology, Dynamics Geological Society, London, UK, Special Publications, 251, 248 pp., https://doi.org/10.1144/GSL.SP.2005.251.01.16, 2005.

Heim, A.: Der alte Bergsturz von Flims, Jahrbuch des Schweizer Alpenclub, Bern, Switzerland, 18, 295–309, 1882.

Hornung, J., Pflanz, D., Hechler, A., Beer, A., Hinderer, M., Maisch, M., and Bieg, U.: 3-D architecture, depositional patterns and climate triggered sediment fluxes of an alpine alluvial fan (Samedan, Switzerland), Geomorphology, 115, 202–214, https://doi.org/10.1016/j.geomorph.2009.09.001, 2010.

Huber, W.: Petrographisch-mineralogische Untersuchungen im südöstlichen Aarmassiv, Schweiz. Miner. Petrog., 2, 557–642, 1948.

Ivy-Ochs, S.: Glacier variations in the European Alps at the end of the last glaciation, Cuadernos de investigación geográfica, 41, 295–315, https://doi.org/10.18172/cig.2750, 2015.

Ivy-Ochs, S. and Kober, F.: Surface exposure dating with cosmogenic nuclides, E&G Quaternary Sci. J., 57, 179–209, https://doi.org/10.3285/eg.57.1-2.7, 2008.

Ivy-Ochs, S., Poschinger, A. V., Synal, H. A., and Maisch, M.: Surface exposure dating of the Flims landslide, Graubünden, Switzerland, Geomorphology, 103, 104–112, https://doi.org/10.1016/j.geomorph.2007.10.024, 2009.

Korup, O. and Tweed, F.: Ice, moraine, and landslide dams in mountainous terrain, Quaternary Sci. Rev., 26, 3406–3422, https://doi.org/10.1016/j.quascirev.2007.10.012, 2007.

Maisch, M.: Die Gletscher Graubündens, Part B, Geographisches Institut Universität Zürich, Zürich, Switzerland, 1992.

Pellitero, R., Rea, B. R., Spagnolo, M., Bakke, J., Hughes, P., Ivy-Ochs, S., Lukas, S., and Ribolini, A.: A GIS tool for automatic calculation of glacier equilibrium-line altitudes, Comput. Geosci., 82, 55–62, https://doi.org/10.1016/j.cageo.2015.05.005, 2015.

Pellitero, R., Rea, B. R., Spagnolo, M., Bakke, J., Ivy-Ochs, S., Frew, C. R., Hughes, P., Ribolini, A., Lukas, S., and Renssen, H.: GlaRe, a GIS tool to reconstruct the 3D surface of palaeoglaciers, Comput. Geosci., 94, 77–85, https://doi.org/10.1016/j.cageo.2016.06.008, 2016.

Scapozza, C.: Kame Terrassen Camischolas (Disentis, Sedrun, GR), Géotope Suisse, no. 284 (GR), Bern, Switzerland, 2012.

Schneider, T.: Geologische Auswertung (Schlussbericht) Sondierbohrungen Tujetsch, NNE Rueras, Bundesamt für Verkehr und AlpTransit, Bern, Switzerland, 1992.

Von Poschinger, A.: Der Flimser Bergsturz als Staudamm, Bulletin für angewandte Geologie, 10, 33–47, https://doi.org/10.5169/seals-225564, 2005.

Wassmer, P., Schneider, J. L., Pollet, N., and Schmitter-Voirin, C.: Effects of the internal structure of a rock-avalanche dam on the drainage mechanism of its impoundment, Flims sturzstrom and Ilanz paleo-lake, Swiss Alps, Geomorphology, 61, 3–17, https://doi.org/10.1016/j.geomorph.2003.11.003, 2004.

Open Access

E&G Quaternary Science Journal

Express report

Disestablishing "*Glacial* Lake Speight", New Zealand? An example for the validity of detailed geomorphological assessment with the study of mountain glaciations

Stefan Winkler[1], David Bell[2], Maree Hemmingsen[3], Kate Pedley[2], and Anna Schoch[4]

[1]Department of Geography and Geology, University of Würzburg, Am Hubland, 97074 Würzburg, Germany
[2]Department of Geological Sciences, University of Canterbury, Private Bag 4800, Christchurch 8140, New Zealand
[3]Primary Science Solutions Ltd., Woodbury Street 75, Russley, Christchurch 8042, New Zealand
[4]Department of Geography, University of Bonn, Meckenheimer Allee 166, 53115 Bonn, Germany

Correspondence:	Stefan Winkler (stefan.winkler@uni-wuerzburg.de)

1   Introduction

The middle Waimakariri River catchment in the Southern Alps of New Zealand, informally defined here as its reach upstream of Waimakariri Gorge to the junction of Bealey River (Fig. 1), is characterised by an outstanding assemblage of various landforms representing different processes of formation and ages. It offers ideal conditions for studying the sediment budget of a major New Zealand braided river within its mountain catchment. Such research has, however, not been carried out yet. It seems to be a legitimate hypothesis considering this catchment as part of a complex sediment cascade. Its numerous voluminous fans, impressive terrace sequences, and wide braided river floodplains are efficient sediment sinks. This would infer that substantial and efficient evacuation of sediment would rather take place under full glacial conditions during glaciations or in their wake, intensified by paraglacial processes, than under current (Holocene) conditions. Detailed studies on the sediment budget may reveal valuable insights into the successive build-up of the Canterbury Plains and their modification by Holocene fluvial action connected to major braided rivers. Additionally, they bear

implications beyond these fluvial aspects. Palaeoseismological studies claim to have detected signals of major Alpine Fault earthquakes in coastal environments along the eastern seaboard of the South Island (McFadgen and Goff, 2005). This requires high connectivity between the lower reaches of major braided rivers and their mountain catchments to generate immediate significant sediment pulses. It would be contradictory to the abovementioned hypothesis though. Obtaining better control on sediment budgets of braided rivers like the Waimakariri River will finally add significant value to multiple scientific and applied topics like regional resource management.

An essential first step of sediment budget studies is to systematically map the geomorphology, conventionally in the field and/or using remote-sensing applications, to localise, genetically identify, and classify landforms or entire toposequences of the area being investigated. In formerly glaciated mountain environments it is also indispensable to obtain all available chronological information supporting subsequent investigations. In our case, only limited chronological and geomorphological information has previously been published. The first major geomorphological mapping was con-
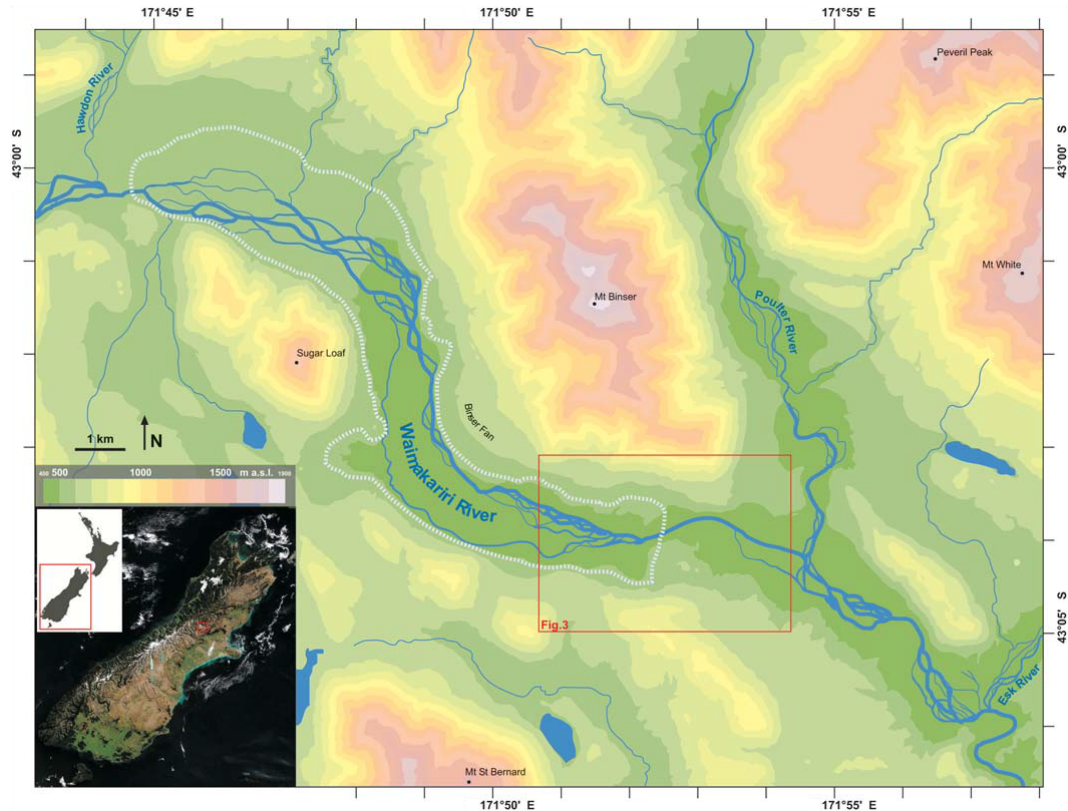
Figure 1. Elevation map of the study area (based on NZ Topo50 map data, Land Information New Zealand, https://www.linz.govt.nz/land/maps/topographic-maps, last access: 9 August 2018). The small insert shows its location within New Zealand and the red frame denotes the area covered by Fig. 3 (i.e. the potential damming site). The approximate outlines of "Glacial Lake Speight" are indicated by a stippled line and based on existing morphological evidence and the figure published in Gage (1958). Please note that the maximum lake level Gage quotes in his text (1550 ft or ~ 472.5 m a.s.l.) matches neither the lake extent indicated in his own figures nor modern topographic data. Even if some inaccuracy may result from the topographic information Gage used at his time, the difference is quite considerable and "1550 ft" is potentially a printing error (1750 or 1850 ft (~ 533 or ~ 564 m would result in a much better match).

ducted by Gage (1958), who introduced a regional stratigraphy that is still in use today despite its lack of numerical age control (see Barrell et al., 2011). Rother et al. (2015) published new numerical (cosmogenic radionuclide) ages and improved our knowledge about Last Glacial Maximum ice extent and subsequent deglaciation. They, however, made no attempt to thoroughly assess Gage's geomorphological map. Except from a few studies merely addressing local topics, no work on a wider regional scale relevant for sediment budget studies has been published. The study area is covered in the glacial geomorphological map of Barrell et al. (2011), which primarily focuses on the chronological aspects of glacial landforms and lacks details due to its scale (1:100 000).

In his study, Gage (1958) introduced the so-called "Glacial Lake Speight" that temporarily occupied a large section of the middle Waimakariri River during deglaciation (Fig. 1). He named it after Robert Speight, a prominent Christchurch-based geologist who investigated glacial landforms and deposits of the region during the first part of the 20th century. Gage's concept of Glacial Lake Speight has been re-

tained since (see Forsyth et al., 2008; Barrell et al., 2011; Rother et al., 2015). Geomorphological evidence in the form of palaeolake shorelines is evident, for example on the large alluvial fans (Fig. 2a, b, Supplement Sect. 3.8). Whereas the existence of this former lake remains unchallenged, already in early preparatory stages of our study the original concept of Glacial Lake Speight comes into conflict with our geomorphological analysis and mapping. We conclude that Glacial Lake Speight potentially has to become disestablished as a temporal lake formed during deglaciation and causally connected to it. Establishing a logical succession of landforms and related processes during landscape evolution reveals that the temporary lake that once occupied the valley must be younger, even without new chronological data. This inevitably requires revisiting statements of Gage (1958) regarding the lifespan of the temporary lake and proposed mechanism of its damming. Glacial Lake Speight and its chronological status is not a major focus of our general study; instead we aim to share our conclusions and put them up for discussion because (a) Glacial Lake Speight is a well-
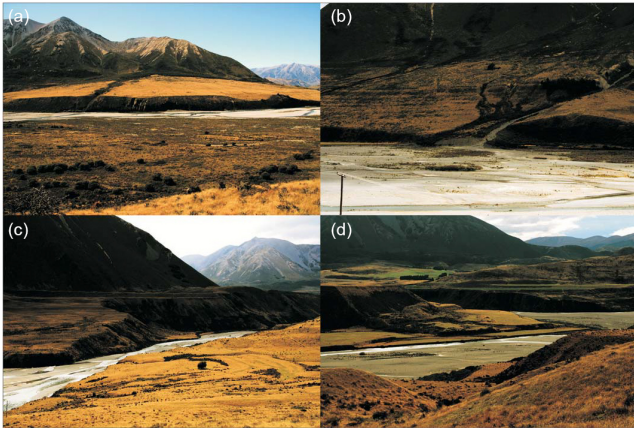
Figure 2. Ground images of selected geomorphological features in the study area: **(a)** Binser Fan as seen from the opposite side of the valley; a sequence of shorelines related to the former lake is visible on its lower part to the right; **(b)** sequence of shorelines formed on the lower part of the prominent fan downstream from Binser Fan as seen from the opposite side of the valley; **(c)** overview of the proposed damming site (see text and Fig. 3) as seen towards the east; **(d)** slump at the confluence of Waimakariri River and Poulter River (entering from the left back) immediately downstream from the proposed damming site (all images Stefan Winkler: **a** 11 March 2018, **b–d** 13 March 2018).

known concept within the regional Quaternary community that surely needs further reassessment, (b) it constitutes another example for apparently universally accepted key localities that might not hold up under detailed re-evaluation, and importantly (c) it demonstrates the unchanged value of basic geomorphological analysis and mapping despite recent technical and methodological progress.

2 Reassessing Glacial Lake Speight

2.1 Original concept and its difficulty

Because of missing shorelines or lake sediments found downstream of the confluence of Poulter Valley, Gage (1958) concluded that the lake existed during deglaciation when the glacier retreated subsequent to the last major advance that formed terminal moraines in this section of the valley, the two-phased "Poulter advance" (ca. 17.5 ka according to Rother et al., 2015, using terrestrial cosmogenic nuclides). The inner of the Poulter moraines is located just upstream the abovementioned confluence (Figs. 1 and 3 and Fig. S4d, e in the Supplement). Gage (1958) suggested that this moraine and debris-covered stagnant ice dammed Glacial Lake Speight but provided no detailed mechanism or timeline. It extended up-valley as far as the Hawdon River confluence (Fig. 1). Among a few other sites, the prominent Binser Fan shows evidence in the form of palaeolake shorelines best described as wave-cut benches (Figs. 2a,

S3.8d). Binser Fan and an adjacent fan to the east (Gooseberry Stream Fan; see Figs. S3.8a, b, c) should have been built up to their present height during the highest lake level according to Gage. This interpretation was repeated by Barrell et al. (2011) mapping this particular fan to be of (Latest) Late Otiran age ($\sim$ 20–14.5 ka), whereas almost all other fans in the area are mapped as Holocene. Gage (1958) interprets the shorelines as signs of an intermittent lake level lowering and states that Glacial Lake Speight existed for hundreds of years. Draining to at least the present floodplain level should have been completed prior to final wastage of early Poulter advance stagnant ice downstream of the lake because the latter protected, according to Gage, glacial sediments east of the Poulter moraine from destruction during drainage (see Gage, 1958, and Fig. 2 therein). Finally, he sees a lower fan intersecting one of the abovementioned fans formed during lower lake levels and consequently judges post-deglaciation fan activity as insignificant.

This original concept immediately creates difficulties with a chronological sequencing of the landforms present in the study area (see below and see Fig. 3). It seems unlikely that the massive Binser Fan fully developed in the short time frame between the former glacier retreating from this part of the valley and the palaeolake reaching its maximum water level. Furthermore, it infers that Binser Fan has been predominately inactive during the subsequent Late Glacial and the entire Holocene. This would be unusual in comparison to most other fans in the wider region. The large extent of the lake and its inferred period of existence would, furthermore, require a rather stable natural dam, somehow difficult to comprehend if stagnant ice was involved. To tackle these and other emerging discrepancies, several questions need to be addressed. (a) Where was the lake's "dam" located? (b) How did it form and what material did it consisted of? (c) When did the lake form and how long did it exist? (d) What was the mechanism of its outburst?

2.2 Geomorphological assessment

Some of the questions raised above are easily solved. There are no features related to the palaeolake located downstream from the confluence of Poulter River. Although there is more than one suitable scar that could be related to potential massive landslides blocking the narrow Waimakariri Gorge further downstream (Figs. S2, S4f), the lack of any morphological evidence at the mouth and within the lower reach of both major tributaries, the Poulter and Esk rivers, rejects this hypothesis. Furthermore, the well-developed terrace sequences along Waimakariri River downstream of the Poulter River confluence (Fig. S3.4a) show no signs of influence by a temporary lake. The feature that once dammed the palaeolake needs, therefore, to be at the location Gage (1958) originally proposed.

Because this location of the former natural dam cannot be separated from its origin and properties, the issue starts to
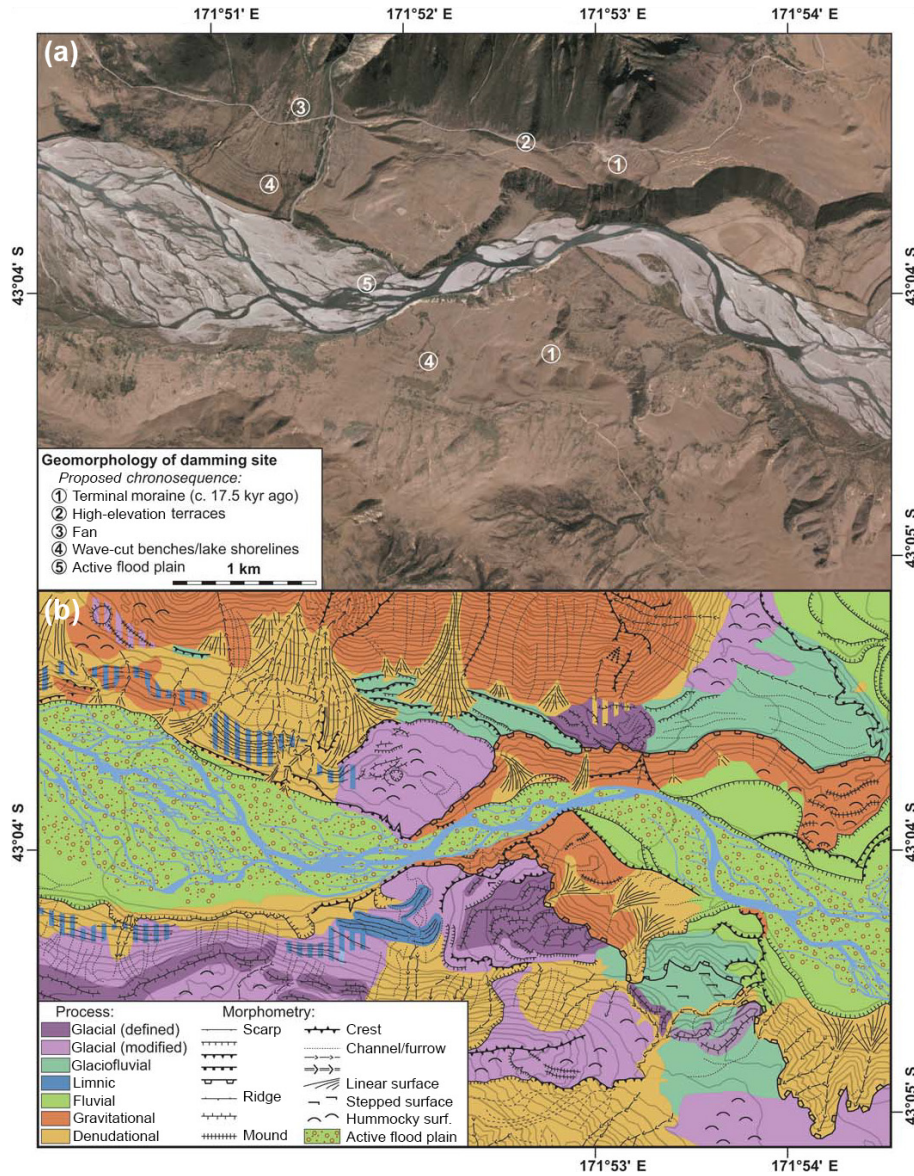
Figure 3. (a) Orthorectified aerial photo of the proposed damming site (modified after Land Information New Zealand, https://data.linz.govt.nz/data/category/aerial-photos, last access: 9 August 2018). A few features mentioned in the text are indicated and set into a proposed chronosequence. **(b)** Preliminary geomorphological map of the proposed damming site covering the same area as the upper panel. The map has been prepared following the slightly modified mapping key of GMK 25 (see Leser and Stäblein, 1985) and some layers (including active processes) have been omitted for clarity. The two different signatures for glacial process area account for landforms of defined origin (e.g. moraine ridges) vs. areas that have merely been overprinted/modified. Different signatures for scarps, ridges, and channels highlight different dimensions (listed small to large here) as outlined in detail in the abovementioned mapping key (contours based on NZ Topo50 map data, Land Information New Zealand, https://www.linz.govt.nz/land/maps/topographic-maps, last access: 9 August 2018).

become quite complex. There is no bedrock structure near the site in the Waimakariri Valley that could have acted as a dam (see S3.4). Given the glacial history of the valley and its occupancy by a large valley glacier during most of MIS 2, it would be hard to assume that a bedrock structure suitable to act as a dam during deglaciation would have survived many thousands of years of glacial erosion and then completely eroded since. Unlike large foreland lakes in the

Southern Alps east of the Main Divide like Lake Ohau or Lake Pukaki, Glacial Lake Speight would not have occupied a glacial foreland depression supporting a permanent lake. While Gage (1958) draws such a comparison, both abovementioned lakes have natural outlets and are actually dammed by massive glaciofluvial fanheads and not any terminal moraine sequences. This is a fundamental difference from the Waimakariri River valley because such settings gen-

erally facilitate the occurrence of stable dams with established outlets. There is neither evidence for a postglacially infilled huge overdeepened basin in this part of the Waimakariri River valley nor does the setup of glacial, glaciofluvial, or fluvial landforms suggest such a basin existed. This requires any potential lake dam to be sufficiently stable to persist until the lake reached its maximum extent before it gradually collapsed or became incised and subsequently eroded.

With the original timeline of Gage (1958), the natural dam needed to allow the lake to exist over many centuries, an assumption that sounds unrealistic for the terminal moraine he proposed, especially if debris-covered stagnant ice should have been involved. If the moraine actually constituted the dam, lake formation must have started immediately during the initial withdrawal of the glacier. It may theoretically include parts of the glacier tongue becoming separated from the active glacier and successively wasting down. But the moraine could only have acted as a dam if no efficient overflow existed from the onset. Increasing hydrological pressure by an enlarging proglacial lake is usually sufficient to widen and incise any meltwater overflow channel (in particular if stagnant ice becomes exposed) and thereby prevent any blockage upstream. With the distance of glacier retreat between the potential damming site and the confluence of Hawdon Valley of ca. 15 km (Fig. 1), it must have taken many centuries if compared to reported concurrent glacier retreat in similar valleys (Rother et al., 2014; Shulmeister et al., 2018). It seems, therefore, doubtful that the Poulter moraine and debris-covered stagnant ice could have provided a stable lake dam over such a long period without an existing depression and a supportive massive fanhead or similar feature.

If the conclusions of Gage (1958) regarding Glacial Lake Speight are accepted, the Waimakariri River needs to have been incised at least a few metres below the lowest palaeo-lake shorelines prior to its formation. As soon as lake formation commenced and the former valley glacier left its position at the Poulter moraine, no further incision would have been possible. This theoretically could reintroduce the abovementioned hypothesis of an overdeepened basin upstream from the Poulter River confluence, but it becomes easily contradicted by the outline and profile of (glacio)fluvial terraces in comparison with the modern floodplain (see Figs. 3, S4c, d, e) and other geomorphological evidence up- and downstream of the damming site (e.g. truncated fans). Furthermore, the position of the Poulter moraine itself (Figs. 3, S3.1) would not match such a low valley floor level as two prominent terraces immediately proximal in high elevation (Figs. 3, S3.2) must have formed shortly after the glacier retreated. The terraces are located above the highest lake shoreline and thus need to be older.

Binser Fan is a typical outsize fan (Jarman et al., 2011) characterised by an anomalous relationship between fan area (ca. 2.2 km^2) and catchment area (ca. 3.4 km^2). There is still discussion whether these fans are formed during rather catastrophic events or by gradual processes over longer periods of time. According to Gage (1958), the fan has been completely built up into the lake during its maximum extension. The palaeolake shorelines on the fan show an erosional character (S3.8) and are likely formed by wave action related to predominant westerly wind directions. The fan seems to be adjusted to a base level below the lowest lake shorelines close or identical to the modern valley floor. Erosion at the base of Binser Fan indicates subsequent shifting of Waimakariri's active river channel towards the east in this section of the valley (see S4c). Binser Fan and its two neighbours cover glacial features (kame terraces, glacially sculptured bedrock ledges) at their lateral upper margins (Figs. 3, S3.8e, S4c). From this morphological age relationship and process sequence, the fans presumably post-date any major glacial activity in the valley including initial deglaciation. Judging by comparison with other formerly glaciated mountain valleys worldwide, morphology and setting of the fans in the study area clearly indicate a postglacial formation, perhaps (but not necessarily) related to the paraglacial process system (Brardinoni et al., 2018). A Late Glacial build-up during the short time frame of the maximum lake level followed mainly by inactivity to allow preservation of the shorelines seems unlikely. The sedimentary architecture of the fan could be investigated using geophysical methods (e.g. ground-penetrating radar) to prove its non-deltaic formation into a lake.

2.3 An alternative model for a non-glacial Lake Speight

Barrell et al. (2011) mapped parts of the area north of the active river channel where Gage (1958) located the Poulter moraines as landslide. A landslide origin for the palaeolake, not necessarily related to deglaciation, would solve some of the abovementioned inconsistencies. Ground inspection reveals, however, that only a part of the terminal moraine complex has been post-depositionally covered by slope material (angular, clast-supported sediment mainly up to pebble grain size; see S3.3). There is no defined source area/scar of a larger landslide at the proposed damming site (S3.2) and both surface material and morphology of the terminal moraine complex are comparable to contemporary ones in other valleys (e.g. Borsellino et al., 2017). Even if we reject its capacity to act as a lake dam we have no doubt that the area constitutes a moraine system subsequently modified by glaciofluvial erosion and slope processes (Figs. 3, S3.1). However, its outline in relation to surrounding geomorphological features (in particular the two major proximal terraces; see S3.6) underlines our conclusion that the moraine itself cannot be considered a lake dam.

Mass movements are very frequent in the Southern Alps. Many are supposed to be coseismically triggered (Davies, 2016) and the proposed damming site is in proximity to an active fault (Esk River Fault; see Forsyth et al., 2008). Mass movements have, of course, many various triggers and without a prominent landslide scar (see S3.2), the narrow active river channel enclosed by steep erosion scars cut into

terrace flights itself moves into the focus. A major slump could easily mobilise enough material to block the narrow course of the Waimakariri River at this site. Successive incision during the latest late glacial or Holocene could have formed a steep-sided channel cut into glacial and glaciofluvial sediment of various origin and properties (see S3.10). Such sediment may not persistently support high cliffs if exposed to some form of external or internal forcing. A slump some hundred metres downstream of the proposed damming site (Fig. 2d) may constitute a miniature analogue for what happened at a larger scale at the narrowing. The proposed damming site is, furthermore, the only stretch within the valley where (glacio)fluvial terraces are not well developed (see S3.4a, 3.5a), instead cut by the abovementioned high erosional scarp (see Figs. 2c, 3, S3.7).

How long would such a slump theoretically need to block the channel in order to dam the palaeolake to its mapped maximum size? Whereas the lake area can be estimated to ca. 24.5 km^2 using existing morphological evidence and contours (Fig. 1), a detailed estimate of its volume is impossible. A generous estimate of 100 m average water depth would yield 2.45×10^9 m^3 for its maximum level. The long-term annual average runoff for the Waimakariri River is ~ 120 m^3 s^{-1} near its mouth and $\sim 90\%$ of this runoff is estimated for it at the Waimakariri Gorge, which represents the mountain catchment (online data: https://www.niwa.co.nz and https://www.ecan.govt.nz, last access: 20 May 2018). Reducing the ratio to 60 % in accounting for three major tributaries (Poulter, Esk, Kowai) entering downstream from the proposed damming site, the modern annual average runoff volume would total 2.27×10^9 m^3. Even if modern runoff data show high annual variability and are not representative for the past, the comparison reveals that filling the temporary lake to its maximum level would only take several years, even if its volume is hugely underestimated. The lake could, therefore, have been a short-lived feature that lasted as short as ~ 10 or fewer years, quite comparable to landslide-dammed lakes that have been observed in the wake of recent earthquakes (Kaikoura, New Zealand). Consequently, after a comparatively short time an outlet could have formed and the lake successively drained. The multiple palaeolake shorelines show that drainage was not catastrophic but more gradual. Such a gradual process also argues for more coherent material of the lake dam and excludes, for example, debris-covered stagnant ice that may have been present in the valley during deglaciation. The latter would, once exposed, cause a sudden drainage. Recent experience at artificially dammed lakes (e.g. Lake Pukaki) demonstrates that shorelines form quite quickly in glacial and glaciofluvial sediments comparable to the ones at Waimakariri River (Bunting, 1977; observations by the authors). The likely short time frame provides another argument against Lake Speight's glacial origin.

3 Conclusions and outlook

Geomorphological mapping and analysis conducted as an initial step towards a sediment budget study of the middle Waimakariri River has revealed serious doubts that a palaeolake that formed in the study area was temporally or causally related to the last deglaciation. Unless a convincing, detailed model of how the Poulter moraine and debris-covered stagnant ice could dam a lake of significant dimensions for many hundreds of years in the specific setting (i.e. without a massive fanhead and pre-existing basin) is developed, the previous concept of *Glacial* Lake Speight that stood unchallenged within the regional Quaternary geology for 70 years should consequently be disestablished. Any such model seriously considered requires, furthermore, to fit with the chronosequence and timescales of para- and postglacial landform development both locally and regionally, in particular with the dominating fans. We propose an alternative model for a comparatively short-lived temporary lake due to blockage by a major mass movement event during the latest late glacial or Holocene. Future detailed work on possible mechanisms and age constraints is highly encouraged. This is inevitably necessary to obtain better control on landscape evolution and effective process systems.

Disestablishing the glacial context of former Lake Speight has implications beyond regional scale. It is an ostensive example that vigorous geomorphological analysis and mapping has inalterable value especially for the study of late Quaternary mountain glaciations. It reveals again that even apparently "established" concepts of key landforms or type localities occasionally have to be challenged. One has to accept that recent scientific progress within the field of dating techniques and palaeoglaciological modelling cannot compensate for what sometimes seems to be the gradual replacement of traditional geomorphology by "big data". Ultimately, Glacial Lake Speight joins an increasing number of key localities that deserve to be re-evaluated and may no longer be carried on in their original interpretation.

References

Barrell, D. J. A., Andersen, B. G., and Denton, G. H.: Glacial geomorphology of the Central South Island, GNS Science Monographs, 27, Lower Hutt, New Zealand, 2011.

Borsellino, R., Shulmeister, J., and Winkler, S.: Glacial geomorphology of the Brabazon and Butler Downs in the Rangitata Valley, New Zealand. J. Maps, 13, 502–510, https://doi.org/10.1080/17445647.2017.1336122, 2017.

Brardinoni, F., Picotti, V., Maraio, S., Bruno P. P., Cucato, M., Morelli, C., and Mair, V.: Postglacial evolution of a formerly glaciated valley: Reconstructing sediment supply, fan building, and confluence effects at the millennial time scale, online first, Geol. Soc. Am. B., https://doi.org/10.1130/B31924.1, 2018.

Bunting, D. G.: Lake Pukaki shore-line stability: a preliminary engineering geological investigation, Unpublished MSc thesis, University of Canterbury, Christchurch, New Zealand, 1977.

Davies, T. R. H.: Mountain process geomorphology: Conceptual progress in the Southern Alps, in: Landscape and Quaternary Environmental Change in New Zealand, edited by: Shulmeister, J., Atlantis Press, 205–233, 2016.

Forsyth, P. J., Barrell, D. J. A., and Jongens, R.: Geology of the Christchurch area, GNS 1:250 000 Geological Maps, 16, Lower Hutt, New Zealand, 2008.

Gage, M.: Late Pleistocene glaciations of the Waimakariri Valley, Canterbury, New Zealand, N. Z. J. Geol. Geophys., 1, 123–155, https://doi.org/10.1080/00288306.1958.10422800, 1958.

Jarman, D., Agliardi, F., and Crosta, G. B.: Megafans and outsize fans from catastrophic slope failures in Alpine glacial troughs: the Malser Haide and the Val Venosta cluster, Italy. Geol. Soc. Spec. Publ., 351, 253–277, https://doi.org/10.1144/SP351.14, 2011.

Leser, H. and Stäblein, G.: Legend of the geomorphological map 1:25.000 (GMK 25) – fifth version in the GMK priority programm of the Deutsche Forschungsgemeinschaft, Berliner Geographische Abhandlungen, 39, 61–89, Berlin, Germany, 1985.

McFadgen, B. G. and Goff, J. R.: An earth systems approach to understanding the tectonic and cultural landscapes of linked marine embayments: Avon-Heathcote Estuary (Ihutai) and Lake Ellesmere (Waihora), New Zealand, J. Quaternary Sci. 20, 227–237, https://doi.org/10.1002/jqs.907, 2005.

Rother, H., Fink, D., Shulmeister, J., Mifsud, C., Evans, M., and Pugh, J.: The early rise and late demise of New Zealand's last glacial maximum, P. Natl. Acad. Sci. USA ,111, 11630–11635, https://doi.org/10.1073/pnas.1401547111, 2014.

Rother, H., Shulmeister, J., Fink, D., Alexander, D., and Bell, D.: Surface exposure chronbology for the Waimakariri glacial sequence in the Southern Alps of New Zealand: Implications for MIS-2 ice extent and LGM glacial mass balance, Earth Planet. Sc. Lett., 429, 69–81, https://doi.org/10.1016/j.epsl.2015.07.033, 2015.

Shulmeister, J., Fink, D., Winkler, S., Thackray, G., Borsellino, R., Hemmingsen, M., and Rittenour, T.: Evidence for slow late-glacial ice retreat in the upper Rangitata Valley, South Island, New Zealand, J. Quaternary Sci. 185, 102–112, https://doi.org/10.1016/j.quascirev.2018.01.006, 2015.

Open Access

E&G Quaternary Science Journal

Proglacial streams and their chronology in the glacier forefields of the Himalayas

Gerrit Tombrink

Institute of Geography, University of Göttingen, Goldschmidtstrasse 5, 37077 Göttingen, Germany

Correspondence: Gerrit Tombrink (g.tombrink@mailbox.org)

The aim of this investigation was to develop a classification of glaciofluvial landforms and to identify a general sequence of these forms in the glacier forefields of the Himalayas. The intention behind this effort was to provide a standard sequence of typical glaciofluvial landforms that can serve as a tool for establishing relative chronological frameworks of fluctuations of glaciers in cases in which the preservation of moraines does not allow for direct determination of the former extents of glaciations. Thus, this research aimed at establishing a standard sequence of landforms that shows a climatic–genetic dependence on recent and historical glacier fluctuations during the Holocene in the study areas of Khumbu Himal (central Eastern Himalayas; Fig. 1a) and Pangong Tso (Western Himalayas; Fig. 1b). An empirical approach, including systematic analyses at the micro-, meso-, and macroscale (Schumm, 1991) of the main study area in Khumbu Himal, allowed such a standard sequence to be identified. This systematic multi-scale approach also proved suitable for the proglacial streams in the semi-arid region near the Pangong Tso southwest shore, which was used to identify convergences and divergences of landforms.

The methods that finally allowed for the establishment of the standard sequence of glaciofluvial landforms included geomorphological field techniques that were applied in two field campaigns in 2012 and 2013, sedimentological analy-sis, satellite image studies, and photo-panorama evaluations. Combination of these methods allowed for the distinguishing of divergent channel-reach morphologies (Montgomery and Buffington, 1997), glaciofluvial terraces, gravel deposits (sandur), sequences of proglacial stream landforms, and longitudinal stream profiles in the study areas of the Himalayas. The influencing factors of the streams, such as geological processes (e.g., tectonic deformation), slope processes (e.g., avalanches, debris flows), climatic processes (e.g., precipitation), and fluvial processes (e.g., glacial lake outburst floods (GLOFs), river inflows), were considered. The roles of these factors were clarified using additional field surveys in tributary valleys.

Microanalysis. In the glacier forefields, proglacial streambed morphologies show a downstream change from cascades into step-pool sequences. Based on these changing morphologies, early and late stages of streambed evolution were reconstructed. This approach allowed for relative classification of the beds of the proglacial streams in Khumbu Himal into early and late stages of streambed evolution. The basal tills underneath the streambeds were rarely deposited during Late Glacial to Neoglacial stages (IV–'VII), but mostly during historical glacier stages (VII–XI) to the recent (XII) glacier stage (glacial stages according to Kuhle, 2005), and stages from 1980 onwards (glacial stages according to Racoviteanu and Bajracharya, 2008). In the proglacial streams at Pangong Tso, the streambed was relatively classified into several late stages of streambed evolution. In these study areas, the basal tills underneath the streambeds were
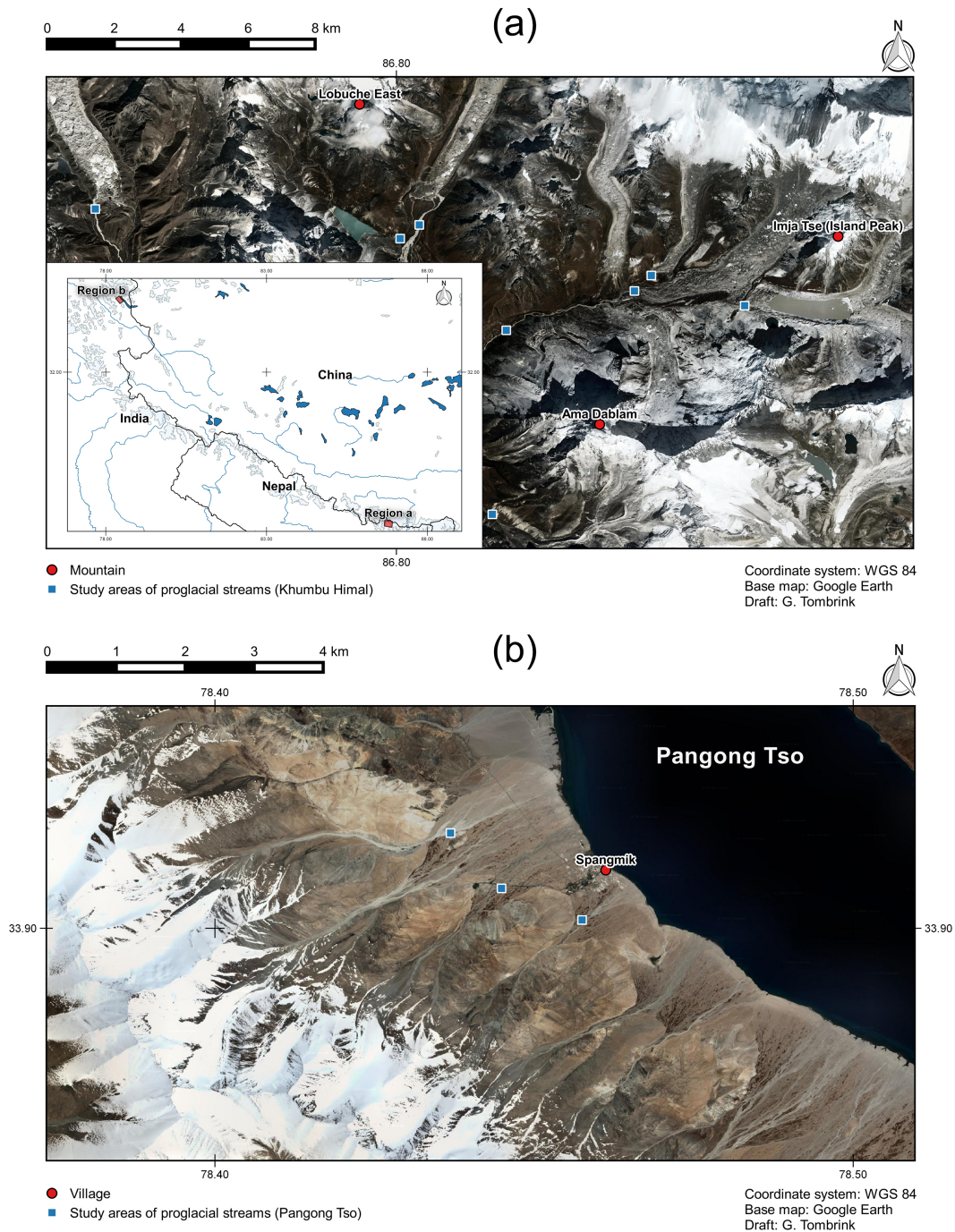
Figure 1. Map of the study areas in Khumbu Himal **(a)** and Pangong Tso **(b)**.

deposited during the Sirkung glacier (IV) to the Nauri glacier stages (V) (glacial stages according to Kuhle, 2013). Step-pool sequences were mapped much further downstream of the channel-reach morphologies in the Khumbu Himal. Thus, a relative chronology of the streambeds was clearly ascertained.

Mesoanalysis. At least four terraces were distinguished in the upper proglacial catchment areas in the Khumbu Himal.

Their number increased up to five (Imja Khola main stream) and six (lower Nare Drangka stream) further downstream. The lowermost terrace orders (one to four) were attributed to recent and historical glacier stages, including their meltdown phases. The higher terrace orders (five to six) were attributed to historical glacier stages, including meltdown phases during the Holocene (glacial stages according to Kuhle, 2013). However, these higher terraces may be influenced by vari-
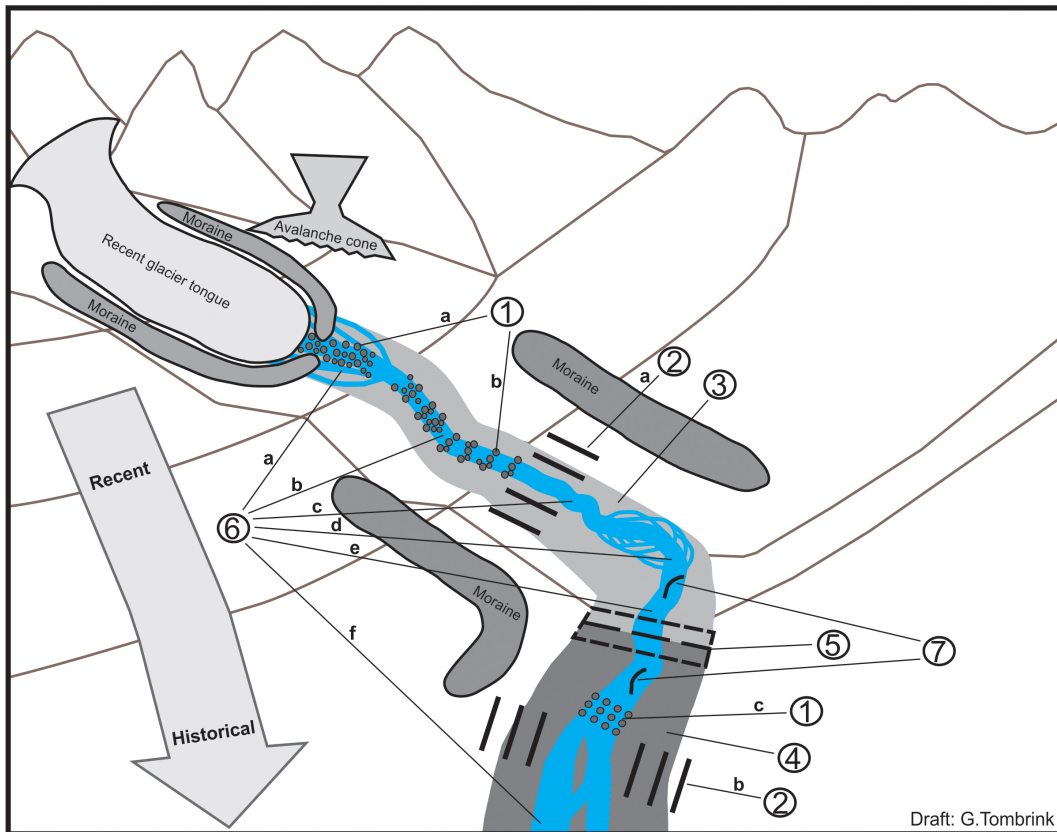
Figure 2. Characteristics of glaciofluvial and fluvial landforms in the glacier forefields of the Himalayas. 1: Horizontal–vertical, chronological sequence of (a) cascades and their (b) stages of evolution to (c) step-pool streambeds. 2: Glaciofluvial terrace sequences of (a) four terraces and (b) up to six or more terraces. 3: Upstream-located recent sandurs. 4: Downstream-located historical sandurs. 5: Vertically nested recent and historical sandurs. 6: Horizontal–vertical proglacial stream chronology comprising (a) braided rivers, partly nested with small-scale streams, (b) high-gradient straight streams, (c) low-gradient small-scale meander forms, (d) pronounced braided rivers, (e) large-scale meandering, and (f) large-scale vegetation-stabilized meandering forms and anabranching rivers. 7: Large-scale convex shapes in an overall concave longitudinal profile.

ous time-dependent factors and may therefore appear morphologically altered. In the study area near the Pangong Tso Lake, a maximum of four terrace orders was identified downstream. The comparable low number of terraces can be explained by the difference in climate and associated glacier oscillations between the study areas.

The sandurs also reflect the chronology of historical and recent landforms. In the investigated proglacial streams, sandurs formed a vertical sequence in wide valleys and a horizontal–vertical sequence in narrow valleys. However, due to sediment rearrangements and inputs, the sandurs could only be used as qualitative indicators of glacier oscillations. Therefore, sandurs need to be systematically reconstructed at different scales to exclude disruptive factors (Schumm and Lichty, 1965). Based on this methodology, it is possible to reconstruct relative chronologies.

Likewise, a sequence of proglacial stream patterns was identified in the study areas. Below the tongue of a glacier, the depositional sequence starts with braided river forms.

The landforms can be divided into high-gradient straight streams and low-gradient small-scale meander forms. Further downstream, pronounced braided rivers can be found in low-gradient streams of the sandur area. These landforms are followed by large-scale meandering stream patterns showing the same stream gradient. At considerable distances further downstream, large-scale vegetation-stabilized meandering forms and anabranching rivers characterize the proglacial river landscape in low-gradient streams. This sequence of proglacial streams can also be found in other high mountain areas, as illustrated by photographs of glacier forefields, e.g., by Röthlisberger (1986) and Winkler (2009).

Macroanalysis. Analysis of the longitudinal profiles of the proglacial streams allowed for the detection of local convex forms within an overall concave longitudinal stream profile of the proglacial streams. These convex shapes – some of these are aligned in steps – were created by sedimentation during past glacier fluctuations and can therefore be attributed to moraine stages. Subsequent erosion and accumu-

lation processes influence the formation and rearrangement of these shapes in the longitudinal proglacial stream profile.

All of the morphological forms described above proved suitable to characterize the glaciofluvial and fluvial sequence of landforms in the glacier forefields of the Himalayas (Fig. 2). In summary, the aim of this work to develop a tool for establishing relative chronologies of glacier fluctuations was achieved through the detailed geomorphological analysis at the micro-, meso-, and macroscale that was carried out in this study. This new tool complements the conventional glacial indicators found in the Himalayas (Kuhle, 1990). It can be used to locate glacier forefields and distinguish different glacial stages in high mountain areas of the Himalayas, where conventional indicators are not well preserved. In addition, the geomorphological indicators used here can serve to compare the intensity of glacier-melting processes. In this way, they also allow for the detection of climatic changes in the proglacial streams of the high mountain areas under investigation. Thus, the outcomes of this study contribute to the understanding of streams in the Himalayas, which also has practical implications, as changes in their total runoff (Tombrink, 2017) may affect landscapes and irrigation systems.

References

Kuhle, M.: The Probability of Proof in Geomorphology – an Example of the Application of Information Theory to a new Kind of Glacigenetic Morphological Type, the Ice-Marginal Ramp (Bortensander), GeoJ., 21.3, 195–222, 1990.

Kuhle, M.: The maximum Ice Age (Würmian, Last Ice Age, LGM) glaciation of the Himalaya – a glaciogeomorphological investigation of glacier trim-lines, ice thicknesses and lowest former ice margin positions in the Mt. Everest–Makalu–Cho Oyu massifs (Khumbu and Khumbakarna Himal) including informations on late-glacial, neoglacial, and historical glacier stages, their snow-line depressions and ages, GeoJ., 62, 193–650, 2005.

Kuhle, M.: The Uplift of High Asia above the Snowline and its Glaciation as an Albedo-Dependent Cause of the Quaternary Ice Ages, Earth sciences in the 21st Century, Nova science publ., New York, USA, 2013.

Montgomery, D. R. and Buffington, J. M.: Channel-reach morphology in mountain drainage basins, Geol. Soc. Am. Bull., 109, 596–611, 1997.

Racoviteanu, A. and Bajracharya, S.: GLIMS Glacier Database, Boulder, CO, USA, National Snow and Ice Data Center, https://doi.org/10.7265/N5V98602, 2008.

Röthlisberger, F.: 10 000 Jahre Gletschergeschichte der Erde: Ein Vergleich zwischen Nord- und Südhemisphäre Alpen, Skandinavien, Himalaya, Alaska, Südamerika, Neuseeland, Sauerländer, Aarau, Switzerland, 1986.

Schumm, S. A.: To interpret the earth: Ten ways to be wrong, Cambridge Univ. Press, Cambridge, UK, 1991.

Schumm, S. A. and Lichty, R. W.: Time, Space, and Causality in Geomorphology, Am. J. Sci., 263, 110–119, 1965.

Tombrink, G.: Flood events and their effects in a Himalayan mountain river: Geomorphological examples from the Buri Gandaki Valley, Nepal, J. Mt. Sci., 14, 1303–1316, 2017.

Winkler, S.: Gletscher und ihre Landschaften: Eine illustrierte Einführung, Wiss. Buchges., Darmstadt, Germany, 2009.

E&G Open Access Quaternary Science Journal

Glacial history of the upper Drac Blanc catchment (Écrins massif, French Alps)

Felix Martin Hofmann

Department of Geology, Lund University, Sölvegatan 12, 22362 Lund, Sweden

Supervisors: Helena Alexanderson (Lund University) & Philippe Schoeneich (Université Grenoble-Alpes)

Numerous studies dealing with Late Glacial and early Holocene glacier variability have been carried out in the Austrian and Swiss Alps. The advent of cosmic ray exposure (CRE) dating, based on the concentration of in situ produced cosmogenic nuclides in the quartz fraction of boulders on moraines, has, since then, enabled the chronology of glacier fluctuations in these regions during this period to be refined (see references in Ivy-Ochs, 2015). However, this holds partly true for the French (Western) Alps. The few available CRE ages from boulders on moraines in this region (e.g. Chenet et al., 2016) indicate glacier fluctuations concomitant with the cooling at 12.7 ka b2k (kiloyears before ∼ 2000 CE; Heiri et al., 2014). Further glacier fluctuations in the French Alps occurred until the early Holocene (e.g. Le Roy, 2012), thereby suggesting a similar pattern as in the Austrian and Swiss Alps where glaciers shaped moraines during the Egesen and Kartell stadials (Ivy-Ochs, 2015). However, precise palaeogeographic and palaeoclimatic reconstructions require additional chronological constraints on Late Glacial and early Holocene glacier variability in the French Alps. The latter application of glacier records is of particular interest, as the lack of biological proxies from the Late Glacial hampers detailed reconstructions of climatic variations in this region.

Considering that a sequence of well-preserved moraines in the Rougnoux valley in the southern Écrins massif (Fig. 1; Di

Costanzo and Hofmann, 2016) has been assigned to glacier fluctuations at the end of the Late Glacial or in the early Holocene, this set of moraines and prominent moraines at two nearby locations (Fig. 1) were considered suitable targets to obtain additional chronological constraints on the related glacier variability. Hence, this study not only contributes to a better understanding of the chronology of Late Glacial and early Holocene glacier fluctuations in the French Alps but also provides a solid base for future palaeogeographic and palaeoclimatic reconstructions.

Based on freely available aerial photographs taken by the French National Institute of Geographic and Forest Information (IGN), an orthophoto and a high-resolution digital elevation model (DEM) were established using the structure-from-motion technique. The use of a combination of a DEM-based hillshade, the orthophoto and photographs as well as extensive field surveys enabled the establishment of geomorphological maps of the study area using the mapping system of Lausanne University. The identification of pre-Little Ice Age (LIA) moraines in the study area was based on a two-fold approach. Firstly, it was assessed whether the ridges in question are characterised by an asymmetric shape and a steeper proximal side. Secondly, it was verified whether the landforms are composed of a diamicton, if outcrops were available. All moraines, even small ones, which are indicative for the extent of the two palaeoglaciers in the study area, were then assigned to former positions of the glaciers based on their relative position in the field to finally establish a morphostratigraphy.
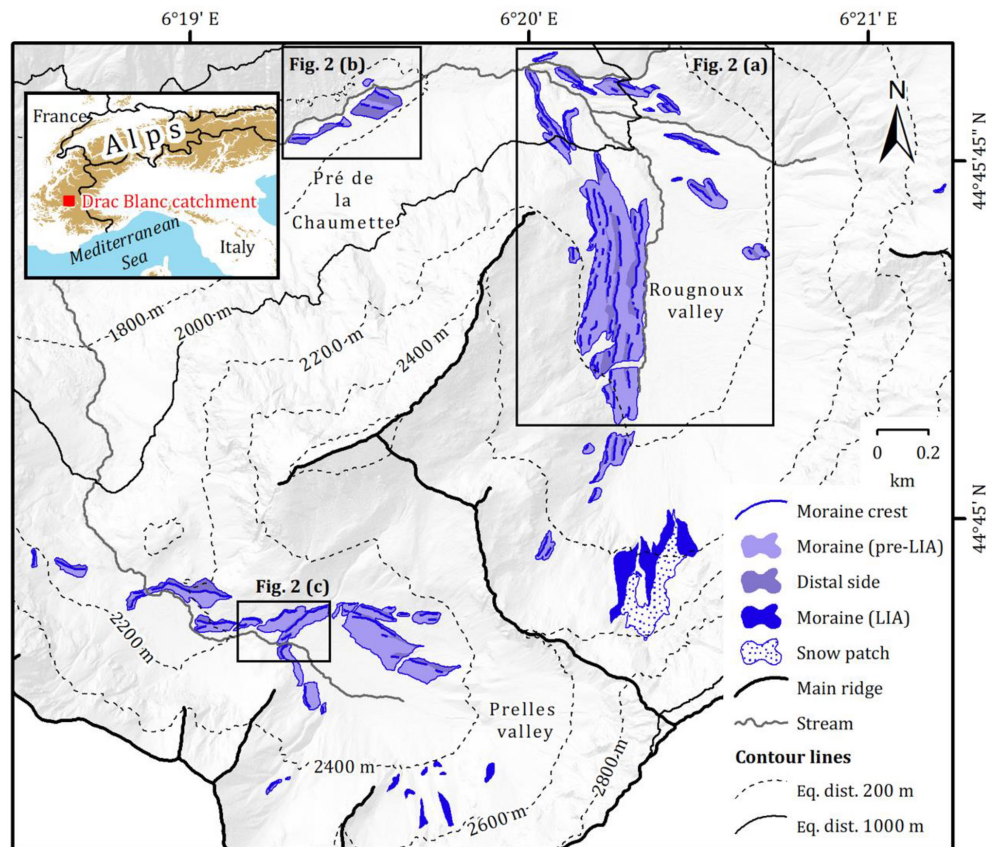
Date: 3.10.2018; Author: Felix Martin Hofmann; Data source: IGN 2012; Coordinate system: WGS 1984 UTM zone 32N

Figure 1. Moraines in the upper Drac Blanc catchment.

Due to the lack of organic material in the moraines suitable for radiocarbon dating, the measurement of the concentration of the in situ accumulated cosmogenic nuclide ^{10}Be in the quartz fraction of samples from boulders on selected moraines was deemed the only solution to overcome this limitation and to be able to constrain their ages. The ^{10}Be production rate of Young et al. (2013) was chosen for the determination of the CRE ages. Considering that the CRE ages with a snow shielding correction are believed to be most realistic, they are presented below. Given that, in most cases, three CRE ages were obtained from each moraine, landform ages were computed (Fig. 2). First, reduced χ^2 statistics was applied. If reduced χ^2 turned out to be roughly 1, the average CRE age was chosen as landform age to eliminate the scatter due to analytical uncertainties, whereas the oldest CRE age from a moraine was considered the landform age if reduced χ^2 was significantly larger than 1, as most sampled boulders were small, thereby increasing the likelihood for post-depositional exhumation. The computed CRE ages were compared with previously published ^{10}Be CRE ages from boulders on moraines at key sites in the Alps, recalculated according to a recent ^{10}Be production rate (Young et al., 2013), and data from palaeoclimatic proxies other than glaciers.

Thirdly, DEMs of the palaeoglaciers during the deposition of their outermost LIA moraines and the further down-valley moraines were established using the GlaRe ArcGIS toolbox (Pellitero et al., 2016). Generally, the basal shear stress as primary input of the GlaRe toolbox was adjusted to fit the DEMs of the palaeoglaciers to the preserved moraines. A second ArcGIS toolbox enabled the equilibrium line altitudes (ELAs) of the palaeoglaciers to be determined, whereby the most common accumulation area ratio of 0.67 was assumed. This ratio is believed to be appropriate for Alpine glaciers being in equilibrium with the climate (Gross et al., 1977). Lastly, ELA depressions with respect to the end of the LIA were computed to allow for stratigraphical correlations between sampled and not-sampled moraines.

In total, 10 and 8 pre-LIA positions of the Rougnoux and Prelles palaeoglaciers were identified, respectively. An enigmatic ^{10}Be CRE age of a boulder on the lowermost sampled moraine (PdC M10-11) indicates that it may have stabilised after a period of stable ice margins at or before 17.2 ± 1.8 ka b2k (Fig. 2). Given its location at the confluence of two valleys, the moraine was probably deposited at the common margin of the glaciers from both valleys. During this potential event, the ELA of the palaeoglacier from
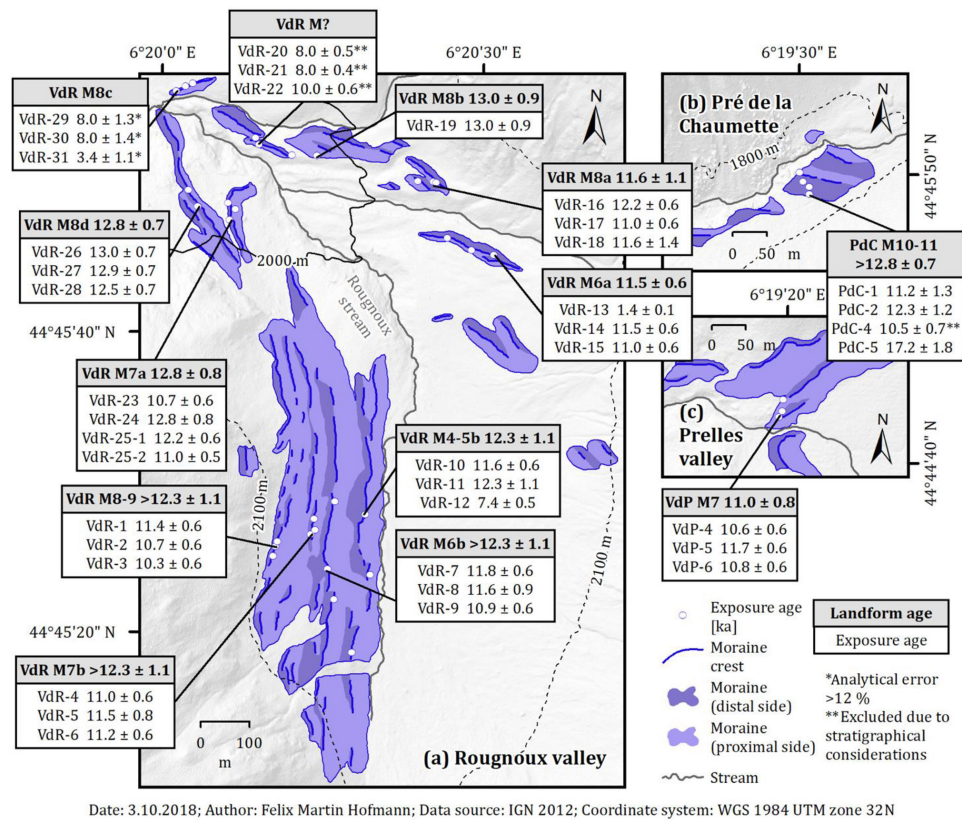
Figure 2. ^{10}Be CRE ages from boulders on moraines in the **(a)** Rougnoux valley, **(b)** at Pré de la Chaumette and in the **(c)** Prelles valley. See Fig. 1 for the location.

the Rougnoux valley was depressed by about 210 m relative to the LIA ELA, whereas the ELA of the formerly confluent two glaciers from the northern valley must have been situated at a 500–600 m lower elevation relative to the LIA. The moraine was certainly reached, or alternatively re-occupied, by the glacier from the Rougnoux valley slightly at around 12.8 ± 0.7 ka b2k when the ELA was 220 m lower than at the end of the LIA. It can be excluded that the palaeoglaciers from the northern valley reached the frontal moraine during this event, since the required ELA depression of the order of 500–600 m to trigger a re-advance of both glaciers up to the moraine can be considered unrealistically high for a glacial re-advance at around 12.8 ± 0.7 ka b2k. Considering that the required ELA lowering (ca. 200 m) for an advance of the Prelles palaeoglacier up to its lowermost pre-LIA moraine matches well the ELA depression during the deposition of the latter moraine, both landforms can probably be correlated.

The ^{10}Be CRE ages from the Rougnoux valley (Fig. 2) provide evidence for multiple periods of stable ice margins at the end of the Late Glacial and potentially in the earliest Holocene (Fig. 2). These events were associated with ELA depressions between 220 and 160 m. One of the youngest periods of stable ice margins in the Prelles valley that was

associated with an ELA depression of 150 m relative to the LIA occurred at or before 11.0 ± 0.8 ka b2k (Fig. 1).

Considering that the inferred age of the event during which the lowermost moraine was last reached by a glacier matches the cooling at around 12.7 ka b2k registered in regional and hemispheric palaeoclimatic archives, it can be inferred that the PdC M10-11 moraine and the outermost arcuate pre-LIA moraine in the Prelles valley were deposited during a glacial re-advance concomitant with this climatic downturn. The new ^{10}Be CRE ages agree well with previously published ^{10}Be CRE ages from moraines at different sites in the Central and Eastern Alps that have been assigned to the Egesen and Kartell stadials (e.g. Moran et al., 2016), thereby reinforcing the hypothesis of a common climatic forcing of the corresponding glacier fluctuations. Uncertainties associated with CRE dating as well as an asynchronous response of the palaeoglaciers to the same climatic signal due to local factors, such as topography, are invoked as explanations for the slight variations in the ^{10}Be CRE ages.

Overall, this study improves the knowledge about the chronology of Late Glacial and early Holocene glacier fluctuations in the Écrins massif, as the youngest periods of stable ice margins have been dated for the first time. This study highlights that a holistic approach relying on converg-

ing lines of evidence, such as geomorphological mapping, CRE dating and ELA reconstructions, should be applied to decipher the glacial history of a region with the greatest possible accuracy.

References

Chenet, M., Brunstein, D., Jomelli, V., Roussel, E., Rinterknecht, V., Mokadem, F., Biette, M., Robert, V., Léanni, L., and ASTER Team: ^{10}Be cosmic-ray exposure dating of moraines and rock avalanches in the Upper Romanche valley (French Alps): Evidence of two glacial advances during the Late Glacial/Holocene transition, Quaternary Sci. Rev., 148, 209–221, https://doi.org/10.1016/j.quascirev.2016.07.025, 2016.

Di Costanzo, H. and Hofmann, F. M.: Le retrait du glacier du Drac Blanc (massif des Écrins, Alpes françaises), Méditerranée, Revue géographique des pays méditerranéens, Paléo-environnements, géoarchéologie, géohistoire, 5, https://doi.org/10.15496/publikation-13788, 2016.

Gross, G., Kerschner, H., and Patzelt, G.: Methodische Untersuchungen über die Schneegrenze in alpinen Gletschergebieten, Zeitschrift für Gletscherkunde und Glazialgeologie, 12, 223–251, 1977.

Heiri, O., Koinig, K. A., Sp.tl, C., Barrett, S., Brauer, A., Drescher-Schneider, R., Gaar, D., Ivy-Ochs, S., Kerschner, H., Luetscher, M., Moran, A., Nicolussi, K., Preusser, F., Schmidt, R., Schoeneich, P., Schwörer, C., Sprafke, T., Terhorst, B., and Tinner, W.: Palaeoclimate records 60–8 ka in the Austrian and Swiss Alps and their forelands, Quaternary Sci. Rev., 106, 186–205, https://doi.org/10.1016/j.quascirev.2014.05.021, 2014.

Ivy-Ochs, S.: Glacier variations in the European Alps at the end of the last glaciation, Cuadernos de investigación geográfica, 41, 295–315, https://doi.org/10.18172/cig.2750, 2015.

Le Roy, M.: Reconstitution des fluctuations glaciaires holocènes dans les Alpes occidentales – Apports de la dendrochronologie et de la datation par isotopes cosmogéniques produits *in situ*, PhD thesis, Grenoble University, Grenoble, 363 pp., 2012.

Moran, A. P., Ivy-Ochs, S., Schuh, M., Christl, M., and Kerschner, H.: Evidence of central Alpine glacier advances during the Younger Dryas–early Holocene transition period, Boreas, 45, 398–410, https://doi.org/10.1111/bor.12170, 2016.

Pellitero, R., Rea, B. R., Spagnolo, M., Bakke, J., Ivy-Ochs, S., Frew, C. R., Hughes, P., Ribolini, A., Lukas, S., and Renssen, H.: GlaRe, a GIS tool to reconstruct the 3D surface of palaeoglaciers, Comput. Geosci., 94, 77–85, https://doi.org/10.1016/j.cageo.2016.06.008, 2016.

Young, N. E., Schaefer, J. M., Briner, J. P., and Goehring, B. M.: A ^{10}Be production-rate calibration for the Arctic, J. Quaternary Sci., 28, 515–526, https://doi.org/10.1002/jqs.2642, 2013.

Open Access

E&G Quaternary Science Journal

Research article

New data from the Middle Palaeolithic Cotencher cave (Swiss Jura): site formation, environment, and chronology

Judit Deák[1], **Frank Preusser**[2], **Marie-Isabelle Cattin**[1], **Jean-Christophe Castel**[3], **and François-Xavier Chauvière**[1]

[1]Office du patrimoine et d'archéologie Neuchâtel (OPAN), section Archéologie, Hauterive, Switzerland
[2]Institute of Earth and Environmental Sciences, University of Freiburg, Freiburg, Germany
[3]Muséum d'histoire naturelle Genève, Département d'archéozoologie, Genève, Switzerland

Correspondence: Judit Deák (judit.deak@ne.ch)

How to cite: Deák, J., Preusser, F., Cattin, M.-I., Castel, J.-C., and Chauvière, F.-X.: New data from the Middle Palaeolithic Cotencher cave (Swiss Jura): site formation, environment, and chronology, E&G Quaternary Sci. J., 67, 41–72, https://doi.org/10.5194/egqsj-67-41-2019, 2019.

Abstract: Cotencher cave is one of the oldest Palaeolithic sites of Switzerland and is known for its rich faunal and Mousterian artefacts, the latter suggesting one or several passages of Neanderthal hunter–gatherer tribes. This interdisciplinary study summarises novel data concerning site formation processes and anthropic attendance of the site. While the lithic artefacts indicate tool production at the site, the faunal remains do not yield any evidence of a link to human occupation. The sedimentary sequence permits us to unravel several important environmental changes that occurred during the Late Pleistocene. The presence of a local glacier around 70 ka (Marine Isotope Stage, MIS 4) is revealed followed by ice-free conditions characterised by alternating soil formation processes and landscape destabilisation during MIS 3. Solifluction processes suggesting recurrent frozen ground were responsible for the displacements of part of the artefacts and faunal remains. Evidence of local glacier development around 36 ka is related to the particular geomorphological conditions of the studied region and shed new light on the complexity of glacier dynamics. The recognition and dating of recurrent hostile glacier landscapes might contribute to understanding the reasons for the Middle and Upper Palaeolithic attendance hiatuses known in the studied region.

Kurzfassung: Die Cotencher-Höhle ist eine der ältesten paläolithischen Fundstätten der Schweiz und bekannt für ihre reiche Fauna und mousterischen Artefakte. Letztere weisen darauf hin, dass Neanderthaler-Sippen aus Jägern und Sammlern die Region einmal oder mehrere Male durchstreift haben könnten. Diese interdisziplinäre Studie fasst neue Daten zu Standortbildungsprozessen und zu Aufenthalten von Menschen zusammen. Während die Steinartefakte eine Werkzeugproduktion an der Fundstelle anzeigen, geben die Faunenreste keine Hinweise auf eine Anwesenheit von Menschen. Die Sedimentabfolge erlaubt es, einige wichtige Umweltveränderungen während des späten Pleistozäns zu entschlüsseln. Die Präsenz eines lokalen Gletschers vor etwa 70 ka (Marines Isotopen Stadium, MIS 4) ist erkennbar, gefolgt von eisfreien Bedingungen, die durch sich abwechselnde Bodenbildungsprozesse und Landschaftsdestabilisierung während des MIS 3 charakterisiert sind. Solifluktionsprozesse, die auf wiederkehrend gefrorene Böden schließen lassen, waren verantwortlich für die Verlagerung eines Teils der Artefakte und Faunenreste. Die Bildung eines Lokalgletschers vor etwa 36 ka

ist bedingt durch die speziellen geomorphologischen Gegebenheiten der untersuchten Region und geben neue Befunde über die Komplexität der Gletscherdynamik. Die Identifikation wiederkehrender lebensfeindlicher glazialer Landschaften könnte einen Beitrag dazu leisten, die phasenweise Abwesenheit von Menschen im Untersuchungsgebiet während des Mittel- und Oberpaläolithikums zu erklären.

1 Introduction

While Alpine glaciers extended several times onto the Swiss Plateau during the Pleistocene (Ivy-Ochs et al., 2008; Preusser et al., 2011), the Jura Mountains were also recurrently covered by local and sometimes Alpine ice bodies (Campy, 1992; Graf et al., 2007; Buoncristiani and Campy, 2011). During the Last Glacial Maximum (LGM), the ice cover reached up to 1200 m in the western part of the Swiss Plateau (Campy, 1992; Bini et al., 2009; Cupillard et al., 2015) and most sediments and soils previously covering the landscape as well as their archaeological content were removed by glacial erosion. As a consequence, Lower and Middle Palaeolithic sites are scarce in the region and the Middle Palaeolithic is documented at only about 20 open air, rock shelter, and cave sites (Le Tensorer, 1993, 1998; Tillet, 2001; Crotti, 2008; Detrey, 2010, 2013). Among these, Cotencher cave is the first Middle Palaeolithic site ever discovered in the Jura Mountains of Switzerland (Egloff, 1989).

Only a few records of Pleistocene environmental change are available from the Swiss Alpine foreland and in the Jura Mountains for the time before the LGM (Ivy-Ochs et al., 2008; Preusser et al., 2011; Heiri et al., 2014; Cupillard et al., 2015). Cave and rock shelter deposits have the potential to provide valuable additional information in this context due to their relatively protected setting compared to potentially more easily eroding open-air sites. These landscape elements were also places of human activity, and geoarchaeological studies aim at understanding the processes behind site formation (Goldberg and Macphail, 2006). Cave deposits are subdivided into clastic and chemical sediments (Goldberg and Macphail, 2006; White, 2007). The clastic sediments originate from either inside (autochthonous) or outside (allochthonous) of the cave and comprise weathering detritus, rock breakdown, entrance talus, infiltrates, and fluvial, glacial, and aeolian deposits. In addition, biogenic debris and anthropogenic layers may occur. Chemical deposits are considered to be in situ formed (autochthonous) and include speleothems, evaporates, ice, and phosphate and nitrate minerals originating from guano and bone alteration. Thus, caves and rock shelters are locations of numerous simultaneous or superposed depositional processes. Understanding these processes and their environmental causes is particularly challenging and often performed within interdisciplinary investigations (e.g. Goldberg et al., 2003; Angelucci et al., 2013; Boschian et al., 2017).

The most common approach to determine the age of cave deposits is radiocarbon dating of organic remains, in particular charcoal and bones, incorporated into sediments (Hajdas, 2008; Taylor and Bar-Yosef, 2014). Usually, this method is considered reliable despite potential problems related to reworking that may lead to radiocarbon ages older than the time of sediment deposition (e.g. Lee et al., 2011). Furthermore, radiocarbon ages $\geq 30\,000$ ^{14}C yr tend to underestimate the real age, and ages beyond $50\,000$ ^{14}C yr are generally not considered reliable (e.g. Hajdas et al., 2007; Higham, 2015). Other approaches include the dating of speleothem formation with the U-series methodology, in particular when applied to flow stones (St Pierre et al., 2009). An important improvement was the introduction of luminescence dating to date cave deposits (Feathers, 1996; Roberts, 1997; Roberts et al., 2015). Using optical stimulation, this approach allows us to directly date the deposition age of quartz and feldspar grains from sediments found in caves. However, the method is also affected by several potential problems that need careful consideration (Jacobs and Roberts, 2008). First, the luminescence signal might not have been fully reset prior to deposition (partial bleaching), which will lead to overestimation of ages. As grains have individual light exposure histories, measuring very few or even individual grains allows the detection of and correction for this effect using statistical approaches (e.g. Duller, 2008). Indication for partial bleaching is a wide-spread and positively skewed distribution, in combination with high overdispersion values (e.g. Rittenour, 2008). Second, while quartz is mainly the preferred mineral in luminescence dating, quartz from certain regions including the Alps is problematic with regard to its signal properties (e.g. Preusser et al., 2006). At the same time the luminescence signal in feldspar can be affected by unstable signal components that may lead to age underestimation. While the signal loss can be monitored in the laboratory and approaches have been suggested to correct for it (Huntley and Lamothe, 2001), these procedures have been shown to often be problematic (e.g. Wallinga et al., 2007; Lowick et al., 2012). An alternative might be to use more stable signal components from feldspar (Thomsen et al., 2008), but at the cost of a slower resetting by daylight (Buylaert et al., 2012), which might be problematic in settings with short-distance transport. Third, reconstructing annual dose rate can be complex in cave settings (e.g. Guérin et al., 2017) and radioactive disequilibrium in the uranium decay chain may occur (e.g. Olley et al., 1997).

Sediments of Cotencher cave have delivered rich faunal assemblages and more than 400 artefacts that were found in two distinct stratigraphical units. Already Dubois and Stehlin (1932/1933) discussed the relationship between the sedimentary sequence and past glaciations. More recent geoarchaeological studies define and characterise several stratigraphic units positioned between the Eemian and the Holocene (Adatte et al., 1991; Rentzel, 1990). The dating of the sequence is based on techno-typological elements, variation in the mineralogy, and a few charcoal radiocarbon ages. The latter, originating from two individual archaeological find layers, are at the upper dating limit and suggest a minimum age of 40 ka for the lower part of the site. The youngest find layer was interpreted as being deposited during the Late Pleistocene (Marine Isotope Stage – MIS 3, cited as Interpleniglacial in Adatte et al., 1991). Based on clay mineralogy, the oldest archaeological layer is interpreted as last interglacial soil redeposited during the early Late Pleistocene (Adatte et al., 1991). According to the most favoured hypothesis the lithic artefacts represent Mousterian Charentian of oriental Quina type originating from a single archaeological level situated originally at the entrance of the cave and redeposited during the two time intervals mentioned above (Bernard-Guelle, 2004).

As part of a regional landscape and natural resource coordination plan (Chauvière et al., 2018b, c; Deák, 2018a, b) two sections close to the entrance of the cavity were investigated. Establishing a more precise and detailed chronology of the sedimentary sequence was the main target, as the radiometric and archaeologic dating available so far were imprecise and incomplete. The present study focuses on the pre-Holocene sedimentary sequence hosting numerous Pleistocene faunal remains and Palaeolithic artefacts. We present the results of an interdisciplinary approach that provides not only a more detailed chronological framework but also completes our knowledge concerning the environmental changes recorded in the sediment fill. Furthermore, the archaeological finds are discussed in the larger context of Middle Palaeolithic occupations in Switzerland and neighbouring France.

2   Research context

2.1   Regional setting

Cotencher cave is located in the Areuse canyon, which is part of the Travers Valley (Canton Neuchâtel, Switzerland; Fig. 1). The entrance is at 660 m in altitude and situated 140 m above the present-day valley bottom. The cave is about 18 m long and consists of a 7 m long and 13 m wide rock shelter as well as an 11 m long underground gallery (Gigon, 1976; Fig. 2a and b). There is no evidence of recent or past karst springs or underground river activity. The cave is formed in Upper Jurassic limestones (Méia and Becker, 1976), more precisely at the interface between Kimmeridgian and Thitonian (Portlandian) strata (Dubois and Stehlin,

1932/1933). Late Quaternary undifferentiated glacial and glaciofluvial deposits interpreted as being of penultimate glacial (Rissian) age are present discontinuously on the neighbouring slopes (Méia and Becker, 1976); sediments attributed to the last interglacial and early phases of the last glacial cycle are apparently absent in the valley (Pasquier et al., 2013). Prior to previous archaeological excavations the cave was almost fully filled with sediment and one could enter it only by crawling (Gigon, 1976; Fig. 2b). Indeed, the maximum height of the internal gallery is about 5 m (Gigon, 1976, Miéville, 2005), where the sedimentary fill reached thicknesses of up to 4 m.

2.2   Research history

Cotencher cave has been mentioned as early as 1523 CE (Miéville, 2005), but the first excavations inside the cavity only date back to the second half of the 19th century (Otz, 1867; Desor, 1868, 1872). The latter permitted researchers to unravel the presence of old bones mainly attributed to cave bears (*Ursus spelaeus*). A high variety of faunal remains were confirmed by subsequent excavations that took place in 1915 and between 1916 and 1918 (Stehlin and Dubois, 1916; Dubois, 1917, 1918, 1920; Dubois and Stehlin, 1932/1933). The 1916–1918 excavations have a benchmark value and the results published in a monography (Dubois and Stehlin, 1932/1933) were the first to describe the complete stratigraphic sequence and defined (from youngest to oldest) the following stratigraphic units: (i) cryoclastic sediment (*éboulis*) containing Holocene archaeological remains (Dubois and Stehlin, 1932/1933; Vouga, 1943; De Rougemont, 1982); (ii) sterile white clay (*argiles blanches*); (iii) "gravelly layer" (*couche à galets*); (iv) "brown layer" (*couche brune*); and (v) a yellow basal clay (*argile du fond*). Detailed investigation of the sedimentary sequence and study of the various finds permitted scholars to recognise the changing environmental conditions recorded in the cave. Thousands of animal bones (belonging to about 60 species and sometimes burnt), dismantled fire places, and more than 400 lithic Mousterian artefacts attest to the presence of Neanderthal people during the time when the gravelly layer and the brown layer were formed (Dubois and Stehlin, 1932/1933; Egloff, 1976; Le Tensorer, 1998). This rich archaeological assemblage was further completed by illegal digs outside the cave in the 1950s. In 1964, a mandible fragment attributed to a ca. 40-year-old Neanderthal woman was discovered in the brown layer in the innermost part of the cave (Moll, 1971, 1974, 1977; Bay, 1981).

The first sedimentological analyses were performed in the 1950s (Schmid, 1958). Between 1988 and 1990, new excavations were accompanied by detailed sedimentological and mineralogical studies, permitting researchers to complete the understanding of the stratigraphic and environmental history (Fig. 3) (Rentzel, 1990, 1992; Adatte et al., 1991). According to these data the sedimentary record of the cave in-
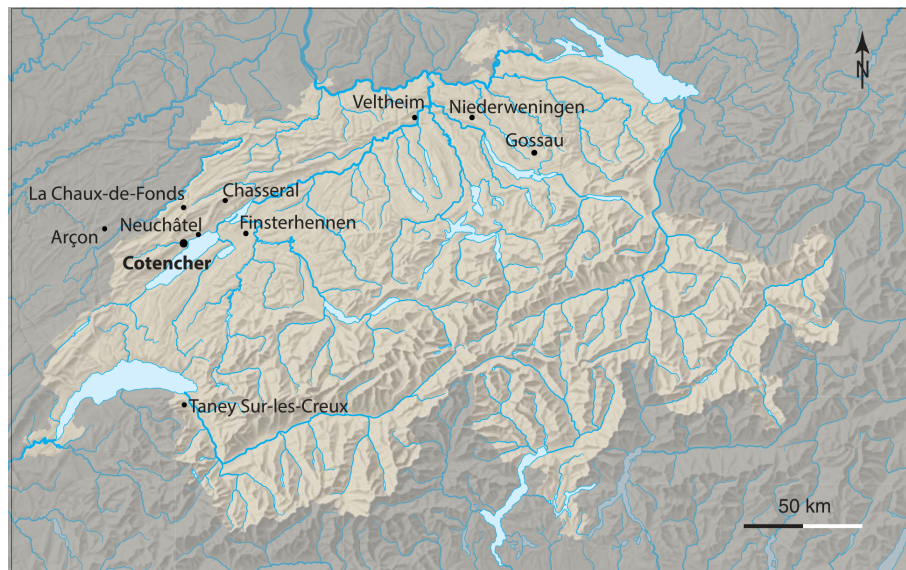
Figure 1. Location of Cotencher cave and of mentioned sites.
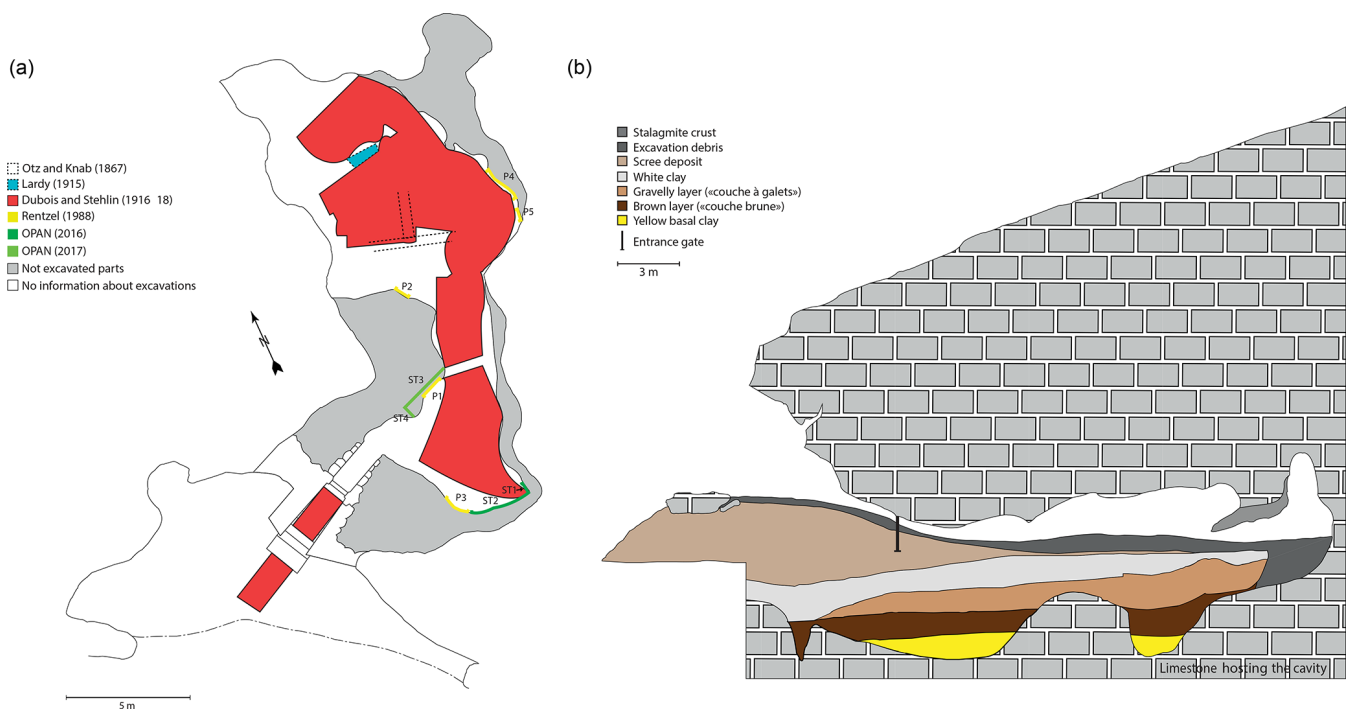
Figure 2. Map of the cavity with the localisation of the various interventions and sections mentioned in this paper **(a)** and longitudinal section of it based on Dubois and Stehlin (1932/1933) **(b)**.

cludes (i) Holocene cryoclastic deposit (Layer I), (ii) two post-glacial finely textured layers (II and III), (iii) an Interpleniglacial gravelly layer (V), and (iv) sediment (brown layer or VI) interpreted as reworked Eemian soil. Three charcoal fragments found in the archaeological layers (two in the gravelly layer, one in the brown layer) gave radiocarbon ages of around 40 000 ^{14}C yr BP, considered minimum ages.

These results together with palaeontological and palynological data have been included in the synthetic work dedicated to the Palaeolithic in Switzerland by Le Tensorer (1998), who attributed the lowest archaeological find layer to the final part of the Odderade interstadial, while the gravelly layer was correlated with the Dürnten (Hengelo) phase.
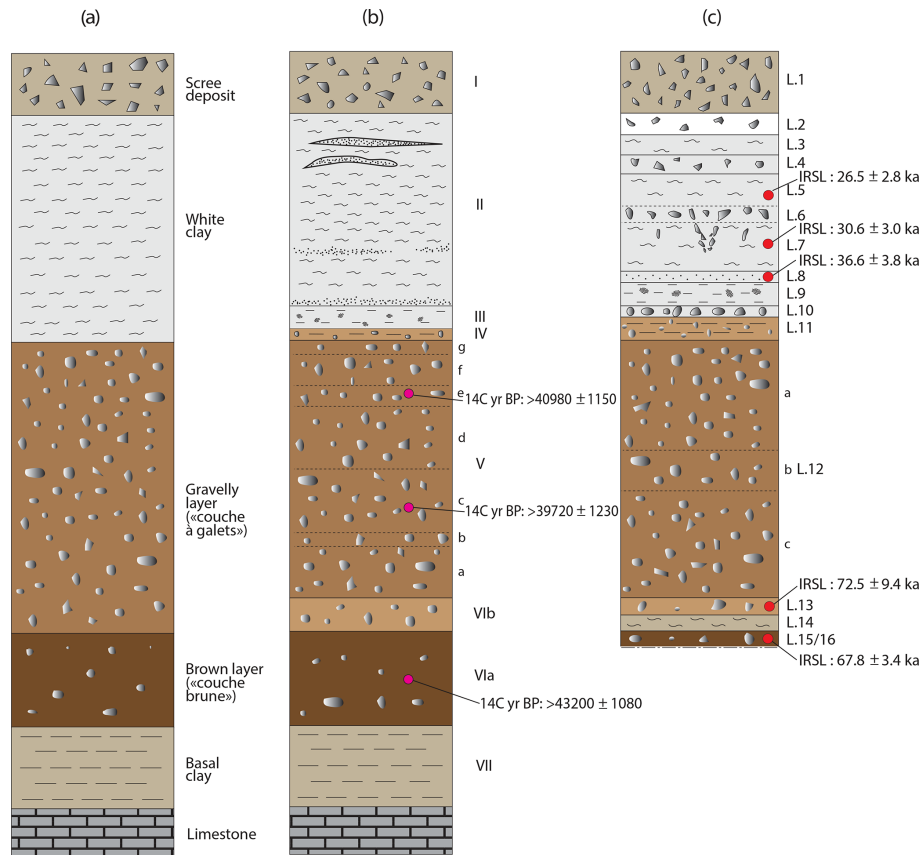
Figure 3. Synthetic overview of the stratigraphy of the site as recorded by the various studies. **(a)** Dubois and Stehlin excavations (Dubois and Stehlin, 1932/1933); **(b)** study by Renzel 1988 (Rentzel, 1990); **(c)** 2016 intervention presented in this paper and the dates obtained. Legend: on the right side of the columns the stratigraphic nomenclature used by the various authors is indicated.

2.3 Climate and environment

Present-day climate in the study region is characterised by mean annual temperatures of 9.4 °C (Neuchâtel 485 m a.s.l.) and 6.3–6.4 °C (La Chaux-de-Fonds 1018 m a.s.l.; Chaumont 1136 m a.s.l.). For the same stations mean annual precipitations are 987, 1468 and 1289 mm (Météosuisse, 2016). The mean annual evaporation for the Neuchâtel station is 573 mm (Météosuisse, 2005); thus on an annual basis leaching conditions prevail.

Reconstruction of the Late Pleistocene terrestrial environmental history of the northern Alpine foreland and the Jura Mountains is based on discontinuously dated evidence from (i) lake pollen records, glacier melt-out and outwash deposits, and a few cave sites – all of them covered by the ice during the LGM, and (ii) some dolina deposits and loess–palaeosol sequences described in localities situated outside of the reach of LGM glaciers (Preusser et al., 2003, 2011; Preusser, 2004; Blant and Deriaz, 2007; Ivy-Ochs et al., 2008; Gaar and Preusser, 2012; Becker et al., 2013; Leesch et al., 2013; Heiri et al., 2014; Bichet et al., 2016). According to Preusser (2004), five rather cool to cold periods (stadials, S1–5) are delimited from warmer phases. The first marked

cooling (S1/MIS 5d) after the last interglacial was possibly accompanied by a first glacier advance into the major alpine valleys, but its extension is not defined. It was followed by a period of rather warm conditions with boreal forest and some deciduous trees. This phase is usually correlated with the Brørup interstadial and MIS 5c. The geographical extension of the S2 glacier advance (MIS 5b) cannot be delimited due to subsequent erosion (Ivy-Ochs et al., 2008). The second interstadial of the Early Würmian (MIS 5a) was again characterised by boreal forest with some temperate taxa. For S3 (equivalent of MIS 4), glacial outwash deposits are documented relatively close to the studied site (Fig. 1), at Finsterhennen (Preusser et al., 2007) and at Arçon (Cupillard et al., 2015; Bichet et al., 2016). For the subsequent period (Middle Würmian, corresponding to MIS 3) a succession of more or less mild interstadials has been recognised at Gossau in the Lake Zürich area (Preusser et al., 2003). Its first phase, the Dürnten Interstadial of Welten (1981), featured open woodland vegetation with pine and spruce and likely dates to about 55 ka (Wegmüller et al., 2002). Sites with faunal remains found both inside and outside the LGM limits indicate open tundra–steppe environment but temporarily with patches of

boreal vegetation (Becker et al., 2013). The site of Nieder-weningen, dating to ca. 45 ka (Hajdas et al., 2007; Preusser and Degering, 2007), has been particularly well investigated, with detailed reconstructions pointing towards open wood-land conditions (Drescher-Schneider et al., 2007) and a rich fauna (Furrer et al., 2007). During the Late Würmian (MIS 2, LGM) all the alpine valleys and the surrounding lowlands were largely covered by ice (Ivy-Ochs et al., 2008) and the northern lobe of the Valais (Rhone) Glacier started to de-posit proglacial sediments at Finsterhennen just after 30 ka (Preusser et al., 2007). In the Jura Mountains local glaciers spread over substantial parts of the landscape (Campy, 1992; Buoncristiani and Campy, 2011). On its eastern flanks, dur-ing the most extensive phase of the LGM, local glaciers were subjugated by the Valais Glacier (Campy, 1992; Pasquier et al., 2013) and Cotencher cave was buried under about 500–600 m of ice (Campy, 1992).

3   Methods

3.1   Excavation and documentation of archaeological finds

Two almost perpendicular sections, situated close to the en-trance of the cave (2.5 and 2 m high, respectively), have been cleaned for this study (Figs. 4 and 5). The sections have been divided into 50 cm large vertical bands and along each band the profiles were successively cleaned by horizontal seg-ments. In the upper parts of the sections, the horizontal clean-ing and sampling segments were 10 cm, while in the lower parts, containing the archaeological find layers, the segments were 5 cm thick. All sediments originating from this cleaning process have been collected to be sieved and analysed. Sam-ples for luminescence dating were taken by forcing metal tubes into the sediment exposure and additional material was taken for high-resolution gamma spectrometry. Undisturbed blocks were taken for thin section preparation and they are used here to estimate porosity. Detailed micromorphological studies are planned for a subsequent phase of this project.

All samples and the lithic and faunal finds discovered during the cleaning process were three-dimensionally posi-tioned. The bulk samples were wet sieved (see below) and all bones and archaeological lithic fragments were carefully collected and documented. The sediments in the lower part of the studied sections are leftovers of former excavations or result from natural collapse of the cave walls. These have been 2 mm dry-sieved in front of the cavity and artefacts were collected. A detailed photographic documentation of the suc-cessive stages of field work was also performed (Fig. 4).

The entire collection of lithic artefacts (457), including the finds of the 2016 excavation, has been re-examined accord-ing to standard procedures. So far, only the bone assemblage of the 1916–1918 excavations has been assessed in detail with the purpose of verification of the identified bone frag-ments and their thorough examination, according the current

standards with regard to the presence or absence of traces of human activity (Castel, 2010; Castel et al., 2017). The bone fragments found during the 2016 intervention will be anal-ysed during a later phase of this project.

3.2   Sedimentology and soil science

Sedimentological and pedological observations were made on both sections to record the morphology, the nature and lateral variability in the soil, and the sediment characteristics. These observations were completed during infrastructure in-stallation works in 2017. Although former studies (Dubois and Stehlin, 1932/1933, Rentzel, 1990) already proposed a nomenclature of the layers (Fig. 3), we observed a more detailed stratigraphy and renumbered layers starting from Layer 1 (L.1) at the upper part of the sequence. In order to assure the representativeness of derived data, samples had a weight between 1.1 and 15 kg, the heavier samples being the gravelly layers. The bulk samples were air-dried, weighed, and subsampled for subsequent analyses. The remains were wet-sieved (8 mm, 4 mm, 2 mm, and 500 µm sieves) in or-der to recover archaeological material and to characterise the quantity and nature of the coarse fraction of the vari-ous layers. The material left on each sieve was air-dried and weighed. It is important to restate that for preservation issues sampling was restricted to a thin external part of the sections. As a consequence the granulometric values of the coarse fraction calculated here should be considered only as indica-tive. For detailed analyses of the fine fraction, we rely on Rentzel (1990). The organic carbon content was determined using the Walkley and Black method, while the $CaCO_3$ con-tent was measured with a calcimeter; both methods are ex-plained in Mathieu and Pieltain (2003).

Petrographic and morphological investigation of the frac-tion > 8 mm of a set of selected samples, representative for each stratigraphic unit, was performed according to a pro-tocol set up for this study. As the first screening revealed marked difference in size, petrography, and morphology of the pebbles from different layers, it was attempted to iden-tify the stratigraphic origin of the calcareous rock fragments. As the available petrographic collections did not permit a clear stratigraphic attribution of the facies recognised, a site-specific catalogue was established. Based on petrographic composition and morphology, different groups of gravel fa-cies (GF1, GF2, etc.) were defined (Table 6). For all selected samples, weight, size, and morphology (roundness, surface roughness; Bullock et al., 1985) of the components of each group was recorded. Limestone banks enclosing the cavity on both the outside and inside were sampled as local lime-stone reference material (Ref. I, Ref. II., Table 6).

Based on the comparison with the reference material and morphological observations, five major coarse fraction groups have been defined (Table 6 and Fig. 9). Group A in-cludes fresh rock fragments originating from the limestone layers hosting the cave. Group B includes rock fragments

Figure 4. Field view of the observed and sampled sections. **(a)** Section 1 (ST1 location; see Fig. 2). Note the ice wedge cast at the contact between layers L.5 and L.7 and filled up with the gravels of L.6. **(b)** Section 2 (ST2 – location; see Fig. 2). Note the gully eroding the gravelly deposit L.12. (Photos: Marc Juillard, Laténium).

similar to limestone strata enclosing the cave but at least shortly transported. Group C includes rock fragments similar to the limestone strata enclosing the cave, but strongly rounded. Group D includes rock fragments not present in the strata enclosing the cave. Group E includes particular features. The rock fragments of groups A and B are considered to be autochthonous, originating from either the breakdown of limestone banks enclosing the cave or those forming the rock shelter. Rock fragments of groups C and D are clearly allochthonous as they either bear evidence of significant transport and/or their petrography is not present around the cave. The few rock fragments belonging to group E might be related with some human activity, but their quantity is too small to allow further interpretation.

3.3 Luminescence dating

Sample preparation for equivalent dose (D_e) determination was carried out in a red-light laboratory and included wet-sieving (100–150 µm) followed by removal of carbonates (20 % HCl) and organic matter (30 % H_2O_2). Clay particles were dispersed during combined Na oxalate and ultrasonic treatment. K feldspar and quartz fractions were separated using heavy liquids (Na polytungstate). The latter fraction was etched in 40 % HF for 1 h, followed by > 1 h HCl (10 %) and re-sieving (to remove feldspar grains). Infrared (IR) screening revealed strong contamination of the quartz fraction with feldspar that could not be removed by further HF etching and all further work focused on K feldspar. It has to be noted

that the amount of feldspar received during preparation was quite small due its low presence in the samples, and this limited the number of experiments and replicate measurements. Feldspar extracts were fixed on stainless steel discs using a 1 mm stamped spot of silicone oil, which will represent ca. 60 individual grains per disc.

Measurements for D_e determination were performed using a Freiberg Instruments Lexsyg Smart device (Richter et al., 2015), equipped with a Hamamatsu H7360-02 photomultiplier and using a combination of a Schott BG39 (3 mm) and a Brightline HC 414/46 interference (3.5 mm) filter. We applied the post-IR (pIR) infrared stimulated luminescence (IRSL) (Buylaert et al., 2009), with a preheat at 250 °C for 60 s, a first IR stimulation at 50 °C for 90 s (IR-50), and a subsequent second IR stimulation at 225 °C for 100 s (pIR-225), both with a power of 130 mW cm^{-2}.

The performance of the protocol was monitored in dose recovery tests and we received recovery ratios of 0.90 for IR-50 and 1.12 for pIR-225, which are at the limits of the recommendations given by Wintle and Murray (2006) for such tests. To investigate potential residuals, six aliquots were exposed to the light of the inbuilt blue diodes subsequently three times for 30 s (100 mW cm^{-2}), followed by D_e determination using the pIR protocol. This shall exemplarily mimic repeated exposures of samples suspended in water (UV cut-off) to daylight. However, due to the complexity in nature with regard to light level, spectrum, and exposure times, this gives only a very rough idea of the dif-
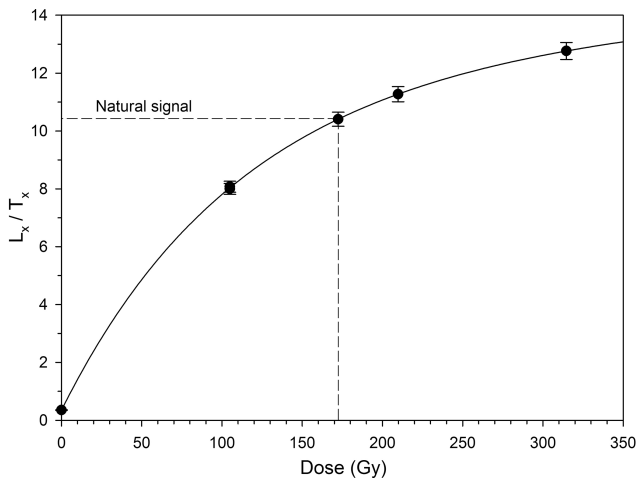
Figure 5. Drawing of sampled sections: morphology of the layers and localisation of the samples mentioned in this paper. **(a)** Section 1 (ST1); **(b)** Section 2 (ST2).

Figure 6. Example of a normalised dose response curve for an aliquot of sample COT-3 IR-50.
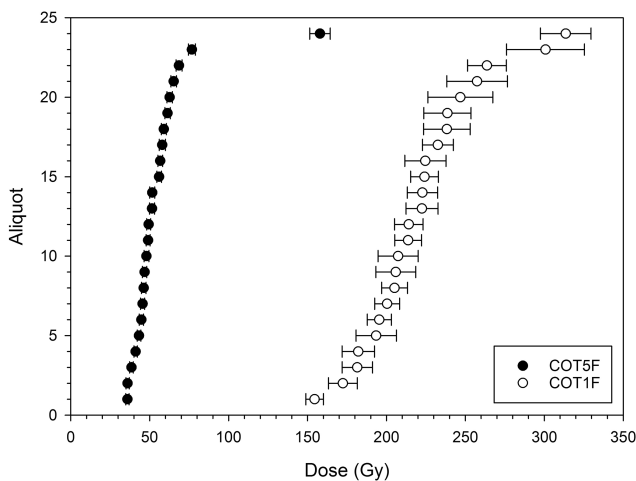

Figure 7. Dose distribution plots exemplified for IR-50 of two samples.

ferent behaviour of IR-50 and pIR-225. For sample COT-3, we received average values of 5.99 ± 1.39 Gy (IR-50) and 54.25 ± 18.03 Gy (pIR-225), and this represents apparent residual ages of ca. 3 and 27 ka, respectively. The third test aims at investigating the stability of different signals with time. For this, four previously measured aliquots were used and the normalised luminescence signal (L_x/T_x) was monitored with different time intervals between irradiation and measurement (Auclair et al., 2003), with a maximum of 5500 s. This results in average g values of 1.5 ± 0.7 % per decade for IR-50 and of 0.5 ± 0.3 % per decade for pIR-225, based on four replicate measurements for COT-3.

Material for dose rate determination was taken around the position sampled for measuring D_e. During sampling it was attempted to collect material representative for the depositional context by taking between 500 and 1000 g. The material was dried, crushed, and homogenised. High-resolution gamma spectrometry was carried out at VKTA Rossendorf e.V. (by Detlev Degering). To investigate for radioactive disequilibrium different decay products in the uranium decay chain are compared (cf. Zander et al., 2007). Dose rate and ages were calculated using Adele software (designed by Detlev Degering). Average sediment moisture was estimated on the measurement of the present-day water content and the geological setting (Table 4). These values roughly correspond to the porosity evaluated through the observation of undisturbed samples in thin sections. Nevertheless, as discussed below, a wide range of environmental and depositional changes occurred during the sedimentation and in situ evolution of the analysed sequence. In addition to the humidity inherent to the karstic environment, the water content of samples was affected by (i) COT1 evolved mostly in dry conditions; although during its own deposition there was surely some water flow. Moreover, during deposition of the overlying sediments (L.14 and L.13) it was subject to some (1000 years?) years of water/ice saturation. (ii) COT2 was deposited by water (Figs. 4b, 5b and Table 5), but it is impossible to estimate how long it was water saturated; the overlying deposit (L.12) was mainly deposited by solifluction on frozen ground with no evidence of water flow and was thus mostly dry. (iii) COT.3, COT.4, and COT.5 are water-laid deposits and they were affected by freeze–thaw processes probably for several thousand years. Conversely, water saturation was absent after deglaciation. Taking all these elements into consideration and in order to avoid circular reasoning, the luminescence age was calculated including a large uncertainty (Table 4) to account for potential moisture changes in the past.

Cosmic dose rate calculation follows Prescott and Hutton (1994) corrected for geographic position and using a rock cover of 10 m. For feldspar, an internal K content of 12.5 ± 1.0 % was used (Huntley and Baril, 1997), supported by measurements from the Swiss Plateau (Gaar et al., 2014). The efficiency of alpha particles in causing radiation damage (alpha efficiency, a value) was assumed to be 0.05 ± 0.01, following Preusser (1999) and Preusser and Kasper (2001) as the geographically closest a value assessments.

4 Results

4.1 Lithic artefacts

The lithic assemblage studied so far (flint and flaked quartzite) is composed of 457 pieces, most of them found in the gravelly layer (L.12), while only a few have been gathered from the brown layer (L.15) (Table 1). The majority of these finds (428 objects) originate from excavations performed between 1916 and 1918 (Dubois and Stehlin, 1932/1933,) but data regarding the vertical and horizontal distribution of these artefacts have not been processed so far. During the 2016 excavations in addition to the chips (see be-

Table 1. Overview of the lithic artefacts found in the cavity by the successive interventions. Based on modified Bernard-Guelle (2004).

Stratigraphic unit	Dubois-Stehlin (1916–1918)		Pittard's series (1926–1936)	Moll's series (1964)	Friedli's series (1966)	1988 excavation	2016 intervention		Total
	Brown layer (L.15/16)	Gravelly layer (L.12)				V	L.11	L.2 to 13	
Lithic artefacts									
1. Tools									
Limace		1							1
Straight side scraper		2			1				3
Convex scraper	1	13							14
Concave scraper		3							3
Double convex side scraper		3							3
Double concave–convex side scraper		1							1
Convergent straight scraper		1		1					2
Convergent convex scraper		10			1				11
Convergent concave scraper		4			1				5
Offset (side) scraper		12		1	2		1		16
Straight transverse scraper		2							2
Convex transverse scraper		3		1					4
Concave transverse scraper		1							1
Atypical end scraper		2							2
Notch		4		3					7
Denticulate		2		1					3
Biface		1							1
Various		2							2
Subtotal tools	4	66	1	9	9	1		1	81
2. Flaking by-products									
Knapping waste products	34		287	1	13	4			339
Core	1		18						19
Knapping waste products (off stratigraphy)			18						18
Total	39	389		2	9	13	4	1	457
3. Flakes and fragments less than 1 cm long									
Chips								20	20

Note that (i) several of the interventions (Pittard, Friedli, Moll) were oriented solely for archaeological material collection and they do not give information concerning the stratigraphic position of the finds; (ii) the flacking by-products documented during the 1988 excavation contain one chip.

low) only one flint object was found, a canted scraper with a thinned base (Chauvière et al., 2018a). The 1988 and 2016 operations revealed the presence of 1–2 cm long chips (flakes and fragments of flakes, Table 1). These artefacts were absent in the inventories compiled before 1988, when no sieving was performed. These chips indicate that flaking operations and manufacturing and sharpening of tools were probably conducted in the cave and/or close to its entrance. Moreover, some chips have a curved profile and their distal part conserves a portion of the dorsal surface of the original flake. These two observations constitute diagnostic criteria to identify them as retouch flakes. The 20 chips of 2016 excavations were found in layers 10, 12b, 12c, and 13 of sections 1 and 2 (Figs. 4a, b, 5a, b), but also in layers 2, 3, 4, and 5 of section 1. For L.2 to L.5 these chips possibly originate from overlaying deposit due to pedoturbation processes. Indeed, L.1 is known to contain Holocene archaeological remains (Dubois and Stehlin, 1932/1933). Thus, based on the available data we suggest that these are likely related to Tardiglacial or Holocene use of the site. Finally, it is worthwhile to mention that the layer enclosing the scraper found in 2016 (L.11) contained only a few bone fragments and no flint chips.

To summarise, the lithic industry of Cotencher cave with its numerous scrapers (63 of 83 tools) can be classified as Mousterian Charentian of oriental Quina type, characterised by a discoidal debitage (non-Quina) (Bernard-Guelle, 2004). Nevertheless the scarcity of "scalariform" retouches and the high number of canted scrapers (16), some of them with thinned bases, indicate a certain distinction compared with the typical Charentian sites (ibid).

4.2 Faunal remains

The assemblage of faunal remains discussed here concerns the finds collected during the 1916–1918 excavations and originates from the two main archaeological find layers (L.15 and L.12), with a high number of pieces and rich in species (Table 2). It is composed of herbivores, carnivores, and omnivores that indicate a wide variety and sometimes divergent ecological background, from temperate to severely cold. The simultaneous presence of reindeer and wild boar, for example, two species with very contrasting ecological backgrounds, suggests a complex environmental and sedimentary history (Le Tensorer, 1998). The interpretation of the environmental significance of this assemblage is still incomplete, as the data processing concerning their horizontal and vertical distribution is still in progress. Nevertheless, the available information already indicates a polygenetic depositional history. A closer look at the rodent species gives some more details, as L.15 (brown layer) contains both arctic–steppic and forest species, while L.12 (gravelly layer) only contains heliophile and forest species (Table 3).

Noteworthy is the fact that the studied bone assemblages did not yield any faunal remains with undeniable cut marks.

Indeed, the long bone fracture surfaces are typical dry bone fractures that are characteristic for bones whose breaking is not interesting for nutrition or those that are frequently found in natural accumulations (in open-air sites or in caves) for which the question of anthropogenic contribution does not arise. In the current state of research, the main criteria for identifying human activity (Castel et al., 2012) appear to be absent from the Cotencher bone assemblages. As a consequence, with the available data there are no arguments to infer a synchronous accumulation of the silex and the bone finds. Similar conclusions have been obtained for several other Mousterian sites situated in mountain environments and raise the question of the reasons for human passage in these areas marginal to the main occupation territories. The absence of hunting and food consumption evidence has been explained as an indication of sites preferentially used for tool preparation (Castel et al., 2012).

4.3 Luminescence dating

The performance of IR-50 and pIR-225 is generally good (e.g. low recuperation, recycling values close to unity), and even for the oldest samples signal levels do not approach saturation (Fig. 6). In most samples, the distribution of D_e values is skewed and overdispersion exceeds 0.20, implying the presence of at least some partial bleaching. This is illustrated in Fig. 7, showing a tight distribution for IR-50 of sample COT5, with one prominent outlier at the upper edge. For IRSL of sample COT1, an overdispersion of 0.15 and a Gaussian-like distribution are interpreted to represent complete resetting of the IR-50 signal prior to deposition in this particular sample. As this represents the only well-bleached sample in the data set, its value was used as input parameter sigma_b when applying the minimum age model (MAM; Galbraith et al., 1999) to all other samples. Even after applying MAM, mean De values of pIR-225 are much higher compared to IR-50 and not in agreement with radiocarbon dating available for the upper part of the sequence (Table 4). The pIR-225 ages are also internally inconsistent. This is interpreted to represent high residual levels in the pIR-225 signal at the time of deposition that are masked by averaging effects in the multigrain feldspar aliquots. With respect to incompletely bleached samples, this may result in age overestimation even when the MAM is applied because signals from incompletely bleached grains mask the signals of well-bleached grains on the aliquots. Such an observation is not unexpected considering the literature (e.g. Buylaert et al., 2012; Lowick et al., 2012, 2015) and the results of the bleaching experiment carried out here. The pIR-225 estimates are hence not considered in further discussion. While signal instability could affect the IR-50, the measured g values are rather small, at the lower edge of values reported by Lowick et al. (2012). As these authors observe uncorrected IR-50 ages in good agreement with independent dating control, we also refrain from carrying out fading corrections.

Table 2. Overview of the vertebrate faunal remains according to their stratigraphic position, based on the material documented by Dubois and Stehlin (1932/1933). Based on Le Tensorer (1998, p. 103–106).

	Taxonomy	Brown layer (L.15/16)	Gravelly layer (L.12)
Order	Family or species		
Carnivora	*Ursus arctos*	×	×
	Ursus spelaeus	×	×
	Panthera spelaea	×	×
	Panthera pardus	×	×
	Lupus lupus	×	×
	Cuon alpinus	×	×
	Gulo gulo		×
	Lynx cf. *pardina*	×	×
	Lynx lynx		×
	Alopex lagopus		×
	Vulpes corsac	×	×
	Vulpes vulpes	×	×
	Felis sylvaticus		×
	Mustela putorius	×	
	Mustela nivalis	×	
	Martes martes	×	×
Perissodactyla	*Equus* sp.	×	×
	Dicerorhinus kirchbergensis		×
	Coelodonta antiquitatis	×	
Artiodactyla	*Sus scrofa*	×	×
	Cervus elaphus	×	×
	Rangifer tarandus	×	×
	Bovidae	×	×
	Capra ibex	×	×
	Rupicapra rupicapra	×	×
Lagomorphs	*Lepus timidus*	×	×
Rodentia	*Marmota marmota*	×	×
	Arvicola sp.		×
	Arvicola terrestris	×	
	Microtus gregalis	×	
	Microtus nivalis	×	×
	Microtus raticeps	×	
	Microtus arvalis	×	
	Clethrionomys rutilus	×	
	Dicrostonyx torquatus	×	×
	Sciurus vulgaris	×	
	Martes ermina	×	×
	Cricetus cricetus	×	
	Allocricetus bursae	×	
	Eliomis quercinus	×	×
	Glis glis	×	×
	Apodemus sylvaticus	×	×
Soricidae		×	
Chiroptera	*Miniopterus schreibersi*		×
	Plecotus auritus	×	
	Myotis myotis	×	×
	Rhynolophus ferrum equinum	×	

Table 2. Continued.

	Taxonomy	Brown layer (L.15/16)	Gravelly layer (L.12)
Order	Family or species		
	Aquila chrysaetos		×
	Pyrrhula pyrrhula	×	
	Anatidae		×
	Pyrrhocorax graculus	×	×
	Pyrrhocorax pyrrhocorax	×	×
	Falco peregrinus		×
	Bucephala clandula		
	Tetrao uragallus		×
Aves	*Corvus corax*	×	
	Bubo bubo		×
	Lagopus mutus		×
	Apus melba		×
	Turdus sp.		×
	Picus canus		×
	Fringilla montifringilla		×
	Tetrao tetrix	×	
	Tetrao urogallus		×
Amphibia		×	×
Pisces		×	×

Table 3. Summary of the ecological significance of the rodent remains according to their stratigraphic position. Based on Le Tensorer (1998, Tables I and II, modified).

Ecological groups	Brown layer (L.15/16) (%)	Gravelly layer (L.12) (%)
Arctic species	35	0
Steppic species	14	0
Heliophilic species	8	39
Forest species	40	71
Wet species	2	0
Total	100	100

Regarding dose rate determination, we found very similar values for the three samples from the upper part of the sequence, which implies a quite homogenous composition of the sediment. Furthermore, the results for different isotopes of the uranium decay chain are in good agreement, indicating the absence of significant radioactive disequilibrium (Table 4). Interestingly, the concentration of dose-rate-relevant isotopes is about 50 % higher in the two lower samples, in particular in sample COT2. Furthermore, both samples show evidence for radioactive disequilibrium, indicated by different values observed for U-238, Ra-2226, and Pb-210 (Table 4). The observed surplus in U-238 is likely the result of carbonate precipitation rich in this isotope but devoid of the daughter isotopes (Ra-2226 and Pb-210), as these are not

solvable in water. The pronounced changes in environmental conditions in the past inhibit proper modelling of U uptake. Carrying out a correction for U uptake appears inappropriate considering the uncertainties related to the environmental history but our screening implies it will not exceed 10 % with regard to age calculation (cf. Preusser and Degering, 2007).

4.4 Sedimentary dynamics and site formation

The stratigraphic succession comprises 16 layers (L.1 to L.16), most of which are strongly calcareous (Table 5). For accessibility reasons only L.5 to L.16 were investigated in detail; therefore the discussion below will mainly concern these layers. Despite careful searching, no charcoal fragments were found in the analysed sections. A summary of the recent observations and comparison with former stratigraphic interpretations is shown in Fig. 3.

4.4.1 Layers 16 and 15 and the brown layer

The sediments labelled as L.15 and L.16 represent the upper part of the cave's oldest archaeological find layer known as the brown layer (Fig. 3). This upper part is characterised by involutions. Due to technical restrictions, a merely 20 cm thick band of this deposit could be investigated discontinuously over 3 m; therefore as reasoned in Table 5 the two facies of this layer are discussed together. L.15 and L.16 have a reddish (L.15) or black (L.16) colour and relatively high organic carbon values (0.8 %–0.9 %), while the $CaCO_3$ is markedly low (11 %–14 %), revealing significant pedo-

genetic processes (Fig. 8b and Table 5). The fine material is fluffy. Our study of the > 8 mm fraction indicates that it is composed of weathered bedrock limestone with some (ca. 8 %) rolled limestone gravel (Fig. 8a).

The underlying brown layer is present all over the cave and fills up the natural depressions inside the cavity, with a maximal thickness of 1.5 m (Fig. 2). The coarse fraction is absent in its lower part and varies between 10 % and 50 % in its upper part (Rentzel, 1990, and Table 5). Locally large limestone blocks probably originating from the ceiling are also present (Dubois and Stehlin, 1932/1933, Rentzel, 1990). A few small (ca. 1 cm) alpine pebbles and a notable amount of sand grains of alpine origin are attributed to reworking of older glacier deposits (Dubois and Stehlin, 1932/1933). The fine material is characterised, at least locally, by traces of stratification (Dubois and Stehlin, 1932/1933). X-ray mineralogy reveals some calcite and quartz grains in the bulk samples, while the clay fraction is characterised by the marked presence of mica, kaolinite, and pedogenetic phyllosilicates. The later data are interpreted as an indication of a relationship to previous Eemian soil cover that occurred in the surroundings (Rentzel, 1990; Adatte et al., 1991). The fine material contains common phosphate-rich impregnations or nodules with values of ca. 12 % to 74 % $CaCO_3(PO_4)_2$ (Dubois and Stehlin 1932/1933; Rentzel, 1990). Rare occurrences of charcoal fragments were mentioned by Rentzel (1990).

All these data suggest that the layer is the result of compound accumulation processes: (i) deposition inside the cave of a soil formed under and in front of the rock shelter, (ii) breakdown and in situ weathering of bedrock, and (iii) important input of biogenic phosphorus-rich organic material (decomposed faunal remains and coprolites and/or bat guano). The significant quantity of weathered, but not rolled, cave bear bones scattered throughout the layer (Dubois and Stehlin, 1932/1933) and the high amount of faunal remains (Table 2) argues for in situ phosphorus accumulation. The IRSL age for the upper part of this deposit is 67.8 ± 3.4 ka (COT1, Table 4).

4.4.2 Layer 14

This stratified sediment, composed of alternating sandy, clayey, or heterometric gravelly strata, has been observed by Rentzel (1990) both close to the entrance of the cavity and in its inward side. During the 2016 work we distinguish only a few thin discontinuous lenses of this layer, while towards the inner part of the cavity, explored in 2017, a stratified deposit up to 57 cm thick was observed (Table 5). In this inward part, large limestone blocks (at least 40 or 20 cm) are present at the upper part of this deposit. X-ray mineralogy of the bulk samples indicates a high amount of quartz and feldspar, while interstratified phyllosilicates and kaolinite in the clay fraction are less common compared to the underlying layer (Adatte et al., 1991). The sedimentological characteristics suggest deposition by running water.

Table 4. Results of luminescence dating with the average activity of K and Th (the latter given as an average of different isotopes; cf. Preusser and Kasper, 2001) and assumed average sediment moisture during burial and resulting dose rate (D). The number of replicate measurements (n) is given together with the relative overdispersion (od) for IR-50 and pIR-225, equivalent dose (D_e), and age for the tow different approaches.

Lab code	K (Bq kg⁻¹)	Th (Bq kg⁻¹)	U-238 (Bq kg⁻¹)	Ra-226 (Bq kg⁻¹)	Pb-210 (Bq kg⁻¹)	Moisture (%)	D (Gy ka⁻¹)	n	od	D_e IR-50 (Gy)	D_e pIR-225 (Gy)	Age IR-50 (ka)	Age pIR-225 (ka)
COT5	237 ± 25	16.7 ± 1.1	24.8 ± 3.9	21.2 ± 1.4	19.9 ± 4.2	10 ± 5	1.87 ± 0.11	24	0.30/0.17	49.1 ± 4.3	161.1 ± 15.0	26.5 ± 2.8	87.0 ± 9.5
COT4	297 ± 31	20.2 ± 1.3	22.9 ± 4.0	26.0 ± 1.7	25.8 ± 3.7	10 ± 5	2.19 ± 0.12	24	0.21/0.17	66.4 ± 5.4	164.5 ± 15.2	30.6 ± 3.0	75.7 ± 8.2
COT3	267 ± 27	18.0 ± 1.2	21.1 ± 3.2	24.1 ± 1.4	24.1 ± 2.9	10 ± 5	2.03 ± 0.11	24	0.30/0.36	73.8 ± 6.4	133.4 ± 17.9	36.6 ± 3.8	66.2 ± 9.6
COT2	401 ± 42	29.4 ± 1.9	102 ± 9	79.2 ± 5.1	43.8 ± 4.8	15 ± 5	3.51 ± 0.17	24	0.37/0.20	250.8 ± 30.3	468.7 ± 61.1	72.5 ± 9.4	135 ± 11
COT1	177 ± 16	14.1 ± 1.0	83.2 ± 7.0	65.9 ± 3.9	41.1 ± 4.9	15 ± 5	3.27 ± 0.13	24	0.15/0.49	217.6 ± 7.1	313.1 ± 16.1	67.8 ± 3.4	97.6 ± 6.3

Table 5. Brief descriptions of the sediments.

Layer no.	Brief description	Coarse fraction	Thickness (cm)	HCl
1	Angular and more or less platy limestone fragments (2–14 cm diameter) in a granular humiferous silty matrix. The lower part of the layer the fine material is less humiferous and there are travertine- and stalagmite-like concretion fragments. Common present-day roots. Lower boundary is sharp.	u.p. 40 %; l.p. 50 %	38	±±±
2	White (5Y 8/1.5) strongly porous granular silt with common angular limestone fragments (5–12 cm diameter) in its upper layer and a few small (2–3 cm diameter) limestone fragments in its lower part. Abundant present-day roots in its lower part. Lower boundary is gradual.	u.p. 30 %–40 %; l.p. 2 %–5 %	20	+++
3	Grey homogeneous clayey–sandy silt. Observed only in section 1. Lower boundary is gradual.		8–10	++
4	Slightly brownish clayey–sandy silt with common angular rock fragments (3–5 cm diameter). Lower boundary is gradual but laterally shows pocket-like morphology.	30 %	10–30	
5	Light grey to white (5Y 7.5/2) sandy, slightly clayey silt. Separated in three layers based on the coarse material. From up down: for L.5a the upper part has a few angular limestone gravels more or less vertically oriented; for L.5b the middle part has almost no coarse fraction and is more sandy with small (0.2–0.6 cm diameter) stratified gravel; L.5c has a homogenous lower part with rare calcareous gravel (2–3 cm diameter). Its lower part fills up the gully that erodes L.12 and that is partially filled by L.7 to L.10. Compact, brittle, and fine (1 mm thick) lamellar structure in the upper part, with coarser lamellar (up to 1 cm) in depth. Lower boundary is sharp.	u.p. 10 %; m.p. < 1 %; l.p. 2 %–3 %	20–70	+++
6	Former gravel level: 0.5–11 cm in depth angular or sub-rounded limestone gravels. A few of the gravels are still at this contact. Most of them are situated along vertical fissures until the deeper part of the layer. One cluster of them suggests an ice wedge cast. Lower boundary is sharp.		10	
7	Homogeneous, light grey (5Y 7.5/3) silty to clayey silty sediment. More and more clayey in depth. Compact and brittle. Large platy structure which becomes angular blocky in depth. Partially fills up the channel marked by the underlying layers. Lower boundary is sharp with involutions of the underlying layer.	20 %–30 %	20–60	+++
8	White, well-sorted, fine bleached sand. Upper limit with involutions. Lower boundary is sharp.	0	5–10	+++
9	Grey-brownish (2.5Y 7/2) clayey sediment. Stratified with involutions and angular clayey soil fragments incorporated. Former studies describe a chaotic related distribution of these fragments. Plugs the lower part of a depression created by the deposition L.10, while it eroded L.12. Lower boundary is sharp.	0	10–15	+++
10	Angular calcareous boulders (10–20 cm diameter) and rounded/sub-rounded calcareous gravels present in the lower part of the depression eroding the underlying layer 12. Lower boundary is sharp.	100 %	15	

Table 5. Continued.

Layer no.	Brief description	Coarse fraction[a]	Thickness (cm)	HCl
11	Heterometric, rather compact sediment composed of limestone and one crystalline rock fragment in a slightly humiferous light greyish brownish silty (2.5Y 7.5/2) fine material. The fine material resembles layer 9. Some of the gravels are rounded, while the others are angular. This sediment is only present at the entrance of the cavity. An artefact was found at its lower boundary. Lower boundary is sharp and irregular.	40 %–50 %	15–50	+++
12	Gravelly layer contains angular, sub-rounded, and rounded gravels in a humiferous silty-sandy fine material. Its upper part is eroded at the level of section 1. Frequent present-day roots. Subdivided in three sub-layers based on the size and amount of gravels and the colour of the fine material.		70–200[b]	++ to +++
	12a has somewhat more brownish (2.5Y 5.5/3), less humiferous fine material and seems to be more compact than the underlying 12b and 12c; coarse fraction: 2–5 cm diameter;	12a: 30 %		
	12b has somewhat more sandy and darker (2.5Y 5–5.5/3), more humiferous fine material. The coarse fraction (3–5 cm diameter) is more abundant and several of the stones are rather rounded. Some bone fragments. The gravels give an impression of sloping towards the interior of the cavity. Some of the rock fragments are vertically oriented.	12b: 50 %		
	12c has rather sandy fine material and is slightly lighter coloured (2.5Y 5/4) compared with the overlying. The coarse material is less abundant and somewhat finer (mostly less than 1 cm diameter; a few 2–3 cm diameter) compared with the overlying layers. Granular structure. Lower boundary is gradual.	12c: 20 %–30 %		
13	Light brown (2.5Y 6.5/4), silty to silty clayey sand with small gravel (±3 mm diameter). Seems to be the fill of depressions cut in the underlying L.15. Lower boundary is sharp and irregular.	5 %–10 %	15–20	+++
14	The entrance of the cavity is represented by a fine sandy, stratified, yellowish-greenish (2.5Y 7.5/1.5–3) well-sorted deposit present as irregular spots at the upper part of layer 15 or incorporated in its upper part. Observed in a very limited area. In some of the fragments internal involutions could be observed.	0	3–10	+++
	Inside the cavity (2017 intervention) is represented by a stratified deposit composed of the following. (i) Lower part includes sandy and clayey layers containing mostly angular limestone pebbles in their upper part; (ii) middle part includes alternating grey and white, well-sorted sandy layers followed by sandy-silty heterometric deposit containing about 40 % rolled gravels (0.5–1 cm diameter); (iii) upper part includes stratified clayey deposit having lamellar structure covered by well-stratified white sandy deposit. (iv) In its upper part there is a level of at least 40 cm of large angular limestone blocks. Lower boundary is sharp.		57	
15/16	Orange sandy silt (10YR 7.5–4.5/3–6) with a few rather weathered calcareous rock fragments (5–8 cm diameter). Fluffy and very friable. The upper surface has involutions and this irregular upper surface is highlighted by a 1 cm thick iron impregnation. Observed over a very limited length and only over a 20 cm thickness. On a very restrained surface its upper part is slightly darker (7.5YR 3.5/4) and this was designated as L.16. The technical restrictions of the field intervention inhibited further observation.	5 %–10 %	> 20	− or +

Legend: The colours are according to the Munsell colour chart (Munsell Color, 1994, revised version). They were measured on air-dried and mostly undisturbed samples under natural light.
u.p.: upper part; m.p.: middle part; l.p.: lower part.
Reaction with HCl: ±±±: very strong; +++: strong; ++: weak; +: very weak.
[a] Based on field estimation using the abundance chart, according to Bullock et al. (1985). [b] A value of 70 cm at the entrance up to 200 cm towards the internal part of the cavity (Adatte et al., 1991).

Table 6. Petrographic and morphologic descriptions of the various rock fragment groups.

Code*	Brief description	Comments	Coarse fraction group*
Ref. I	Light grey to slightly beige, very compact, indurated, fine crystalline limestone. Undulating to rough (microkarst-like) external surfaces with a thin discontinuous white, slightly powdery coating. Locally thin hard, hard, and granular crust. Cutting external edges.	Sampled outside of the cavity: limestone bank forming the ceiling of the rock shelter. Upper strata.	
Ref. II	Brownish grey, very compact, indurated, fine crystalline limestone. Undulating to smooth external surfaces with thin white crust. Cutting external edges.	As above: upper part of the middle strata.	
Ref. III	Dark grey, compact, indurated, finely crystalline limestone. Undulating external surfaces with a very thin white crust. Cutting external edges.	As above: lower part of the middle strata.	
Ref. IV	Light grey, slightly yellow beige, very compact, indurated fine crystalline limestone. Undulating to smooth external surfaces with bright white coating on surfaces and along fissures. On some sides more granular crust resembling a lichen mat and providing a rough surface.	As above: lowest strata.	
Ref. V	Light grey to yellowish whitish, very compact, indurated, fine crystalline limestone. Rough external surfaces covered by a slight powdery white crust and organic matter.	Isolated limestone block situated in front of the cavity, covered my mosses and litter.	
Ref. VI	Brownish grey, very compact, indurated, fine crystalline limestone. Rough external surfaces covered by a white, irregular, rather hard crust. Some Fe impregnations towards its external rim.	Sampled inside the cavity: limestone outcrop situated on the floor of the cavity, at the level of sections 1 and 2.	
Ref. VII	Light grey to white compact limestone or fine sandstone with some internal holes (former fossils?). Globally rather powdery aspect, with a more pronounced trend toward the external part of the fragment. Irregular, rough external surfaces.	Sampled inside the cavity: limestone from the lateral wall, 2–3 m inward from section 2.	
Ref. VIII	Beige to yellowish grey, very compact, indurated, fine crystalline limestone. Undulating to smooth external surfaces with an irregular thin white crust. Resembling to Ref. IV(3)	Sampled inside the cavity: limestone outcrop on the floor situated towards the inner third of the cavity.	
GF1	Strongly porous, tuff-like $CaCO_3$ nodules and platy, rather angular, compact $CaCO_3$ crust fragments.		A
GF2	Light grey to dark grey, very compact, indurated finely crystallised angular to subangular rock fragments. Undulating surfaces covered by a thin indurated $CaCO_3$ crust. Rather sharp edges.	Resemble Ref. II and III.	A

Table 6. Continued.

Code	Brief description	Comments	Coarse fraction group
GF3	Light grey to whitish, very compact, indurated, fine crystallised angular to subangular rock fragments. Undulating external surfaces covered by thin, indurated, white CaCO$_3$ crust.	Resemble Ref. I.	A
GF4	Very compact, indurated, sub-rounded to sub-angular limestone rock fragments. Rough and porous external surfaces (alteration, dissolution of fossils) covered by thin, hard, white crust. Under this crust: brownish grey, fine crystalline. Locally more brownish hard precipitations.	Resemble Ref. VI.	A
GF5	Rather porous weathered rock fragments at least partially covered by orange-brownish (phosphorus?) precipitation crust. Sometimes sandy aspect. Sometimes part of them is whitish, suggesting a least weathered limestone. Weak to moderate reaction with HCl.	Weathered and phosphorus impregnated rock fragments (Ref. VIII).	A
GF6	Subangular to sub-rounded limestone fragments having a rough white external surface with partially preserved microkarst features. Inside compact light grey.	Might correspond to Ref. I	B
GF7	Subangular to sub-rounded, polished surfaced, indurated, strongly compact limestone fragments. White at the surface, yellow-brownish grey fine crystallisation inside.	Resemble Ref. IV and VIII.	C
GF8	Sub-rounded light grey yellowish limestone fragment with smooth surfaces suggesting rolling processes.	Resemble Ref. I.	C
GF9	Bright white rounded fine sandstone gravels.	Might be rolled fragments of Ref. VII.	C
GF10	Brownish grey, rounded limestone gravel with smooth/polished surfaces.		D
GF11	Grey to dark grey, rounded to sub-rounded limestone or fine sandstone gravels with smooth surfaces.		D
GF12	Greyish white, laminated fine sandstone gravels.		D
GF13	Rounded Alpine rock fragments.		D
GF14	Strongly rolled 1–2 cm diameter gravels. Mostly limestones, but rare alpine rock fragments.		D
GF15	Small (±1 cm) irregular CaCO$_3$ concretions, resembling loess dolls.		D
GF16	Dark grey to black angular limestone. Thin CaCO$_3$ crust.	Might correspond to Ref. III, but it might be a fragment of a black limestone.	E? or D?
GF17	1–2 cm large, angular calcite crystals.		E
GF18	Angular yellowish small limestone fragments.	Might be lithic artefacts.	E

Legend:
Ref. I to VIII: limestones hosting the cavity or blocks situated inside and outside of it;
GF1 to GF18: site-specific gravel facies defined for this study.
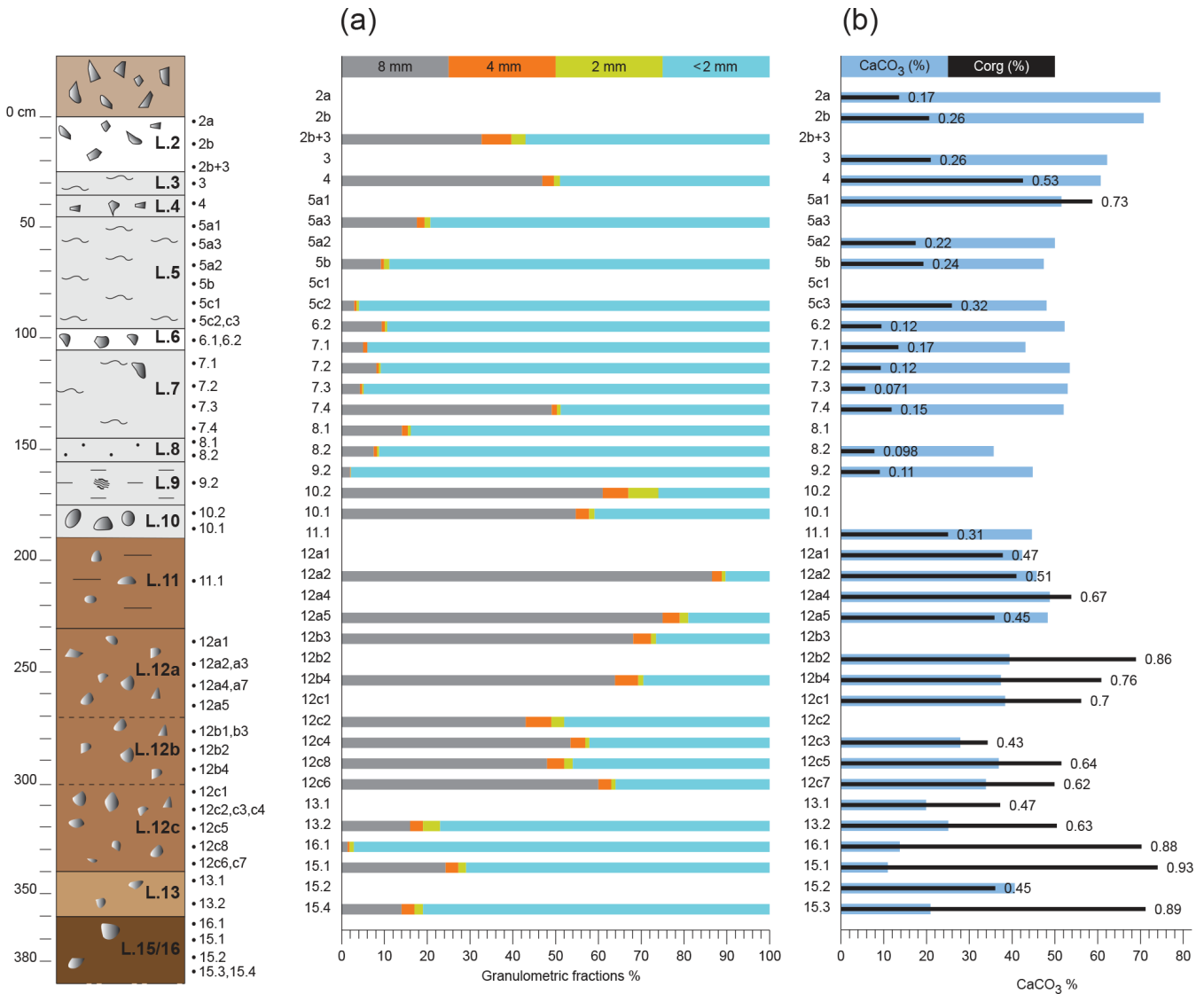See explication in Sect. 3.2.

Figure 8. Variation in granulometric and chemical soil characteristics throughout the studied layers. **(a)** Granulometry. **(b)** Variation in organic carbon and $CaCO_3$ content. Legend: 2a to 15.4 – sample numbers; their location is presented in Figs. 4a, b and 5a, b.

4.4.3 Layer 13

This heterometric relatively finely textured sediment has been observed in a gully-like depression in section 2, towards the entrance of the cave. The 8 mm fraction is mainly composed of slightly reworked local limestone fragments, but in the fine gravel fraction (1–2 cm) small quantities of rounded limestone pebbles of various origins and one rounded quartzite were detected (Figs. 8a and 9). Field and laboratory observations and the analytical data (organic carbon and $CaCO_3$ content, Fig. 8b) suggest that it is a partial reworking of the underlying L.15 and L.16 with some fresh sediment input. The latter is suggested by the rounded small gravels and the relatively higher $CaCO_3$ content compared to the underlying L.15 and L.16. The morphology in

the channel-like depression suggests torrential flows at this external part of the cavity. The sections examined do not permit us to state whether L.13 and L.14 are the result of two clearly distinct sedimentary events or if they are the different sediment facies deposited during the same landscape destabilisation phase. This layer has been dated to 72.5 ± 9.4 ka (COT-2, Table 4) but this sample shows a high overdispersion, implying the presence of partial bleaching. This is in contrast to COT-1, which appears to be well bleached. Altogether, the environmental proxy data and IRSL dating of this lower part of the studied sequence imply correlation to the periods of severe cooling of the S3 stadial (MIS 4).
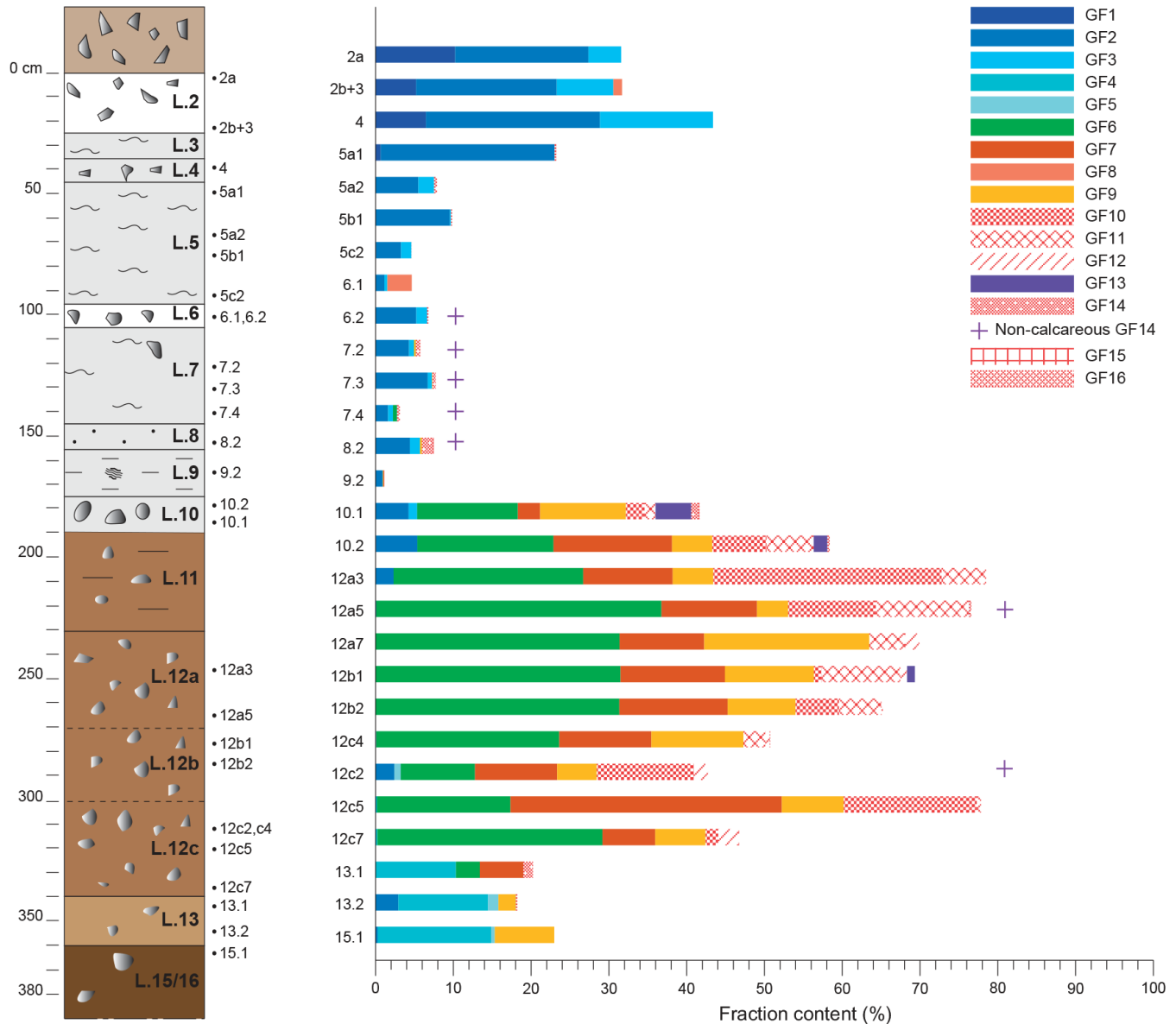
Figure 9. Petrographic composition of the more than 8 m fraction of selected samples. Legend: 2a to 15.1 – sample numbers; their location is presented in Fig. 5a and b. GF: gravel fractions as described in the methods and Table 6. GF1 to GF5: fresh rock fragments originating from the limestone layers hosting the cave (group A); GF6: pebbles similar to limestone strata enclosing the cave but at least shortly transported (group B); GF7 to GF9: pebbles similar to the limestone strata enclosing the cave, but strongly rounded (group C); GF10 to GF16: pebbles not present in the strata enclosing the cave (group D). Note the presence of non-calcareous gravels of GF14 is indicated by a cross as their quantity is too small to be visible on the graph.

4.4.4 Layer 12

This rich coarse material, up to 180 cm thick, sediment (Figs. 4a, b, 5a, b, 8a; Table 5) is present all over the cavity (Dubois and Stehlin, 1932/1933; Rentzel, 1990). The coarse fraction varies between 50 % and 92 % and the > 8 mm fraction, composed mainly of 3–8 cm large pebbles, dominates in this deposit (Fig. 8a). Petrographic observations (Fig. 9) indicate that throughout this deposit the coarse material is composed of (i) more or less rolled limestone fragments similar

to the limestone banks hosting the cavity and (ii) rolled limestone and sandstone pebbles that are allochthonous. Part of the gravel has a powdery, and thus weathered, external part, while others are more polished and little weathered. Non-calcareous components are very rare and are represented by one ca. 3 cm large rolled schist or gneiss fragment (sp.12.5) and a few rolled ca. 5–10 mm pebbles. The variability in petrography and morphology of the calcareous coarse fraction has already been highlighted by Dubois and Stehlin

(1932/1933). They also stated that the alpine components are very rare, all rounded, and dominated by quartzite, with a few gneiss pebbles.

The < 2 mm fraction is more important in the lower part of the deposit (30 %–40 % in L.12c and L.12b) and it decreases in the upper part (less than 20 % in L.12a). Throughout L.12 this fine material is rather rich in CaCO$_3$, but except in the upper part of the layer (L.12a), values are less than 40 %. The organic carbon values show some variability, but generally they are rather high (Fig. 8b). In the lower part of the deposit (L.12c and L.12b) organic contents are highest and increases upward (L.12b), while in the uppermost part (L.12a) these values are generally lower, although certain variability is present. The CaCO$_3$ content, on the contrary, is markedly lower in the lower part of the deposit (L.12c and L.12b) and increases towards the top (L.12a). All this suggests that the fine material constituting this unit has undergone noticeable pedogenetic processes that had a more important fingerprint in the lower part of the deposit (L.12c and L.12b).

The clay and silt fractions are dominated by mica (Adatte et al., 1991). Weathered clay minerals (interstratified phyllosilicates) are present mainly in the lower part of the deposit while in the upper part chlorite increases in parallel to the quasi-fading of the interstratified constituents.

Bone fragments are present all over the layer and all through the cavity; some of them are strongly rolled, part of them are clearly reworked, and part of them seem to be rather fresh (Dubois and Stehlin, 1932/1933). Although former studies mention the presence of charcoal (Rentzel, 1990), we did not find any despite the large number of samples sieved. No in situ fireplaces have been observed so far but sieving revealed pebbles bearing traces of heating. A concentration of burned rock fragments, associated with a fresh lithic tool, has been documented towards the upper part of this deposit, during the 2017 campaign. This feature will be studied during a later phase of this project.

To summarise, all these data suggest a complex environmental history recorded in this deposit. The heterogeneous and allochthonous coarse fractions indicate that part of the sediment source was originally situated outside the cavity. The traces of pedogenetic processes all over this layer indicate that this sediment evolved as a soil outside the cavity. Eventually the heterometric soil and its faunal and artefact constituents were deposited inside the cavity during several depositional phases. The chronological setting of these processes is specified by the stratigraphic position of L.12 (Fig. 3) and will be discussed below.

4.4.5 Layer 11

This heterometric coarse-material-rich (Table 5), rather compact sediment is present only towards the entrance of the cavity and it wedges out towards the inside. Due to technical reasons it was only briefly examined and sampled during the 2016 operations. The fine material is moderately humiferous and rather strongly calcareous (Fig. 8b), while the coarse fraction is composed of rounded and angular limestone fragments and at least one rounded pebble of alpine origin (Table 5). The poorly sorted nature of this deposit suggests deposition by mass movement. Similarly to L.12, the origin of the sediment is most probably related to a deposit situated earlier at the cavity entrance, but as indicated by the chemical soil characteristics this deposit was little affected by the pedogenetic processes. The presence of the alpine rock fragment can be explained as either originating from reworked glacial sediment or it could be related to human activity.

4.4.6 Layer 10

This sediment is composed of mostly rolled, but also angular, coarse gravel, blocks of autochthonous and allochthonous limestone, and a few alpine pebbles (Table 5 and Figs. 8a, 9). Earlier studies also described a more heterometric facies of this deposit with an irregularly surfaced gravelly layer composed of rounded limestone and alpine pebbles, rich in bone fragments, and having a sandy-silty matrix (Rentzel, 1990). As for the non-calcareous components, the largest rounded pebble (9 cm) found in L.10 (sp.10.1) is proven to be a stone tool, while the others are 2–4 cm large rounded to sub-rounded quartzite and angular schist fragments accounting for 3 % of the coarse material of sample 10.2 (Figs. 8a, 9). As argued for L.12 and L.11 above, the few non-calcareous components are most likely reworked from sediments that already existed in the region. The clay mineralogy of the fine sediment is similar to L.12, but no interstratified, pedogenetic minerals are present in the clay fraction (Adatte et al., 1991). L.10 has been observed at the bottom of the depression cut in the L.12. This gully – traversing the rock shelter parallel with the main valley – removed, at its deepest part, at least 40 cm of the gravel-rich L.12 (Fig. 4b).

These elements indicate that an important water flow traversed this landscape position and reworked and disturbed sediments towards the entrance of the cavity. It eroded the fine material of L.12 and rolled and re-sedimented part of its coarser fraction, including the bone fragments. Limestone fragments from the cavity fallen due to frost shattering completed the sediment body accumulated.

4.4.7 Layer 9

This layer is a highly calcareous, stratified, finely textured clayey, silty sediment. The few coarse components found by sieving (Fig. 8a) are probably related to underlying L.10. In some parts the clayey band is discontinuous and chaotically oriented. The layer partially fills the channel cut before the deposition of L.10 (Figs. 4b, 5a, b), but it is also present in the inner parts of the cavity (Rentzel, 1990). These sedimentary features indicate fine material deposition by low energy flow and decantation in a pond environment. The presence of standing water in highly porous rock and at this landscape

position further argues for a frozen landscape. The chaotically oriented clayey bands indicate freeze–thaw processes affecting this layer. The absence of pollen in the test samples (Bezat, 1990), the low organic carbon content, and the absence of the organic layers in the sequence are in good agreement with a vegetation-free glacial environment.

4.4.8   Layer 8

This strongly calcareous, stratified, well-sorted, fine sandy layer with some gravels (Figs. 4b, 8a; Table 5) indicates an episode of significant water flow. The size and morphology of the coarse fraction (Fig. 8a) indicate episodes of more energetic water flow and also some cryoclastic rock fall from the ceiling during the deposition of this layer. The involutions observed at its surface are related to freeze–thaw processes occurring during and/or after the deposition of layer 7. The IRSL age of this layer indicates deposition around 36.6 ± 3.8 ka (COT3, Table 4).

4.4.9   Layer 7

This strongly calcareous, lightly coloured, clayey silty deposit (Table 5 and Figs. 4a, b, 8a, b) has been described at the entrance of the cavity, but earlier studies suggest that it is probably present all over the cave (Dubois and Stehlin, 1932/1933; Rentzel, 1990). It coarsens upward. Traces of stratifications have been reported by Rentzel (1990). It is a rather compact and brittle sediment with platy structure. In the sections investigated it can be up to 40 cm thick and represents the upper fill of the gully eroding the upper part of the L.12. The coarse fraction, except its lowest part, represents less than 10 % (Fig. 8a) and is mainly composed of angular rock fragments similar to the limestone strata hosting the cavity. A low abundance (a few grains per sample), but systematic presence, of small (ca. 5 mm) rounded alpine pebbles was observed (Fig. 9). These are probably related to the presence of older alpine material in the surroundings. The organic carbon content is very low, among the lowest measured in this stratigraphic sequence (Fig. 8b). Screening for palynological content revealed an absence of pollen (Bezat, 1990), whereas mineralogical analyses document the lack of weathered minerals (Adatte et al., 1991). In former studies this and the overlying layer (L.5) have been described as one single deposit (Dubois and Stehlin 1932/1933; Rentzel, 1990). Our subdivision is based on the occurrence of a gravel layer (L.6) on top of L.7 and an ice wedge cast filled with these gravels (Figs. 4a, 5a). The IRSL age of the upper part of the layer is 30.6 ± 3.0 ka (COT4, Table 4).

4.4.10   Layer 6

This layer is composed of mostly angular limestone pebbles and some smaller blocks resembling the limestone strata hosting the cavity. It is present as (i) a discontinuous gravel layer occurring on top of L.7 and (ii) dispersed or concentrated vertical stones inside the underlying L.7 (Figs. 4a, 5a). The morphology of the latter is interpreted as a former ice wedge cast and fill of the former cryodesiccation features. All these elements indicate the absence of fine sediment input, strong freezing conditions favourable of permafrost, ice wedge formation, and cryoclastic breakdown of the surrounding limestone walls.

4.4.11   Layer 5

This strongly calcareous sandy, slightly clayey silt is present all over the cavity (Table 5 and Rentzel, 1990), with its maximal thickness of about 60 cm towards the entrance (Fig. 2b). It appears rather homogeneous but shows some stratification and a distinct platy structure (Table 5 and Rentzel, 1990). In addition some faint vertical cryodesiccation features could also be observed. Except for the upper part, coarse material is scarce (Fig. 8a) and composed of almost exclusively angular, local limestone fragments (Fig. 9). The organic carbon content is low except for the uppermost sample (Fig. 8b), which is likely contaminated by present-day roots. Mineralogical analyses indicate the absence of weathered minerals (Adatte et al., 1991).

    Sedimentation of this layer indicates that water-flow processes were regularly active again at this landscape position. The texture suggests that part of the fine material might be of aeolian origin. The platy structure, the cryodesiccation fissures and the cryoclasted rock fragments incorporated in the sediment witness a particular cold environment during the accumulation of this deposit. IRLS dating of the sample from the lower part of the layer indicates an age of 26.5 ± 2.8 ka (COT5, Table 4).

4.4.12   Layers 3 and 4

These strongly calcareous heterometric sediments, with abundant angular limestone fragments in L.4 (Figs. 4a, 5a, 9), were found only at the entrance of the cavity. The common angular limestone fragments in L.4 suggest important cryoclastic breakdown of the cavity roof that possibly indicates cold climatic phases. The lack of chronological, field, and analytical data does not permit a discussion of the deposition processes and environmental significance of these layers.

5   Discussion

As recognised already by former scholars in the first quarter of the twentieth century (Dubois and Stehlin, 1932/1933) the sedimentary sequence of the Cotencher cave is an outstanding record of the environmental changes that occurred during the Late Pleistocene. Regional climatic fluctuations (Fig. 10) are also documented in different sections of the alpine foreland (Preusser, 2004) and in the Jura Mountains (Cupillard et al., 2015). The deposits of the Cotencher cave reinforce
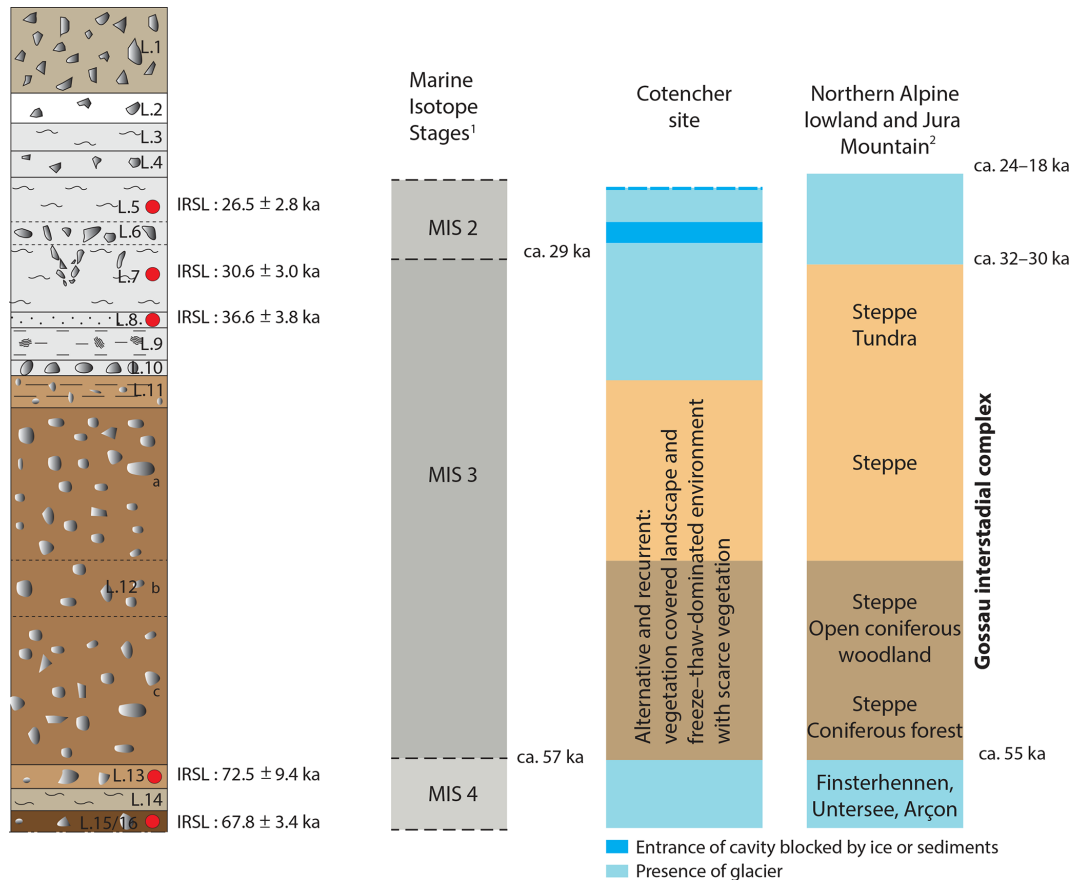
Figure 10. Syntheses of the Cotencher data in comparison with the regional chronological and palaeoenvironmental record. [1] based on Lisiecki and Raymo (2005). [2] based on Preusser (2004), Ivy-Ochs et al. (2008), Cupillard et al. (2015), and Bichet et al. (2016).

some of the former environmental records and permit us to further decipher the complexity of Jura and Alpine glacier dynamics.

5.1 Early last glacial: evidence of landscape destabilisation

Based on mineralogical arguments, the brown layer present in the lower part of the stratigraphic sequence has been interpreted as sediment originating from Eemian soil (Adatte et al., 1991). Its spatial (vertical and horizontal) distribution (Fig. 2b) suggests the presence of a reasonably large sediment platform in front of the cave and under the rock shelter. Pedogenetic processes transformed this sediment and the resulting rather weathered soil has been subsequently reworked into the cave. The observations available so far do not permit an exhaustive discussion about the deposition processes, but the stratified sandy layer described by Dubois and Stehlin (1932/1933) clearly suggests at least some water flow towards the cavity, while the large limestone blocks witness gravitational accumulations. The important quantity of biogenic phosphorus (Dubois and Stehlin, 1932/1933; Rentzel, 1990) and the presence of numerous cave bear (*Ur-*

sus speleous) bones together with the presence of animal bones indicating both steppe and forest vegetation cover (see Sect. 4.2) suggest slow sediment build-up over a long time span and sediment accumulation during several depositional phases. Involutions in the upper part of this layer may reflect cryoturbation processes but could also be related to faunal turbation, such as digging by bears in order to prepare hibernation dens (e.g. at the rock shelter of Tanay Sur-les-Creux; Braillard et al., 2004). Larger sections would be needed to formulate a trustworthy interpretation.

The L.15 observed and analysed in this work represents only the uppermost part of this stratigraphic unit known as the brown layer (Fig. 3). For this part of the sequence the IRSL chronology suggests reworking processes around 67 ka (see discussion below). As a result we can only deduce that the accumulation of the brown layer containing part of the Mousterian artefacts occurred during several phases of the early Last Glacial, but this can be detailed only through more suitable sections and further dating.

5.2   Evidence of glacier processes around 70 ka

In the lower part of the studied sequence several converging sedimentary and chronological facts indicate the presence of a glacier environment in the surroundings of Cotencher cave. First of all, layers L.14 and L.13 suggest water flow processes both at the entrance and towards inner parts of the cavity. The presence of running water despite the steep slopes and strongly permeable environment both inside cavity and under the rock shelter at about 140 m above the river valley bottom implies that something kept up the water. The geomorphological context as described above suggests the presence of a neighbouring glacier during the deposition of these sediments. The high $CaCO_3$ content of the various sublayers, their low organic carbon content, and the cyroclasted coarse components (Table 5) further sustain the hypothesis of a cold environment characterised by sparse or absent vegetation cover. Altogether, the environmental proxy data and IRSL dating of this lower part of the studied sequence (COT1 and COT2, Table 4) imply correlation to the periods of severe cooling with the S3 stadial (MIS 4). This evidence is further completed by the information provided by the sedimentary data recorded in L.12. Indeed the coarse fraction of this layer reveals that the sediment source of this deposit is not only limited to physical breakdown of the limestone hosting the cavity. As such, the thickness of this layer, the wide variety of stone fragments, their morphology, and particularly the allochthonous and rolled pebbles (Fig. 9) reveal the presence of a rather thick and heterometric sediment outside the cavity that was originally deposited, at least partially, by water. Once more, the evidence of water flow, depositing coarse material in the studied geomorphological context, strengthens the hypothesis of the presence of a glacier. Layer L.12 was deposited after 67 ka. Moreover, before its deposition it has undergone pedogenetic processes. Therefore we can conclude that the deposition of the sediment source of L.12 in the surroundings of the cavity also occurred during the severe cold period of S3 stadial (MIS 4).

To summarise, during the S3 stadial the studied landscape was occupied by ice masses and thick associated deposits. In this environment the seasonal meltwater deposited the finer sediments of L.14 and L.13 inside the cavity and possibly reworked the upper part of the brown layer, sampled as L.15 here. Similarly accumulation of heterometric sediment (source of L.12) at the entrance of the cave and on the surrounding slopes was related to ice-marginal debris supply resulting in the deposition of lateral moraine or kame terraces. The petrographic data suggest that this glacier was of local (Jura Mountains) origin. The very few alpine elements can be well explained as reworking of deposits of older glacial material, which extended westward beyond the LGM (Campy, 1992) and were also mapped in the neighbourhood of the studied region (Méia and Becker, 1976; Pasquier et al., 2013).

This climatic cooling of MIS 4 is rarely evidenced in the regional terrestrial record. Two sites witnessing glacier advances have been reported: in the northern Alpine foreland at Finsterhennen glacier-outwash deposits have been dated to about 70 ka (Preusser et al., 2007), while in the Jura Mountains recent studies of an outcrop at Arçon also described glacio-fluviatile sediments situated under organic sediments dated to ca. 48 ka and interpreted as possibly deposited during this period (Bichet et al., 2016). As such the Cotencher sedimentary record represents additional evidence for this rarely recorded climatic event in terrestrial context and its importance lies also in its geographical position, situated between the above-mentioned locations (Fig. 1).

It is interesting to mention that the hypothesis of glacial sedimentation in front of the cavity has already been formulated by Dubois and Stehlin (1932/1933). Similar to our reasoning, they tried to understand the presence of the wide variety gravels in the *couche à galets*. They concluded that only the presence of a glacier, different from the one known for the main Würmian with an alpine source, could explain waterlaid deposits high above the valley bottom. Based on the scientific data of their time, they interpreted this glacier activity ("Areuse precursor glaciation") as representing a cooling that occurred before the LGM-dated Rhone glacier conquered the Alpine foreland and the slope of the Jura Mountains (Dubois and Stehlin, 1932/1933).

5.3   Alternation of pedogenetic and cryogenic processes during MIS 3

Layers L.12 and L.11 witness evolution outside and recurrent sediment transport towards the cavity. The organic matter accumulation and the associated $CaCO_3$ content trends, the slight weathering of the limestone fragments, and the notable presence of pedogenetic minerals, particularly in its lower part, indicate that the sediment generating L.12 was affected by pedogenetic processes; thus it evolved outside the cavity. As indicated by $CaCO_3$ and organic carbon content, the soil-forming processes affected the lower part of the deposit more strongly than its upper part (particularly L.12b, but also L12c). The same chemical soil properties suggest a perceptible weakening of the impact of the pedogenetic processes in the upper part of the deposit (L.12a) as well as in L.11.

Subsequently the heterometric soil sediments were transported into the cavity. As explored earlier (Dubois and Stehlin, 1932/1933) the karstic chimneys of the cavity are completely plugged by metres of limestones; therefore the coarse deposit must have been transferred by horizontal transport. Although some fine material might have been deposited by water seepage through karstic fissures of the cavity roof, the morphology of the deposits (intermixed coarse and granular fine fraction, absence of stratification, homogeneous presence of granular, humiferous fine material) indicate deposition by mass movement, in which the fine and

coarse materials were transported together. In addition, the distinct layering (L.12c to L.12a,) observed both in 2016 and by former studies (Dubois and Stehlin, 1932/1933; Rentzel, 1990) and the presence of a considerable amount of organic matter clearly indicate that deposition of this sediment occurred in several phases. Solifluction processes and soil creep triggered by repeated intensive freezing conditions and the presence of frozen ground (Bertran et al., 1997) can best explain the morphology of the L.12 and its characteristics, such as (i) the heterometric nature of the deposit, (ii) rounded allochthonous gravels associated with more angular, more or less polished local limestone fragments, and (iii) homogeneous distribution of the organic material throughout a 180 cm thickness. The L.11, occurring only at the entrance of the cavity, might be a solifluction deposit.

To conclude, L.12 and L.11 are the result of combined deposition of heterometric soil sediments stemming from the cavity entrance and of fragments resulting from the physical breakdown of the limestone hosting the cavity. They record multiple cycles of alternation of soil formation processes and frost-related sedimentation that occurred after ca. 67 ka and before ca. 36 ka. This period corresponds to the time span of Gossau PAZ2 to Gossau PAZ5 (Preusser et al., 2003), i.e. roughly to the major part of MIS 3 (Fig. 10). For this period, environmental archives support an ice-free but fluctuating cold and milder climate with changing ecosystems alternating among coniferous forest, steppe, and tundra (Preusser et al., 2003; Drescher-Schneider et al., 2007; Becker et al., 2013; Bichet et al., 2016).

The sediment and soil characteristics of L.12 and L.11 are in good agreement with these environmental trends, showing regular organic matter accumulation and some decarbonatation outside the cavity during milder climatic conditions. This was followed by destabilisation of vegetation cover and of soils and physical breakdown of the ceiling during cooler phases. The reworking of these pedosediments towards the cavity suggests repeated periods of frozen subsoils enabling soil creep processes. The numerous faunal remains found all over this layer (Dubois and Stehlin, 1932/1933) also confirm the hypothesis of cyclic soil formation processes and recurrent deposition over a long time span. Whereas the large mammal remains indicate a wide variety of ecosystems (Table 2), the rodent remains are heliophile and forest species (Table 3). A brief pollen study (Bezat, 1990) revealing the dominance of the arboreal and shrub pollen in one sample of L.12 further confirms at least one phase of interstadial climatic conditions.

Based on their stratigraphic position, the soils generating L.12c and L.12b, characterised by marked pedogenetic transformations, can be possibly correlated to the phases Gossau PZ2 and PZ4, respectively. Their transport in the cavity could be related to the colder conditions that are known as Gossau PZ3 and PZ5 (Fig. 10). The upper part of L.12 (L12a) and L.11 show less distinct pedogenetic processes (significant organic matter decrease, the noteworthy CaCO$_3$ and coarse

fraction augmentation). This can be best explained by the more and more important cooling that occurred during the passage towards the LGM. The soil formation and sedimentation trends described here present strong similarities with those described for the Ferrassie rock shelter record in SW France (Bertran et al., 2008) and this highlights the potential of terrestrial sediments to document gradual environmental changes.

5.4 Glacier processes during the Last Glacial Maximum

In the sedimentary record of Cotencher cave the advent of the LGM is marked by the gully incision towards the entrance of the cavity that erodes the upper part of the porous and heterometric sediments of L.12 and deposits the coarse sediment of L.10. Torrential flow at this landscape position (ca. 140 m above the valley bottom) can only be explained by the presence of a glacier that was accompanied by meltwater at its margin and frozen ground in the surroundings. The incision process was followed by the formation of a pond with fine material sedimentation (L.9) and this is a further indication of frozen grounds. This slow deposition was followed by more or less dynamic overland or concentrated water flow (L.8). All these deposits underwent severe and repeated freeze–thaw processes as indicated by the cryoturbation features. This cluster of sedimentary and morphological evidence reveals severe climatic deterioration, the quasi absence of vegetation, and the presence of a glacier in the surroundings. Petrographic data (Table 6, Fig. 9) suggest that a local glacier occupied parts of the Areuse canyon. Our data are in good agreement with Pasquier et al. (2013), who documented till deposits composed of gravels of local origin underlying fine sediments and tills of alpine origin. The timing of these events triggered by the local glacier is about 36.6 ± 3.8 ka (COT-3) and gives a novel and valuable chronological indication for an early onset of a glacial environment in the Jura Mountains, more precisely in the Travers Valley. This date is several thousand years older than those known in the lowlands of the northern Alpine foreland. At Finsterhennen (ca. 40 km from the site), the northern lobe of the Rhone glacier started to deposit proglacial sediments at about 30 ka (Preusser et al., 2007). Similarly, higher up in the Jura Mountains, the landscape was also not yet covered by ice, as is indicated by dates provided by various faunal records. Indeed, at the Baume de Longaigue (820–920 m), situated higher up in the studied valley, an ibex bone has been accelerator mass spectrometry (AMS) dated to 34 840 ± 340 BP (Leesch et al., 2013) and an open landscape suggesting faunal assemblage found in a cave at La Chaux-de-Fond (1020 m, Fig. 1) has been AMS dated to 32 590 ± 630 BP (Oppliger, 2010, in Leesch et al., 2013).

This apparent relatively early formation of a local glacier in the Areuse canyon was possibly due to its particular geomorphological, climatic, and microclimatic conditions in a severely cooling regional climate. As highlighted by Buon-

cristiani and Campy (2011), the morphology of some of the valleys in the Jura Mountains, the average cool conditions, and the exposure to northeast winds created sufficiently arctic conditions for local glacier development. The importance of the local geomorphological factors is still evident in the present-day climatic conditions. Indeed, higher up in the valley the sunshine-sheltered "Creux-du-Van" setting is a place where a ca. 20 m thick permafrost still exists in the scree situated under the mountain cliff at about 1200 m (Pancza, 1988/1989; Delaloy and Reynard, 2001). This location could have been the place of birth of the local glacier that invaded the valley downstream and caused sediment deposition at the level of the studied site. Furthermore, the Jura Mountains are a geomorphological barrier for the Atlantic humid air masses, and the high precipitation associated with low evapotranspiration was probably an additional factors triggering early local glacier development.

The first phase of erosion–sedimentation processes revealing the existence and closeness of a local glacier was followed by the deposition of L.7. The transition from the underlying pond environment is gradual and reveals a glaciolacustrine setting. The analytical data further support an environment with no or scarce vegetation cover. The stratigraphic position and the dating performed indicate that this sedimentation took place between ca. 36.6 ± 3.8 and 30.0 ± 3.0 ka (COT3, COT4), thus just prior to the LGM and in continuity of sedimentary processes discussed for L.10 to L.8. The deep freeze–thaw processes were probably very active and the cryoturbation processes recorded by the underlying L.8 and L.9 are probably related at least partially to this period. The deposition of L.7 corresponds to the expansion of glaciers of the LGM in both the Jura and the northern Alpine foreland (Preusser, 2004; Preusser et al., 2011). However the continuous fine sediment accumulation indicates that the surroundings of the cave were not yet completely covered by ice, but torrential water flow associated with its margins was replaced by calmer overland and lateral water flow processes.

A break in the fine sediment input is recorded by the L.6. This period, which lasted from about 30.0 ± 3.0 to 26.5 ± 2.8 ka (COT4, COT5) was characterised inside the cave by intensive (cryo)shattering of the cave roof and the formation of ice wedge in the already existing sediments. The sedimentary hiatus unravelled here can be interpreted as an indication that the cavity entrance was plugged by ice and/or sediment.

The next sedimentary phase materialised by L.5 indicates renewed overland water flow possibly accompanied by aeolian sediment input in an environment with absent or little vegetation cover. The accumulation of this sediment was also accompanied by frost shattering of the limestones hosting the cavity and deep freeze–thaw processes. These processes started at about 26.5 ± 2.8 ka (COT5) but we do not have data to further constrain the time span of this sediment accumulation. The onset of sedimentary processes and the absence of vegetation cover might be interpreted as (i) evidences of

deglaciation at the level of the cave or (ii) the sedimentary fingerprint of the complex processes associated with the passage between the local glacier and the alpine glacier. This date is consistent with existing chronological evidences that expect the start of deglaciation at the maximum extent of the Rhone glacier not later than 24 ± 2 ka (Ivy-Ochs, 2015). First vegetation re-colonisation in the lowlands around Neuchâtel Lake is estimated at around 19 ka (Thew et al., 2009).

The sediments of L.10, L.9, L.7, L.8, L.6, and L.5 thus show some important phases of the sedimentary dynamics that occurred in the studied region and at the level of the site during the LGM: (i) presence of a local glacier at the altitudes close to Cotencher cave at about 36.6 ± 3.8 ka triggering erosion processes and sediment deposition, (ii) followed by the growth of the ice body, filling up the valley at the level of the cavity entrance accompanied by a sediment hiatus that lasted from ca. 30.6 ± 3.0 to 26.5 ± 2.8 ka and (iii) fine material sedimentation in an environment with no vegetation cover post 26.5 ± 2.8 ka. A succession of a local till overlaid by glaciolacustrine sediments followed by till of alpine origin covered by glaciolacustrine sediments is documented in cores and outcrops situated upstream of the site (Pasquier et al., 2013; Mojon et al., 2015). The sedimentary evidences and chronological data provided here complete this geological record and bring novel elements into the knowledge and timing of the regional glaciation history.

5.5 Dynamics of human activities

The new chronological and environmental information combined with available archaeological data permit us to readdress the question of the nature, location, and timing of human presence at Cotencher cave and its surroundings. This subject concerns three aspects: the nature of this activity, its location, and its timing.

In the review of Mousterian occupation of the Jura Mountains, Detrey (2013) concludes that the Travers Valley was used not only as passage for Palaeolithic people, but this internal part of the mountain chain was also a place of exploitation of lithic resources and rich in potential prey. The techno-economic analyses of the lithic assemblage of Cotencher cave have been interpreted as indicating temporary dwelling under the rock shelter, with a mixed economic vocation (production and consumption of blanks) that was possibly frequented on several occasions (Bernard-Guelle, 2004). Our study confirms that the tools found in earlier excavations can be characterised as Charentian Mousterian of oriental Quina type. Moreover, the study of the material collected in 2016 unravels the presence of numerous chips witnessing debitage (or flaking) operations, the manufacturing and sharpening of tools at the level of the site. The faunal remains analysed so far could not reveal any unequivocal trace of anthropic action; thus the bone assemblage does not permit further discussion of the nature of human activity.

The location of the human activity remains difficult to assess. Dubois and Stehlin (1932/1933, p. 189) mentioned charcoal and burned stones without lithic tools at the bottom of the cave in the lower part of the brown layer. They interpret these finds as the remains of two fireplaces and if this assumption was correct it would imply an occupation pre-dating 67 ka. The lithic artefacts are present in the deposits situated under L.15 (brown layer) and in L.12 (gravelly layer). The brown layer contains only a minor amount of this find (Table 1) and according to the available data it is mostly situated in the upper part of it. This imprecise information does not permit us to assert the timing of the human activity materialised by the tools found in this stratigraphic unit. Indeed several hypotheses can be formulated, but none of them can be eliminated: (i) they could have been reworked from outside during the deposition of the brown layer or of the L.15 and L.16, and thus might be older than 67 ka; (ii) they might be the results of in situ activity inside the cavity during or by the end of the accumulation of this layer but before the deposition of L.14 and L.13, thus once more reflecting human activity older than 67 ka; (iii) they could be stemming from the overlying L.12 due to bioturbation or cryoturbation processes and in this case they would be the reworked traces of the seasonal anthropic activity, which took place at the level of the rock shelter between ca. 67 and 36 ka. As for the L.12, although burned stones and bones were regularly observed in this layer, so far there are no elements clearly supporting in situ human activity inside the cavity. In absence of these features, we can only formulate that the lithic tools were used at the external rock shelter part of the site and they were deposited as part of L.12 during multiple processes of soil creep that occurred over a time span of some 10 000 years, i.e. after the deposition of the sediment source of L.12 at around 72 ka and before 36 ka. The study of vestiges found in 2017 might give arguments to complete this interpretation.

Based on the study of the lithic industry, Bernard-Guelle (2004) concludes that the lithic artefacts that are spread all over the two find layers (red and gravelly layer) are possibly related to the reworking of one single archaeological level, located initially at the entrance of the cavity. The sedimentological study performed here contests this interpretation. First of all, these two layers have considerably different sedimentological and pedological characteristics and they have been deposited during distinct and rather distant time frames. In addition, sediments supporting the development of a glacier, reaching more or less the level of the cavity, separate the two layers that contain the lithic and faunal finds. As developed here above, the brown layer has been deposited and evolved inside the cavity after the last interglacial and before ca. 67 ka. The sedimentation of L.12 in the cavity post-dates the marked cooling at about 67 ka and it occurred during multiple phases up to about 36 ka. The soil characteristics of this reworked sediment suggest several distinct phases of pedogenetic evolution outside the cavity. As a consequence the artefacts reworked inside the cavity through the successive mass movements are, at least partially, related to recurrent human activity on the soil surface at the entrance of the cavity, over a time span of several thousands of years.

The climatic fluctuations unravelled here also permit us to modestly complete the already existing considerations concerning the relationship between the succeeding climates and distribution of the Palaeolithic sites in the studied region. The Mousterian sites, although not numerous, are present on both sides of the Jura Mountains (Le Tensorer, 1998; Tillet, 2000, 2001; Detrey, 2013). The marked dissymmetry in the frequency of sites between the northwester slopes (more abundant) and southeaster flanks (scarce) has been explained (i) by the erosion processes more active on the Helvetic side due to the glacier passage during the LGM and (ii) by the more abundant silex outcrop on the French side. Moreover, Detrey (2013) highlights the fact that among the sites post-dating MIS 5, there is a hiatus corresponding to MIS 4 and the early part of MIS 3. The Cotencher data acquired here might at least partially explain this fact. As discussed above, around 67 ka a local glacier developed at the level of the cave, but likely also in some other parts of the Jura Mountains (Bichet et al., 2016). The erosion triggered by this glacier passage, as well as the hostile landscape, non-suitable for anthropic activity, could be the cause of this hiatus. As for the early Upper Palaeolithic sites (Aurignacian, Gravettian), they are completely absent in the Jura Mountains (Leesch et al., 2013) and in Switzerland (Cattin et al., 2009; Leesch and Bullinger, 2013). In addition to the erosion processes induced by the glaciers of the LGM, the relatively limited prospection and research programs are thought to be possibly responsible for this lack (ibid). Nevertheless it seems that the Jura Mountains represented a barrier region that the people preferred to avoid during the Upper Palaeolithic in the Jura Mountains (Leesch and Bullinger, 2013). Once more the sedimentary and chronological evidences of the deposits accumulated in Cotencher cave support this fact. The local glacier was active at the level of the cavity as early as ca. 36.1 ± 3.5 ka (COT3) and a glacio-lacustrine type of sedimentation was active at least up to 26.5 ± 2.8 ka (COT1). This environmental setting was once more not attractive for the hunter–gatherer populations.

6 Conclusions

The interdisciplinary study of the sedimentary fill of Cotencher cave permitted us to unravel and date several significant environmental changes encoded in these deposits. According to this, two periods of glacier development are documented for the Late Pleistocene. Compared to the chronology known for alpine glaciers advancing into the lowlands, a particular early development of a local glacier is apparently revealed for the LGM. These data imply new elements for the understanding of the dynamics of this major climatic change. As for the climatic deterioration of MIS 4, the Cotencher sed-

iments support a local glacier build-up and these data complete the scarce regional terrestrial record. The new archaeological information clearly reveals manufacturing and sharpening activities of Mousterian tools at the level of the site. Although it is still not possible to delimit the precise location of the various occupations, this study points out two of their characteristics: (i) at least part of them occurred at the entrance rock shelter part of the cavity and (ii) a repeated visiting of the site occurred over a long time span. The integration of the sedimentological and chronological data also permitted us to formulate a hypothesis concerning some of the questions raised about the dynamics of human passage in the studied region. According to our data the particular hostile glacier landscape explains, at least partially, the absence of traces of human activity for both the period of MIS 4–early MIS 3 and the early Late Palaeolithic.

Data availability. Most of the underlying data are included in the paper. Our site is still under study as part of a larger project of the Neuchâtel Archaeological Service. For this reason part of our underlying data are not yet publicly available.

References

Adatte, T., Rentzel, P., and Kübler, B.: Etude minéralogique et sédimentologique du remplissage de la grotte de Cotencher (Jura neuchâtelois, Suisse), Eclogae Geol. Helv., 84, 671–688, 1991.

Angelucci, D. E., Anesin, D., Susini, D., Villaverde, V., Zapata, J., and Zilhão, J.: Formation processes at a high resolution Middle Paleolithic site: Cueva Antón (Murcia, Spain), Quaternary Int., 315, 24–41, 2013.

Auclair, M., Lamothe, M., and Huot, S.: Measurement of anomalous fading for feldspar IRSL using SAR, Radiat. Meas., 37, 487–492, 2003.

Bay, R.: Der menschliche Oberkiefer aus der Grotte de Cotencher (Rochefort, Neuchâtel, Suisse), Archives suisses d'anthropologie générale, 451, 57–101, 1981.

Becker, D., Oppliger, J., Thew, N., Scherler, L., Aubry, D., and Braillard, L.: Climat et écologie en Ajoie durant la second partie du Pleniglaciaire moyen weichsélien: apport des remplissage des dolines de Courtedoux-Vâ Tche Tchâ (Jura, CH), in: Le peuplement de l'Arc jurassien de la Préhistoire au Moyen Âge. Actes des deuxièmes journées archéologiques frontalières de l'Arc jurassien, Delle (F) -Boncourt (CH), edited by: Richard, A., Schifferdeccker, F., Mazimann J.-P., and Bélet-Gonda, C., 16–18 November 2007, Presses Universitaire de Franche-Compté, Besançon, 13–23, 2013.

Bernard-Guelle, S.: Un site moustérien dans le Jura suisse: la grotte de Cotencher (Rochefort, Neuchâtel) revisitée, Bulletin de la Société préhistorique Française, 101, 741–769, 2004.

Bertran, P., Hétu, B., Texier, J.P. and Steijn, H.: Fabric characteristics of subaerial slope deposits, Sedimentology, 44, 1–16, 1997.

Bertran, P., Caner, L., Langohr, R., Lemée, L., and d'Errico, F.: Continental palaeoenvironments during MIS 2 and 3 in southwestern France: the La Ferrassie rockshelter record, Quaternary Sci. Rev., 27, 2048–2063, 2008.

Bezat, E.: Analyse pollinique, Cotencher Sondage 1988 – P1, in: Neue quatärgeologische Untersuchungen an den Höhlensediementen von Cotencher (Kt. NE), edited by: Renztel, P.,

Labor für Ur- und Frühgeschichte der Universität Basel, 76–81, 1990.

Bichet, V., Buoncristiani, J.-F., and Ravier, É.: Identification de sédiments du stade isotopique 3 (OIS-3) dans les formations proglaciaires du haut Jura, in: De la reconstitution des paysages à l'histoire des sociétés, edited by: Barral, P. M. M. and Ravier E., 10 000 d'archives sédimentaires en zones humides, Infolio, Gollion, Switzerland, 19–27, 2016.

Bini, A., Buoncristiani, J. F., Coutterand, S., Ellwanger, D., Felber, M., Florineth, D., Graf, H. R., Keller, O., Kelly, M., Schlüchter, C., and Schoeneich, P.: Die Schweiz während des letzteiszeitlichen Maximum (LGM) 1 : 500 000, Carte et notice, Bundesamt für Landestopografie Swisstopo, Wabern, 2009.

Blant, M. and Deriaz, P.: Le gisement paléontologique du Pléistocène supérieur de la grotte du Balai (Saint-Croix, Vaud), Stalactite supplément, 16, 155–158, 2007.

Boschian, G., Gerometta, K., Ellwood, B. B., and Karavanić, I.: Late Neandertals in Dalmatia: Site formation processes, chronology, climate change and human activity at Mujina Pećina, Croatia, Quaternary Int., 450, 12–35, 2017.

Braillard, L., Guélat, M., and Rentzel, P.: Effects of bears on rock-shelter sediments at Tanay Sur-les-Creux, southwestern Switzerland, Geoarchaeology, 19, 343–367, 2004.

Bullock, P., Fedoroff, N., Jongerius, A., Stoops, G., and Tursina, T.: Handbook for soil thin section description, Waine Research, Wolverhampton, 1985.

Buoncristiani, J.-F. and Campy, M.: Quaternary Glaciations in the French Alps and Jura, in: Ehlers, J., Gibbard, P. L., and Hughes, P. D., Developments in Quaternary Science. Quaternary glaciations – extent and chronology, Elsevier, Amsterdam, the Netherlands, 117–126, 2011.

Buylaert, J. P., Murray, A. S., Thomsen, K. J., and Jain, M.: Testing the potential of an elevated temperature IRSL signal from K-feldspar, Radiat. Meas., 44, 560–565, 2009.

Buylaert, J. P., Jain, M., Murray, A. S., Thomsen, K. J., Thiel, C., and Sohbati, R.: A robust feldspar luminescence dating method for Middle and Late Pleistocene sediments, Boreas, 41, 435–451, 2012.

Campy, M.: Palaeogeographical relationship between Alpine and Jura glaciers during the two last Pleistocene glaciation, Palaeogeogr. Palaeocl., 93, 1–12, 1992.

Castel, J.-C.: The faunal remains at Roc-de-Marsal and game exploitation in the Mousterian of Southwest France, Variability in Human Hunting Behavior during Oxygen Isotope Stages 4/3: Implications for Understanding Modern Human Origins. ICAZ Paris 2010, S5, 4, 2010.

Castel, J.-C., Luret, M., and Chaix, L.: Hommes et bêtes au Moustérien, in: La Haute-Savoie durant la Préhistoire, edited by: Serralongue, J., Culture 74/08, Haute-Savoie, 60–64, 2012.

Castel, J.-C., Discamps, E., Soulier, M.-C., Sandgathe, D., Dibble, H. L., McPherron, S. J. P., Goldberg, P., and Turq, A.: Neandertal subsistence strategies during the Quina Mousterian at Roc de Marsal (France), Quaternary Int., 433, 140–156, 2017.

Cattin, M.-I., Affolter, J., and Thew, N.: Provenance de diverses matières premières: un indice pour définir circulations et territoires au Magdalénien supérieur en Suisse, in: Le concept de territoires dans le Paléolithique supérieur européen, edited by: Djindjian F., Kozlowski, J., and Bicho, N., actes 15e Congrès

UISPP, Lisbonne, September 2006, Oxford BAR S1938, Lisbonne, 157–165, 2009.

Chauvière, F.-X., Cattin, M.-I., Deák, J., and Brenet, F.: Le petit racloir moustérien: un retour à la grotte paléolithique de Cotencher (Rochefort, NE), Nike-Bulletin, 1, 32–35, 2018a.

Chauvière, F.-X., Deák, J., Cattin, M.-I., Brenet, F., Juillard, M., Castel, J.-C., Oppliger, J., and Preusser, F.: La grotte de Cotencher: une (pré)histoire humaine et naturelle. Archéologie Suisse: Neuchâtel les nouvelles voies de l'archéologie, Archéoloogie Suisse, 41, 16–20, 80, 2018b.

Chauvière, F.-X., Deák, J., Cattin, M.-I., Brenet, F., Juillard, M., Castel, J.-C., Oppliger, J., and Preusser, F.: Die Höhle von Cotencher: eine menschliche und natürliche (Vor-)Geschichte, Archäologie Schweiz: Neuenbourg, neue Wege der Archäologie, Archäologie Schweiz, 41, 16–20, 80, 2018c.

Crotti, P.: Le peuplement paléolithique et mésolithique de la Suisse: la question de l'utilisation des étages montagnards dans les Alpes, Geogr. Helv., 63, 167–175, https://doi.org/10.5194/gh-63-167-2008, 2008.

Cupillard, C., Magny, M., Bocherens, H., Bridault, A., Bégeot, C., Bichet, V., Bossuet, G., Drucker, D. G., Gauthier, E., Jouannic, G., Millet, L., Richard, H., Rius, D., Ruffaldi, P., and Walter-Simonnet, A.-V.: Changes in ecosystems, climate and societies in the Jura Mountains between 40 and 8 ka cal BP, Quaternary Int., 378, 40–72, 2015.

Deák, J.: Geoarchäologie oder das „Gedächtnis der Böden", Archäologie Schweiz: Neuenbourg, neue Wege der Archäologie, Archéologie Suisse, 41, 36–40, 80, 2018a.

Deák, J.: La géoarchéologie ou la mémoire des „sols", Archéologie Suisse: Neuchâtel les nouvelles voies de l'archéologie, AS, 41, 36–40, 80, 2018b.

Delaloy, R. and Reynard, E.: Les éboulis gelés du Creux du Van (Chaîne du Jura, Suisse), Environnements Périglaciaire, 8, 118–129, 2001.

De Rougemont, D.: Monnaies trouvées lors des fouilles de 1917 à Cotencher NE, Gazette numismatique suisse, 28–32, 100–104, 1982.

Desor, E.: Théorie de l'époque glaciaire, Congrès International d'Anthrolpologie et d'archéologie préhistorique, Compte rendu de la 2eme session, Paris, 1867, Paris C. Reinwald, Libraire-éditeur, 275–276, 1868.

Desor, E.: Essai d'une classification des cavernes du Jura, Bulletin de la Société des Sciences Naturelles de Neuchâtel, 9, 69–87, 1872.

Detrey, J.: Nouvelles données sur le Paléolithique moyen dans le canton du Jura (Suisse), Revue Archéologique de l'Est, 59, 7–45, 2010.

Detrey, J.: Présence moustérienne dans l'arc jurassien: un état de la question, in: Deuxièmes journées archéologiques frontalières de l'Arc jurassien. Actes, Le peuplement de l'Arc jurassien de la Préhistoire au Moyen Âge. Besançon, edited by: Richard, A., Schifferdeccker, F., Mazimann J.-P., and Bélet-Gonda, C., Presses Universitaires de Franche-Comté et Porrentruy, Office de la culture et Société jurassienne d'émulation, Delle, France – Boncourt, Switzerland, 16–18 November 2007, 41–70, 2013.

Drescher-Schneider, R., Jacquat, C., and Schoch, W.: Palaeobotanical investigations at the mammoth site of Niederweningen (Kanton Zürich), Switzerland, Quaternary Int., 164–165, 113–129, 2007.

Dubois, A.: Note sur les fouilles exécutées en 1916 dans la grotte de Cotencher, Le Rameau de sapin, IIème série, 14–15, 1917.

Dubois, A.: Les fouilles de la grotte de Cotencher, Le véritable messager boiteux de Neuchâtel, 72–74, 1918.

Dubois, A.: Les Fouilles de la Grotte de Cotencher, Actes de la Société Helvétique des Sciences, 101, 99–122, 1920.

Dubois, A. and Stehlin, H. G.: La grotte de Cotencher: station moustérienne, Emil Birkhaeuser&Cie, Bâle, 1932/1933.

Duller, G. A. T.: Single-grain optical dating of Quaternary sediments: why aliquot size matters in luminescence dating, Boreas, 37, 589–612, 2008.

Egloff, M.: Musée cantonal d'archéologie, Ville de Neuchâtel, Bibliothèques et musées, 1975, 91–95, 1976.

Egloff, M.: Des premiers chasseurs au début du christianisme Histoire du Pays de Neuchâtel, 1. De la préhistoire au Moyen-Age, Attinger, Neuchâtel, 9–160, 1989.

Feathers, J. K.: Luminescence dating and modern human origins, Evol. Anthropol.-Issues, News, and Reviews, 5, 25–36, 1996.

Furrer, H., Graf, H. R., and Mäder, A.: The mammoth site of Niederweningen, Switzerland, Quaternary Int., 164–165, 85–97, 2007.

Gaar, D. and Preusser, F.: Luminescence dating of mammoth remains from northern Switzerland, Quaternary Geochronol., 10, 257–263, 2012.

Gaar, D., Lowick, S. E., and Preusser, F.: Performance of different luminescence approaches for the dating of known-age glaciofluvial deposits from northern Switzerland, Geochronometria, 41, 65–80, 2014.

Galbraith, R. F., Roberts, R. G., Laslett, G. M., Yoshida, H., and Olley, J. M.: Optical dating of single and multiple grains of quartz from Jinmium rock shelter, Northern Australia: part I, experimental design and statistical models, Archaeometry, 41, 339–364, 1999.

Gigon, R.: Inventaire Spéléologique de la Suisse, tome 1: Canton de Neuchâtel, Commission de Spéléologie de la Société helvétique des Sciences Naturelles, Neuchâtel, 1976.

Goldberg, P. and Macphail, R. I.: Caves and rockshelters, in: Practical and theoretical geoarchaeology, edited by: Goldberg, P. and Macphail, R., Blackwell Publishing, Malden, 169–187, 2006.

Goldberg, P., Schiegl, S., Meligne, K., Dayton, C., and Conard, N. J.: Micromorphology and site formation at Hohle Fels Cave, Swabian Jura, Germany, Eiszeitalter und Gegenwart, 53, 1–25, 2003.

Graf, A. A., Strasky, S., Ivy-Ochs, S., Akçar, N., Kubik, P. W., Burkhard, M., and Schluchter, C.: First results of cosmogenic dated pre-Last Glaciation erratics from the Montoz area, Jura Mountains, Switzerland, Quaternary Int., 164–165, 43–52, 2007.

Guérin, G., Valladas, H., Joron, J.-L., Mercier, N., Reyss, J.-L., and Zaidner, Y.: Apports de la datation par la luminescence des sites du Proche-Orient et résultats préliminaires du site de Nesher Ramla (Israël), L'Anthropologie, 121, 35–45, 2017.

Hajdas, I.: Radiocarbon dating and its applications in Quaternary studies, E&G Quaternary Sci. J., 57, 2–24, https://doi.org/10.3285/eg.57.1-2.1, 2008.

Hajdas, I., Bonani, G., Furrer, H., Mäder, A., and Schoch, W.: Radiocarbon chronology of the mammoth site at Niederweningen, Switzerland: Results from dating bones, teeth, wood, and peat, Quaternary Int., 164–165, 98–105, 2007.

Heiri, O., Koinig, K. A., Spötl, C., Barrett, S., Brauer, A., Drescher-Schneider, R., Gaar, D., Ivy-Ochs, S., Kerschner, H., Luetscher, M., Moran, A., Nicolussi, K., Preusser, F., Schmidt, R., Schoeneich, P., Schwörer, C., Sprafke, T., Terhorst, B., and Tinner, W.: Palaeoclimate records 60–8 ka in the Austrian and Swiss Alps and their forelands, Quaternary Sci. Rev., 106, 186–205, 2014.

Higham, T.: European Middle and Upper Palaeolithic radiocarbon dates are often older than they look: problems with previous dates and some remedies, Antiquity, 85, 235–249, 2015.

Huntley, D. J. and Baril, M. R.: The K content of the K-feldspars being measured in optical dating or in thermoluminescence dating, Ancient TL, 15, 11–13, 1997.

Huntley, D. J. and Lamothe, M.: Ubiquity of anomalous fading in K-feldspars and the measurement and correction for it in optical dating, Can. J. Earth Sci., 38, 1093–1106, 2001.

Ivy-Ochs, S.: Glacier variations in the European Alps at the end of the last glaciation, Cuadernos de investigación geográfica, 41, 295–315, 2015.

Ivy-Ochs, S., Kerschner, H., Reuther, A., Preusser, F., Heine, K., Maisch, M., Kubik, P. W., and Schlüchter, C.: Chronology of the last glacial cycle in the European Alps, J. Quaternary Sci., 23, 559–573, 2008.

Jacobs, Z. and Roberts, R. G.: Advances in optically stimulated luminescence dating of individual grains of quartz from archeological deposits, Evol. Anthropol.-Issues, News, and Reviews, 16, 210–223, 2008.

Lee, M. K., Lee, Y. I., Lim, H. S., Lee, J. I., Choi, J. H., and Yoon, H. I.: Comparison of radiocarbon and OSL dating methods for a Late Quaternary sediment core from Lake Ulaan, Mongolia, J. Paleolimnol., 45, 127–135, 2011.

Leesch, D. and Bullinger, J.: Le Plateau suisse et le massif du Jura pendant le Paléolithique supérieur ancien: paléoenvironnment et indices d'occupation humaine, Mémoire LVI de la Société préhistorique française, Le Paléolithique supérieur ancien de l'Europe du Nord-Ouest, 385–394, 2013.

Leesch, D., Bullinger, J., and Cupillard, C.: Le peuplement de l'arc jurassien au Paléolithique supérieur, Le peuplemenr de l'Arc jurassien de la Préhistoire au Moyen Âge, Actes des deuxièmes journées archéologiques frontalières de l'Arc jurassien, Delle, France – Boncourt, Switzerland, 16–18 November 2007, Presses universitaire de Franche-Comté., Annales Littéraires de l'Université de Franche-Compté, série Environnement, sociétés et archéologie 17, Cahier d'archéologie jurassienne, 21, 71–84, 2013.

Le Tensorer, J.-M.: Méthodologie et chronologie La Suisse du Paléolithique à l'aube du Moyen-Age. De l'Homme de Néandertal à Charlemagne, 1. Paléolithique et Mésolithique, Société suisse de préhistoire et d'archéologie, Bâle, 15–38, 1993.

Le Tensorer, J.-M.: Le Paléolitique en Suisse, Jérôme Millon, Grenoble, 1998.

Lisiecki, L. E. and Raymo, M. E.: A Pliocene-Pleistocene stack of 57 globally distributed benthic δ^{18}O records, Paleoceanography, 20, 1–17, 2005.

Lowick, S. E., Trauerstein, M., and Preusser, F.: Testing the application of post IR-IRSL dating to fine grain waterlain sediments, Quaternary Geochronol., 8, 33–40, 2012.

Lowick, S. E., Buechi, M. W., Gaar, D., Graf, H. R., and Preusser, F.: Luminescence dating of Middle Pleistocene proglacial deposits from northern Switzerland: methodological aspects and stratigraphical conclusions, Boreas, 44, 459–482, 2015.

Mathieu, C. and Pieltain, F.: Analyse chimique des sols, Méthodes choisies, Edition Tec and Doc Paris, 2003.

Méia, J. and Becker, F.: Notice explicative et feuille 1164, Neuchâtel, Commission géologique suisse, 1976.

Météosuisse: Evapotranspiration nach Primault. Neuchâtel, 485 m. 1996–2005, Météosuisse, Geneve, Switzerland, 2005.

Météosuisse: Normes climatologique La Brévine (1961–1990), Chaumon (1961–1990), Neuchâtel (1961–1990), La Chaux-de-Fonds (1901–1980), Météosuisse, Genève, Switzerland, 2016.

Miéville, H.: Cotencher. Dictionnaire historique de la Suisse (DHS), available at: http://www.hls-dhs-dss.ch/textes/f/F12556.php (last access: 1 December 2018), 2005.

Mojon, P.-O., Pasquier, F., and Emery-Barbier, A.: Micropaléontologie des dépôts lacustres Tardiglaciaires à Holocènes du Val-de-Travers et de la Vallée des ponts (Jura Suisse Nord-Occidental), Bulletin de la Société Neuchâteloise des Sciences Naturelles, 135, 51–77, 2015.

Moll, H. F.: Rochefort NE. Grotte de Cotencher, Annuaire de la Société Suisse de Préhistoire et d'Archéologie, 56, 177, 1971.

Moll, H. F.: Die Paläolitische Station von Cotencher (Rochefort NE), Kolloquium: Der fossile Mensch im schweizerischen Palaolithicum, Verhandlungen der Schweizerischen Naturforschenden Gesellschaft, Sektion Anthropologie, 6, 48–49, 1974.

Moll, H. F.: Découverte d'un maxillaire supérieur humain à la grotte de Cotencher (commune de Rochefort, canton de Neuchâtel, Suisse), Bulletin de la Société d'Etudes et de Recherches Préhistoriques des Eyzies, 26, 1–15, 1977.

Munsell Color: Munsell soil color charts, 1994, New Windsor, 1994.

Olley, J. M., Roberts, R. G., and Murray, A. S.: Disequilibria in the uranium decay series in sedimentary deposits at Allen's cave, nullarbor plain, Australia: Implications for dose rate determinations, Radiat. Meas., 27, 433–443, 1997.

Otz, H.-L.: Communication à la séance du 4 avril 1867, Bulletin de la société neuchâteloise des sciences naturelles, 7, 534–536, 1867.

Pancza, A.: Un pergélisol actuel dans le Jura Neuchâtelois, Bulletin de la Société neuchâteloise de géographie, 32–33, 129–140, 1988/1989.

Pasquier, F., Burkhard, M., Mojon, P.-O., and Gogniat, S.: Feuille 1163 Travers-Atlas géol. Suisse 1 : 25 000, Notice expl. 162, Office fédérale de topographie, Wabern, Switzerland, 2013.

Prescott, J. R. and Hutton, J. T.: Cosmic ray contributions to dose rates for luminescence and ESR dating: Large depths and long-term time variations, Radiat. Meas., 23, 497–500, 1994.

Preusser, F.: Luminescence dating of fluvial sediments and overbank deposits from Gossau, Switzerland: fine grain dating, Quaternary Sci. Rev., 18, 217–222, 1999.

Preusser, F.: Towards a chronology of the Late Pleistocene in the northern Alpine Foreland, Boreas, 33, 195–210, 2004.

Preusser, F. and Degering, D.: Luminescence dating of the Niederweningen mammoth site, Switzerland, Quaternary Int., 164–165, 106–112, 2007.

Preusser, F. and Kasper, H. U.: Comparison of dose rate determination using high-resolution gamma spectrometry and inductively coupled plasma-mass spectrometry, Ancient TL, 19, 1–24, 2001.

Preusser, F., Geyh, M. A., and Schlüchter, C.: Timing of Late Pleistocene climate change in lowland Switzerland, Quaternary Sci. Rev., 22, 1435–1445, 2003.

Preusser, F., Ramseyer, K., and Schlüchter, C.: Characterisation of low OSL intensity quartz from the New Zealand Alps, Radiat. Meas., 41, 871–877, 2006.

Preusser, F., Blei, A., Graf, H., and Schlüchter, C.: Luminescence dating of Würmian (Weichselian) proglacial sediments from Switzerland: methodological aspects and stratigraphical conclusions, Boreas, 36, 130–142, 2007.

Preusser, F., Graf, H. R., Keller, O., Krayss, E., and Schlüchter, C.: Quaternary glaciation history of northern Switzerland, E&G Quaternary Sci. J., 60, 21, https://doi.org/10.3285/eg.60.2-3.06, 2011.

Rentzel, P.: Neue quatärgeologische Untersuchungen an den Höhlensediementen von Cotencher (Kt. NE), Diplomarbeit, Labor für Ur- und Frühgeschichte der Universität Basel, 131 pp., 1990.

Rentzel, P.: Lithostratigraphie und Geochronologie der Höhlensediemente von Cotencher (Schweiz, Kt. NE), 9e Congrès national de spéléologie, Société Suisse de Spléléologie et Comission de Spéléologie ASSN, 109–112, 1992.

Richter, D., Richter, A., and Dornich, K.: Lexsyg Smart – a luminescence detection system for dosimetry, material research and dating application, Geochronometria, 42, 202–209, 2015.

Rittenour, T. M.: Luminescence dating of fluvial deposits: applications to geomorphic, palaeoseismic and archaeological research, Boreas, 37, 613–635, 2008.

Roberts, R. G.: Luminescence dating in archaeology:from origins to optical, Radiat. Meas., 27, 819–892, 1997.

Roberts, R. G., Jacobs, Z., Li, B., Jankowski, N. R., Cunningham, A. C., and Rosenfeld, A. B.: Optical dating in archaeology: thirty years in retrospect and grand challenges for the future, J. Archaeol. Sci., 56, 41–60, 2015.

Schmid, E.: Höhlenforschung und sedimentanalyse. Ein Beitrag zur Datierung des Alpinen Paläolithikums, Verlag des Institutes für Ur- und Frühgeschichte der Schweiz, Basel, 1958.

Stehlin, H.-G. and Dubois, A.: Notes préliminaires sur les fouilles entreprises dans la Grotte de Cotencher (canton de Neuchâtel), Eclogae Geol. Helv., 14, 240–242, 1916.

St Pierre, E., Zhao, J.-X., and Reed, E.: Expanding the utility of Uranium-series dating of speleothems for archaeological and palaeontological applications, J. Archaeol. Sci., 36, 1416–1423, 2009.

Taylor, R. and Bar-Yosef, O.: Radiocarbon Dating, Walnut Creek, California, Left Coast Press, Walnut Creek, California, 2014.

Thew, N., Hadorn, P., and Coope, G. R.: Hauterive/Rouges-Terres. Reconstruction of Upper Palaeolithic and Early Mesolithic natural environments, Office et musée cantonal d'archéologie, Neuchâtel, 2009.

Thomsen, K. J., Murray, A. S., Jain, M., and Bøtter-Jensen, L.: Laboratory fading rates of various luminescence signals from feldspar-rich sediment extracts, Radiat. Meas., 43, 1474–1486, 2008.

Tillet, T.: Le Moustérien dans l'arc alpin: complémentarité entre sites en grotte et sites en plein-air, in: Les Paléoalpins, hommage à Pierre Bintz, edited by: Tillet, T., Université de Grenoble, Grenoble, 99–106, 2000.

Tillet, T.: Le Paléolithique moyen dans les Alpes et le Jura: exploitation de milieux de contraintes d'altitude, in: Settlement dynam-

ics of the middle Palaeolithic and Middle Stone Age, edited by: Conard, N. J., Kerns Verlag, Tübingen, 421–446, 2001.

Vouga, D.: Le Paléolitique, Mémoires de la Société Neuchâteloise des Sciences Naturelles, 7, 18–28, 1943.

Wallinga, J., Bos, A. J. J., Dorenbos, P., Murray, A. S., and Schokker, J.: A test case for anomalous fading correction in IRSL dating, Quaternary Geochronol., 2, 216–221, 2007.

Wegmüller, S., Preusser, F., and Müller, B. U.: Palynostratigraphische Untersuchung und Lumineszenzdatierung des Profils Galgenmoos und Implikationen für die Chronologie des letzten Glazialzyklus im nördlichen Alpenvorland der Schweiz, Eclogae Geol. Helv., 95, 115–126, 2002.

Welten, M.: Verdrängung und Vernichtung der anspruchsvollen Gehölze am Beginn der letzten Eiszeit und die Korrelation der Frühwürm- Interstadiale in Mittel- und Nordeuropa, Eiszeitalter und Gegenwart, 31, 187–202, 1991.

White, W. B.: Cave sediments and paleoclimate, J. Cave Karst Stud., 69, 76–93, 2007.

Wintle, A. G. and Murray, A. S.: A review of quartz optically stimulated luminescence characteristics and their relevance in single-aliquot regeneration dating protocols, Radiat. Meas., 41, 369–391, 2006.

Zander, A., Degering, D., Preusser, F., Kasper, H. U., and Brückner, H.: Optically stimulated luminescence dating of sublittoral and intertidal sediments from Dubai, UAE: Radioactive disequilibria in the uranium decay series, Quaternary Geochronol., 2, 123–128, 2007.

Fortification, mining, and charcoal production: landscape history at the abandoned medieval settlement of Hohenwalde at the Faule Pfütze (Saxony, Eastern Ore Mountains)

Johann Friedrich Tolksdorf[1], **Matthias Schubert**[2], **Frank Schröder**[2], **Libor Petr**[3], **Christoph Herbig**[4], **Petr Kočár**[5], **Mathias Bertuch**[2], and **Christiane Hemker**[2]

[1]Praktische Denkmalpflege: Bodendenkmalpflege, Bayerisches Landesamt für Denkmalpflege, Thierhaupten, Germany
[2]ArchaeoMontan Research Group, Landesamt für Archäologie Sachsen, Dresden, Germany
[3]Department of Botany and Zoology, Masaryk University, Brno, Czech Republic
[4]Institut für Archäologische Wissenschaften, Goethe-Universität Frankfurt am Main, Frankfurt, Germany
[5]Institute of Archaeology, Czech Academy of Sciences, Prague, Czech Republic

Correspondence: Johann Friedrich Tolksdorf (johann.tolksdorf@blfd.bayern.de)

Abstract: Geoarchaeological reconstructions of land-use changes may help to reveal driving cultural factors and incentives behind these processes and relate them to supra-regional economic and political developments. This is particularly true in the context of complete abandonment of a settlement. Here we present a case study from the site of Faule Pfütze, a small catchment in the Eastern Ore Mountains (Saxony). The historical record of this site is confined to the report of a settlement called Hohenwalde in 1404 CE and two later references to the then-abandoned settlement in 1492 and 1524 CE in this area. Combined geoarchaeological studies allowed for the reconstruction of several phases of land use. While a first phase of alluvial sedimentation occurred during the late 12th century, archaeological evidence for a permanent settlement is absent during this period. The onset of settlement activity is identified during the late 14th century and included a hitherto unknown massive stone building. Mining features are present nearby and are dated to the early 15th century. The local palynological record shows evidence for reforestation during the mid 15th century and thereby corroborates the time of abandonment indicated by written sources. These processes are discussed in the context of a local political conflict (Dohna Feud) leading to the redistribution of properties and the development of a mining economy during this time. Later land use from the mid 16th century onwards appears restricted to charcoal production, probably in the context of smelting works operating in nearby Schmiedeberg as indicated by rising lead concentrations in the alluvial record.

Kurzfassung: Geoarchäologische Rekonstruktionen der Landschaftsgeschichte können dazu dienen, die hinter diesen Prozessen liegenden kulturellen Triebkräfte und Motivationen offenzulegen und diese mit überregionalen ökonomischen und politischen Entwicklungen in Beziehung zu setzen. In besonders hohem

Maße trifft dieses im Umfeld von vollständigen Wüstungsprozessen zu. Im Rahmen einer Fallstudie wird hier die Fundstelle an der "Faulen Pfütze", einer kleinen Siedlungskammer im Osterzgebirge (Sachsen), vorgestellt. Die historische Überlieferung zu dieser Fundstelle beschränkt sich auf die Nennung einer Siedlung "Hohenwalde" im Jahr 1404 sowie zwei spätere Nennungen aus dem Jahr 1492 und 1524, die sich bereits auf eine Wüstung in diesem Gebiet beziehen. Nur durch geoarchäologische Ansätze war es daher möglich, unterschiedliche Phasen der Landnutzungsgeschichte zu rekonstruieren. Während eine erste Phase der alluvialen Sedimentation bereits im späten 12. Jahrhundert festzustellen ist, fehlen archäologische Belege für eine dauerhafte Siedlung zu diesem Zeitpunkt noch völlig. Der Beginn der Siedlungsaktivitäten setzt im späten 14. Jahrhundert ein und umfasst dabei auch ein bislang unbekanntes massives Steingebäude. In unmittelbarer Nähe treten Bergbauspuren auf, die in das frühe 15. Jahrhundert datieren. Die palynologischen Analysen zeigen eine lokale Wiederbewaldungsdynamik ab der Mitte des 15. Jahrhunderts und bestätigen dabei den durch historische Quellen genannten Zeitpunkt der Siedlungsaufgabe. Diese Entwicklung wird vor dem Hintergrund eine regionalen Auseinandersetzung (Dohnaischen Fehde) diskutiert, die vor Ort nicht nur eine territoriale Neuverteilung sondern auch Bergbauaktivitäten zur Folge hatte. Spätere Landnutzung ab der Mitte des 16. Jahrhunderts scheint dann auf die Produktion von Holzkohle beschränkt gewesen zu sein, wahrscheinlich zur Versorgung der Hüttenwerke im nahen Schmiedeberg, was sich auch in steigenden Bleieinträgen in den alluvialen Sedimenten abzeichnet.

1   Introduction

A number of regional case studies have highlighted the influence of mining activities and related timber and charcoal production on central European mountain ranges (e.g. Stolz and Grunert, 2010; Hrubý et al., 2014; Knapp et al., 2015). In the Ore Mountains region silver and tin mining has been present at least since the mid 12th century based on historical sources (Wagenbreth, 1990), but archaeological and palaeoenvironmental investigations on this time period have been scarce compared to other regions. Due to the establishment of a border zone between East Germany and the Czechoslovakia from 1945 to 1990 and low construction activities, this area has not been in the focus of the heritage authorities on both sides of the border for decades. Moreover, the intensive mining activities in later centuries were expected to have destroyed most of the medieval structures. Palaeoenvironmental studies were restricted to pollen profiles from mires in the upper reaches of the Ore Mountains (Stebich, 1995; Schlöffel, 2010). Research activity in this area only resumed after the discovery of well-preserved mining features from the late 12th and 13th century in Dippoldiswalde in 2008 and led to the establishment of two German–Czech ArchaeoMontan research projects (Ziel-3 ArchaeoMontan from 2012 to 2015 and ArchaeoMontan 2018 from 2016 to 2018). In the course of these projects, local studies focussed on the medieval human impact around the town of Freiberg that have flourished as a silver mining centre since the mid 12th century (Tolksdorf et al., 2018) and the effects of mining activities together with timber and charcoal production since the late 12th century in the small mining district of Niederpöbel near Schmiedeberg in the Eastern Ore Mountains (Schröder, 2015; Tolksdorf et al., 2015). The results have indicated a strong impact in the form of deforestation, a sharp decline of tree species like *Abies alba* and changes in forest composition during ongoing land use. This case study addresses the land-use history of a comparatively short-lived village in the Ore Mountains in the context of local mining activities and the regional political history.

2   Site topography and sampling

The site of Faule Pfütze is located in the Eastern Ore Mountains (*Osterzgebirge* in German) about 30 km south of Dresden (Fig. 1a) in a mountain ridge east of Schmiedeberg (Fig. 1b) and was investigated by the ArchaeoMontan 2018 team in 2016 and 2017. Local geology is dominated by quartz porphyries and porphyroid granites (GK 25, 1915; Reinisch, 1915). In the study area the small valley of the Brießnitzbach river opens to the east, and the modern site name "Faule Pfütze" (meaning "brackish pool" in German) relates to the wetlands around the spring area of this river. Microtopographical assessment of lidar data reveals several sunken roads that converge in the area of a modern dam used for the road, creating a small pond. Some mining features (shafts, mining heaps) can be recognized by their specific topography to the southeast. Additional charcoal kilns in the form of round platforms are visible on the surrounding slopes (Fig. 2a).

Immediately downstream of the modern dam, the upper 110 cm of alluvial sediments was accessible in an outcrop cut by the river and sampled as profile 1 for macro-botanical, palynological, geochemical, and ^{14}C analyses. A dense layer of rubble just a few metres upstream of profile 1 was noted as an archaeological feature and labelled profile 3. To substantiate the age of the mining features, profile 2 was situated beside
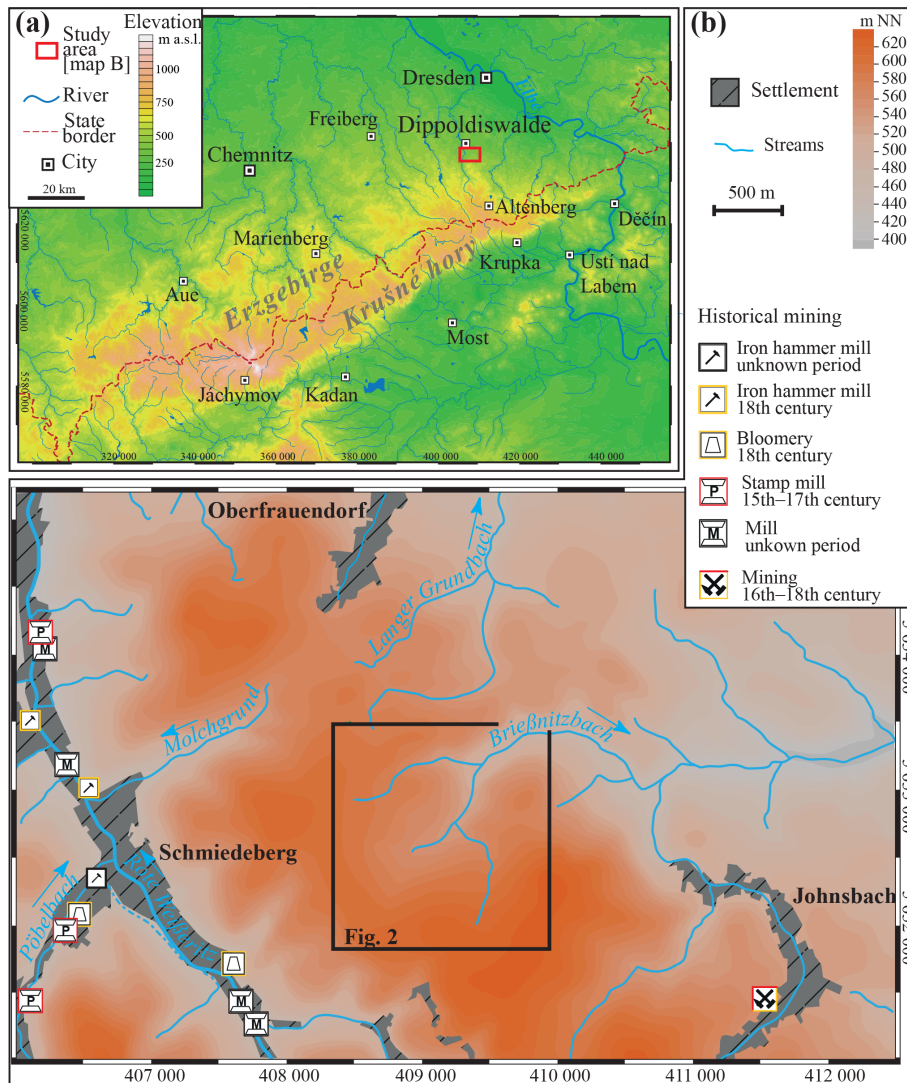
Figure 1. (a) Location of the site of Faule Pfütze in the Ore Mountains (data: SRTM), **(b)** regional topography (data: GeoSN). Historical mining features are mapped according to historical maps (Ur–Oder and Oeder–Zimmermann from early 17th century) and written sources (Müller, 1964) using the symbols and time periods from Göhler and Wehmeyer (2013).

a mining heap in order to sample the palaeo-surface covered by mining waste for botanical (BOT-36) and ^{14}C analyses (MAMS-30882).

The valley bottom above profile 1 yielded numerous ceramic fragments on the surface. Here, profile 4 was recorded to document the relation of settlement layers to alluvial and colluvial sediments, while profile 5 was situated at the transition from the southern hillslope to the alluvial plain. A prominent feature visible in the digital elevation model (DEM) derived from lidar scan is a stone heap with a square layout rising more than 1 m above the valley floor. Profile 6 was used to record a profile in this feature and profile 7 was used for archaeological investigation of the valley floor nearby. Sedimentation history on the valley floor was recorded using a transect consisting of six cores and profiles 1 and 3 (Fig. 2b) from the southeast to the northwest.

3 Methods and material

Botanical macro-remains were retrieved from sediment samples by wet sieving with mesh widths of 2, 1, 0.5, and 0.25 mm and determined according to standard literature (Cappers et al., 2012) and a reference collection of wild and domestic plants. Their attribution to ecological groups is based on the classification by Oberdorfer (2001). Sample preparation for pollen analysis followed standard acetolysis procedure, and a minimum number of 500 palynomorphs were identified according to literature (Beug, 2004) in every sample. A portable X-ray fluorescence (XRF) unit (Olympus
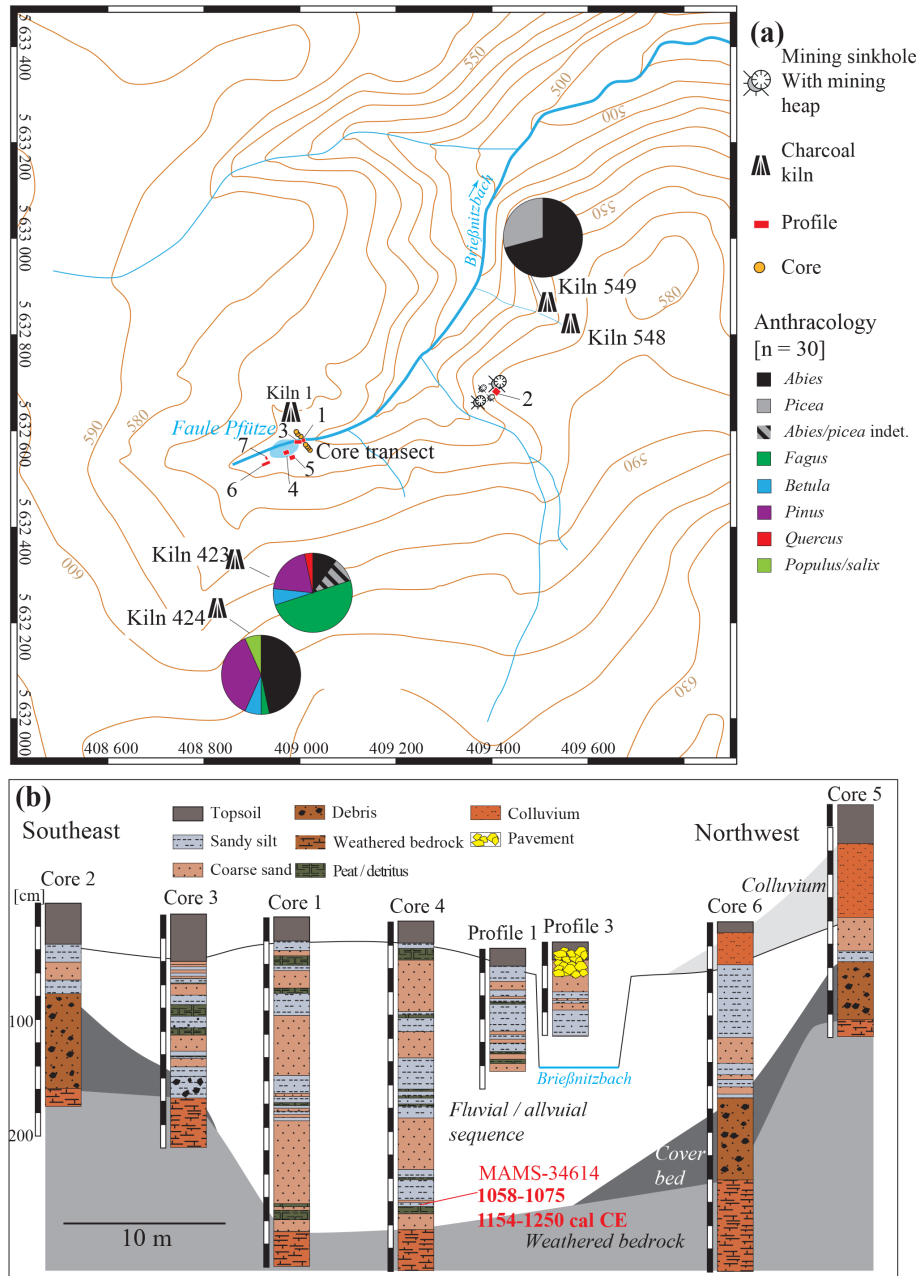
Figure 2. (a) Site topography, sampled records, and results of anthracological analysis of charcoal kilns from this area; **(b)** stratigraphic logs of the core transect through the valley floor.

Innov-X DELTA 50) was used to measure geochemical properties on dried samples from the grain-size fraction < 0.8 mm (CGS Prague Laboratories). Changing concentrations of the elements Pb, As, and Zn were used as potential environmental proxies for metallurgical activities (Hürkamp et al., 2009; Schmidt-Wygaasch et al., 2010). The ^{14}C analyses were performed by the Curt-Engelhorn-Zentrum Archäometrie (CEZ) in Mannheim, and calibrated using IntCal13 (Table 1) and the Bayesian model implemented in OxCal. Samples of 30 charred particles were extracted from three charcoal kilns for

an anthracological assessment. Determination of the taxa is based on wood-anatomical features on fresh cuts with different orientations (Schweingruber, 1990). Due to their anatomical similarity *Populus* and *Salix* were grouped together. The dating of ceramics was based on typological and technological parallels with well-dated archaeological assemblages in the region (Mechelk, 1981). A series of overlapping photos was used to process 3-D models for larger archaeological features by structure from motion (SfM). Consequently, the

Table 1. Results of ^{14}C analyses.

Lab no.	Profile	Material and context	^{14}C	^{14}C (calibrated; IntCal13, 1σ)	^{14}C (calibrated; IntCal13, 2σ)	δ^{13}C (‰)
			(BP)	(cal CE)	(cal CE)	
MAMS-30884	profile 1	charcoal from alluvial layer 18–25 cm below surface	282 ± 16	1528–1544 1634–1650	1522–1573 1630–1657	−23.6
MAMS-30883	profile 1 from alluvial layer	charcoal 49–55 cm below surface	333 ± 17	1499–1504 1512–1527 1555–1601 1617–1633	1487–1638	−23.9
MAMS-32962	profile 1	charcoal from alluvial layer 75 cm below surface	401 ± 19	1447–1479	1441–1498 1601–1616	−17.6
MAMS-30882	profile 2	charcoal below mining heap	510 ± 17	1414–1430	1408–1437	−23.1
MAMS-33862	profile 4	charcoal concentration below alluvial layers, 55 cm below surface	953 ± 22 1086–1124	1029–1049 1065–1155 1137–1150	1023–1059 1065–1155	−25.7
MAMS-33861	profile 6	charcoal, under embankment 80 cm below surface	593 ± 24	1315–1356 1389–1400	1300–1369 1381–1410	−29.2
MAMS-34614	core 4	charcoal from base of alluvial sediments	857 ± 23	1167–1214	1058–1075 1154–1250	−29.0
MAMS-32530	charcoal kiln 423	charcoal kiln	311 ± 21	1522–1575 1586–1590 1625–1642	1495–1602 1616–1646	−23.9

structures were mapped in a local coordinate system with the surrounding surface as the vertical reference level.

4 Results

The auger transect through the valley floor around profile 1 shows a complex sequence of coarse fluvial sands and alluvial silt that partly cover the periglacial cover beds dominated by gravels (Fig. 2b). Fine layers of organic detritus were preserved within some of the alluvial silt units. Colluvial layers appear at the northern slope covering the alluvial layers. A ^{14}C sample from the lowermost alluvial layer in core 4 yielded an age of 1058–1075 or 1154–1250 cal CE (MAMS-34614).

Profile 1 was recorded at a location where the river at the outlet of the modern dam incised into the valley floor. The sequence exposed along the bank consists of alluvial layers with organic detritus and coarse fluvial sands (Fig. 3). Based on three ^{14}C analyses (MAMS-30883, MAMS-30884, MAMS-32962), these layers have been deposited from the early 15th century to the early 17th century. The content of botanical macro-remains differs between the alluvial layers but is consistently dominated by wetland taxa. The ratio of

arboreal to non-arboreal pollen within the three lowermost pollen samples shows recovering forest vegetation up to a depth of 61 cm. The sample at 55 cm is characterized by a high percentage of micro-charcoal and declining arboreal pollen. Geochemical analyses show a relatively stable concentration of zinc and arsenic but a distinct rise in lead concentrations at a depth of about 50 cm. Based on the chronological model, both the drop of arboreal pollen and the rise of lead content are ascribed to the 15th to 16th century.

The detailed analysis of the pollen spectra (Fig. 4) reveals a very high percentage of *Corylus avellana* pollen in the lowermost sample at 90 cm. The subsequent samples at 75 cm show a sharp decline of *Corylus* but increasing percentages of *Abies*, *Pinus*, and *Picea* pollen. At a depth of 61 cm the share of *Abies* pollen declined again while *Pinus* and *Picea* are still expanding. Although pollen from *Secale cereale* and *Centaurea cyanus* as well as ruderal taxa like *Plantago lanceolata* or *Rumex acetosella* are present in these lower three samples, their low number indicates that permanent settlement and arable land could have existed only at some distance. Additional information about the local vegetation is provided by the macro-botanical spectra at 75, 67, and 61 cm depth. These present a dominance of wetland

Table 2. Macro-botanical and anthracological results.

Sample (BOT: macro-remains; HK: anthracology) cf. Figs. 2 and 3 for sample location			BOT-53	BOT-54	BOT-62	BOT-63	BOT-64	BOT-65	BOT-36	BOT-79	BOT-80	BOT-85	HK-14	HK-15	HK-16
Sample size (litres or pieces (pcs.))			0.1 l	0.1 l	0.1 l	0.1 l	0.1 l	0.1 l	0.2 l	0.1 l	0.1 l	0.1 l	30 pcs.	30 pcs.	30 pcs.
Depth (cm)			75	47	51	56	61	67	120	14–29	29–49	200	10	10	10
Profile			1	1	1	1	1	1	2	4	4	4	kiln 423	kiln 424	kiln 529
Taxonomy	**Anatomy**	**Preservation**													
Forest community															
Abies alba	ND	u	5		9		4	9			2				
	ND	ch			21				500		36	180			
	W	ch											3	14	17
Picea abies	ND	u	9				11	11		23	7				
	ND	ch				4									
	W	ch													7
Abies and *Picea* indet.	W	ch											3		
Pinus	ND	ch							5						
	W	ch											6	11	
Populus sp.	FS	u					1	1							
	W	ch												1	
Populus and *Salix* indet.	W	ch												1	
Carpinus betulus	FS	ch								1					
Fagus sylvatica	W	ch											15	1	
Quercus robur	W	ch											1		
Oxalis acetosella	FS	u			1	1									
Forest edges and clearances															
Arctium sp.	FS	u					1								
Betula pendula and *pubescens*	FS	u	11			1		6							
	W	c											2	2	
Carex ovalis	FS	u				1	1	1							
Hypericum hirsutum	FS	u						1							
Sambucus nigra	FS	ch										2			
Rubus fructicosus agg.	FS	u					1								
Meadows															
Cerastium fontanum	R	u	4	1	5		1	3							
Luzula campestris and *L. multiflora*	FS	u		2			1								
Origanum vulgare	FS	u		1											
Prunella vulgaris	FS	u						1							
Rumex acetosella agg.	FS	u				1		1							
Wetlands and river banks															
Carex sp.	FS	u	13	1000	300	359	195	480							
Glyceria fluitans	FS	u	114		32	50	4	115							
Montia fontana s.l.	FS	u	41			8	4								
Potamogeton sp.	FS	u		2											
Ranunculus flammula	FS	u	1	4	8	17	8	8							
Scirpus sylvaticus	FS	u	1		10	33	10	10							
Sparganium emersum	FS	u		1											
Sphagnum	FS	u	+												
Varia															
Chenopodium album type	FS	u					1								
Carduus and *Cirsium*	FS	u					1								
Juncus sp.	FS	u	5	7	9	7	1	2		36	31	60			
Lamiaceae	FS	u		1											
Myosotis sp.	FS	u	1												
Pinaceae	FS	u						1							
Poa sp.	FS	u	5	1											
Polygonum aviculare agg.	FS	u					2								
Sagina procumbens	FS	u					1								
Viola sp.	FS	u		18	1	5		1							
Rumex crispus or *R. obtusifolius*	FS	ch						1							
Indeterminate	FS	u		1											
Indeterminate	W	u	+	+	+		+								
Indeterminate	W	ch	+	+	+	+	+	+							
Indeterminate	R	u	4					4							6

taxa like *Glyceria fluitans* or *Montia fontana* with increasing numbers of *Carex* species. Remains of taxa which tend to occur on more open areas such as meadows or clearances like *Cerastium fontanum*, *Betula*, or *Carex ovalis* are seldom found and even show a decline that is in good accordance with the expansion of forest vegetation visible in the pollen.

However, direct evidence of forest species like fir or pine is rare in these samples.

The trend towards a recovery of the forest vegetation seems to be interrupted at a depth of 55 cm with declining percentages of *Pinus*, *Picea*, and *Abies* pollen accompanied by rising values of *Corylus* and species related to open ar-
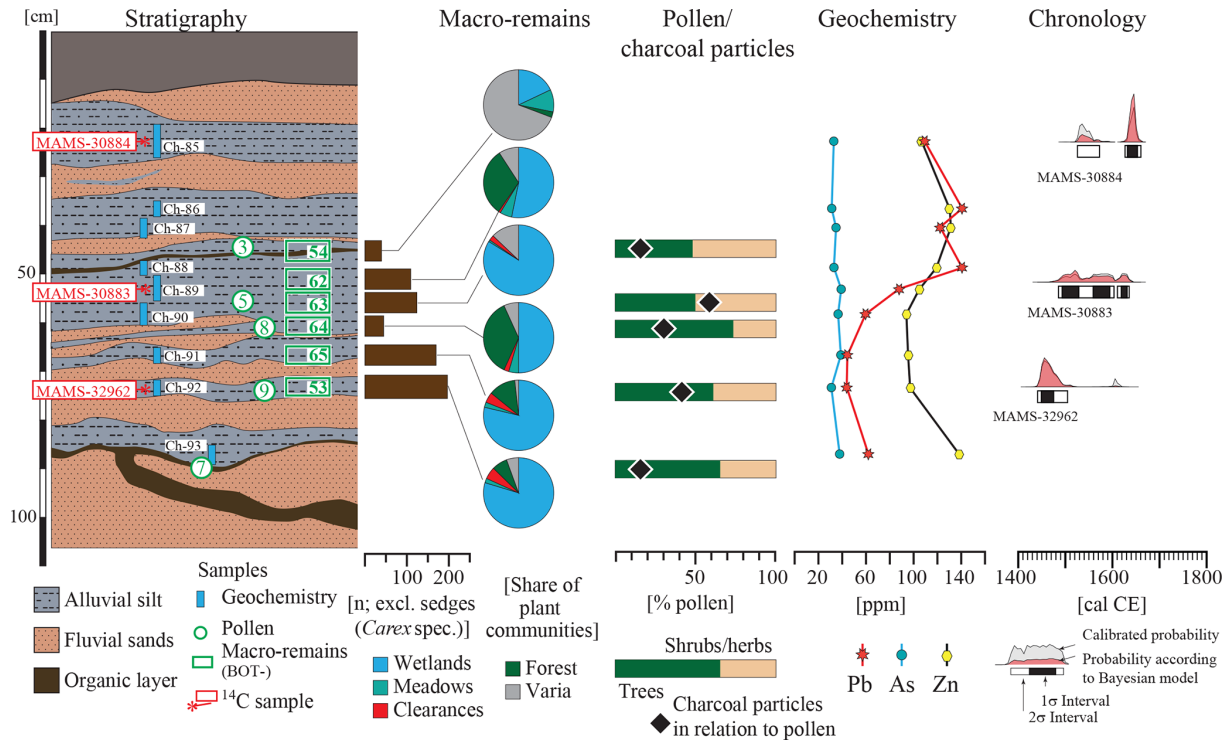
Figure 3. Stratigraphy, chronology, and key results of palynological, macro-botanical, and geochemical analyses in profile 1.

eas, especially Poaceae and Cyperaceae together with *Rumex acetosella* and *Artemisia*. The macro-botanical samples from this layer show a complete absence of taxa related to forest vegetation. While evidence for forest species is visible again in the macro-botanical spectrum at a 51 cm depth, the macro remains at a 47 cm depth and a pollen spectrum at a 45 cm depth are consistent with a reduction of forest taxa. Particularly, the very high number of *Rumex acetosella* pollen in the uppermost sample might indicate the permanent establishment of open areas, perhaps meadows.

Mining activity in this area is proven by profile 2 (Fig. 5a), which revealed a layer of charred material below a mining heap. *Abies alba* needles dominated the charred material by far (BOT-36) and prove that it results from the burning of local vegetation rather than technological processes like fire-setting or smelting. The material yielded an age of 1408–1437 cal CE (MAMS-30882) providing a minimum age for the mining activities.

The square stone heap was investigated at profile 6 (Fig. 5b) and revealed a stone wall construction covered by an embankment. Residues of the former topsoil below the embankment contained ceramic fragments, an iron nail, and charred material, yielding a ^{14}C age of 1300–1369 or 1381–1410 cal CE. It is in very good accordance with the typochronological dating of the ceramic material discovered below the layers of relocated rubble in profile 7 (Fig. 5d). This was assigned to the end of the 14th century and later based on the presence of high- and undercut-shaped collar

rims (*hohe und unterschnittene Kragenränder*) and reddish high-fired earthenware (*rotscherbige hochgebrannte Irdenware*; Mechelk, 1981).

While profile 5 at the transition from the slope to the alluvial plain only yielded relocated coarse material, nearby profile 4 showed intercalating layers of alluvial sedimentation and colluvial material (Fig. 5c). At a depth of 50 cm a dense layer of charred material was covered by alluvial sediments. This material (BOT-85) was dominated by charred *Abies alba* needles but also contained remains of local *Juncus* species. Remains of *Sambucus nigra* could indicate the existence of clearances. A ^{14}C analysis provided an age of 1023–1155 cal CE for this layer. It was covered by colluvial sediments that contained charred remains of *Abies* and *Juncus* but also *Picea* needles (BOT-80). The subsequent alluvial layer from a 30 to 12 cm depth contained charred and uncharred botanical remains (*Picea* together with *Juncus* and *Carex* species) together with ceramic fragments dating to the 14th century by means of typochronology. Remains of fir were absent in this younger layer.

Some small plateaus visible in the DEM were identified as charcoal kilns (Fig. 2a). While kiln 549 only contained remains of *Abies* and *Picea*, the fuel spectra of the kilns 423 and 424 were very broad and contained *Fagus*, *Abies*, *Picea*, *Betula*, *Populus/Salix* (indiff), and *Quercus* of differing proportions. A ^{14}C analysis of kiln 423 provided an age of 1495–1646 cal CE.
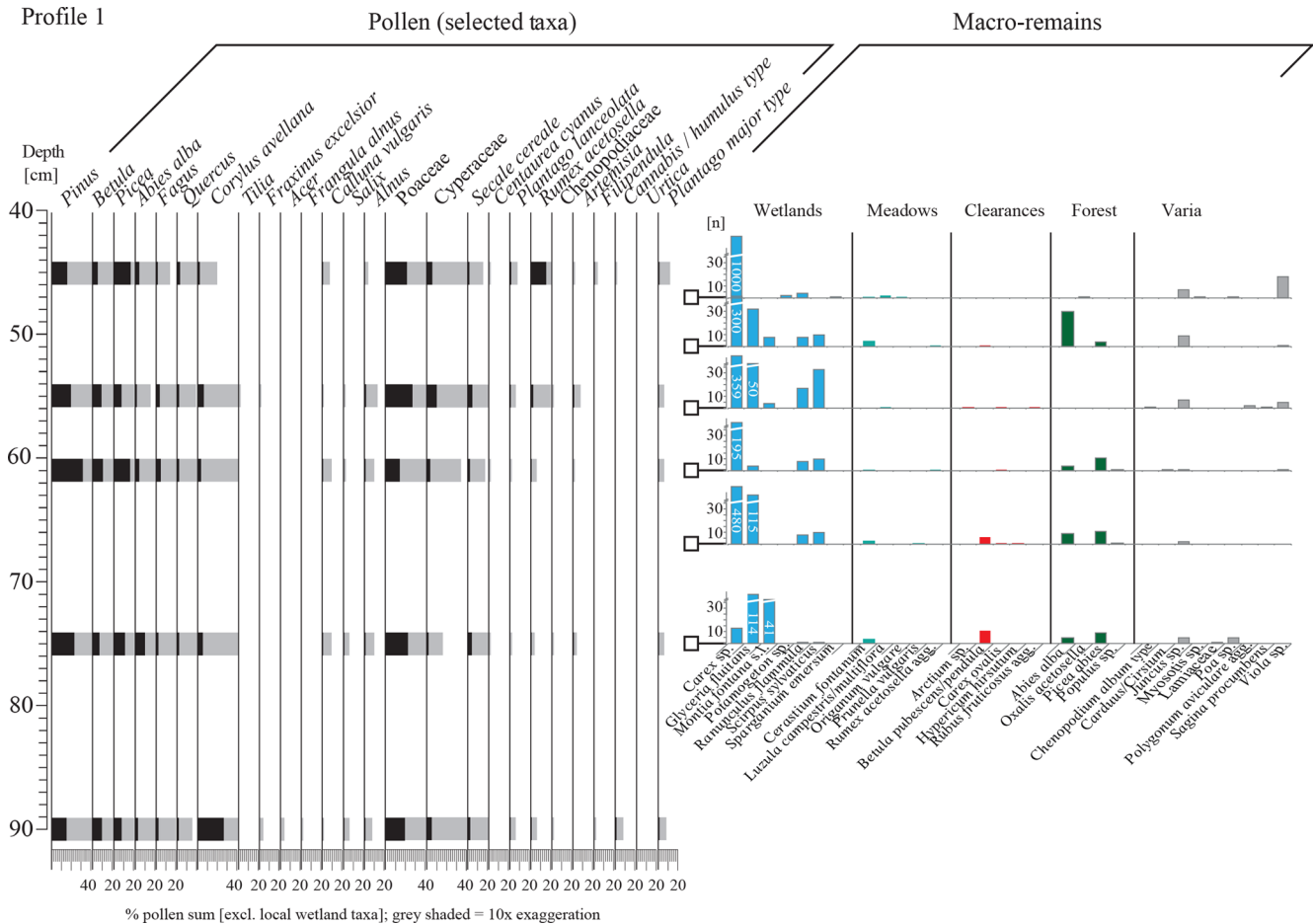
Figure 4. Palynological and macro-botanical spectra from profile 1 (cf. Fig. 3).

5 Discussion

The onset of alluvial sedimentation dates back to the 12th century based on ^{14}C ages from charcoal taken from profile 4 and core 4. Although catastrophic events like wildfires could theoretically trigger local soil erosion (Shakesby and Doerr, 2006), human impact is a more likely cause. From the regional perspective, the 12th century is known as a time period with intensive rural colonization and mining in the Ore Mountains (Billig and Geupel, 1992; Kenzler, 2013). The earliest timber from the nearby medieval mines of Dippoldiswalde (about 7 km NNW) could indicate the start of mining in the region at the turn of the 12th to the 13th century (Hoffmann, 2011; Westphal et al., 2014). However, at the site of Faule Pfütze, the artefact assemblage and archaeological features suggest permanent human activity to have occurred from the 14th century onwards. It may be possible that this settlement phase was preceded by phases of ephemeral land use with low archaeological visibility, e.g. logging or pasture. Botanical spectra from this time preceding the settlement (BOT-80, BOT-85) contain high shares of *Abies alba* (fir) needles compared to other taxa like *Picea abies* (spruce)

or *Pinus sylvestris* (pine) and may indicate the dominance of fir in the forest composition. However, such evidence neither support nor preclude earlier human activities in the area.

Human settlement on this site during the 14th century is undisputed and included the construction of the massive building recorded in profiles 6 and 7. Based on the construction technique, the ground plan, and the archaeological material, this feature represents the remains of what is possibly some sort of fortification (cf. Schwabenicky, 1996), but definitely a solid stone-built structure. The onset of mining may have occurred later as indicated by the ^{14}C age from profile 2 (Fig. 6, phase 1). Identifying the political and economic context of the strong building and the mining activities is problematic as major territorial changes took place in the region after the Dohna Feud (1385–1402 CE) (Ermisch, 1902; Hoffmann, 2011). Eventually, the first historical record concerning the village of Hohenwalde in 1404 CE appears in the aftermath of these events when land ownership had changed (Müller, 1964). It is possible that mining activities have been fostered in this region by the new owner. Another aspect worth discussing is the function of the massive building. It may have either protected the settlement and
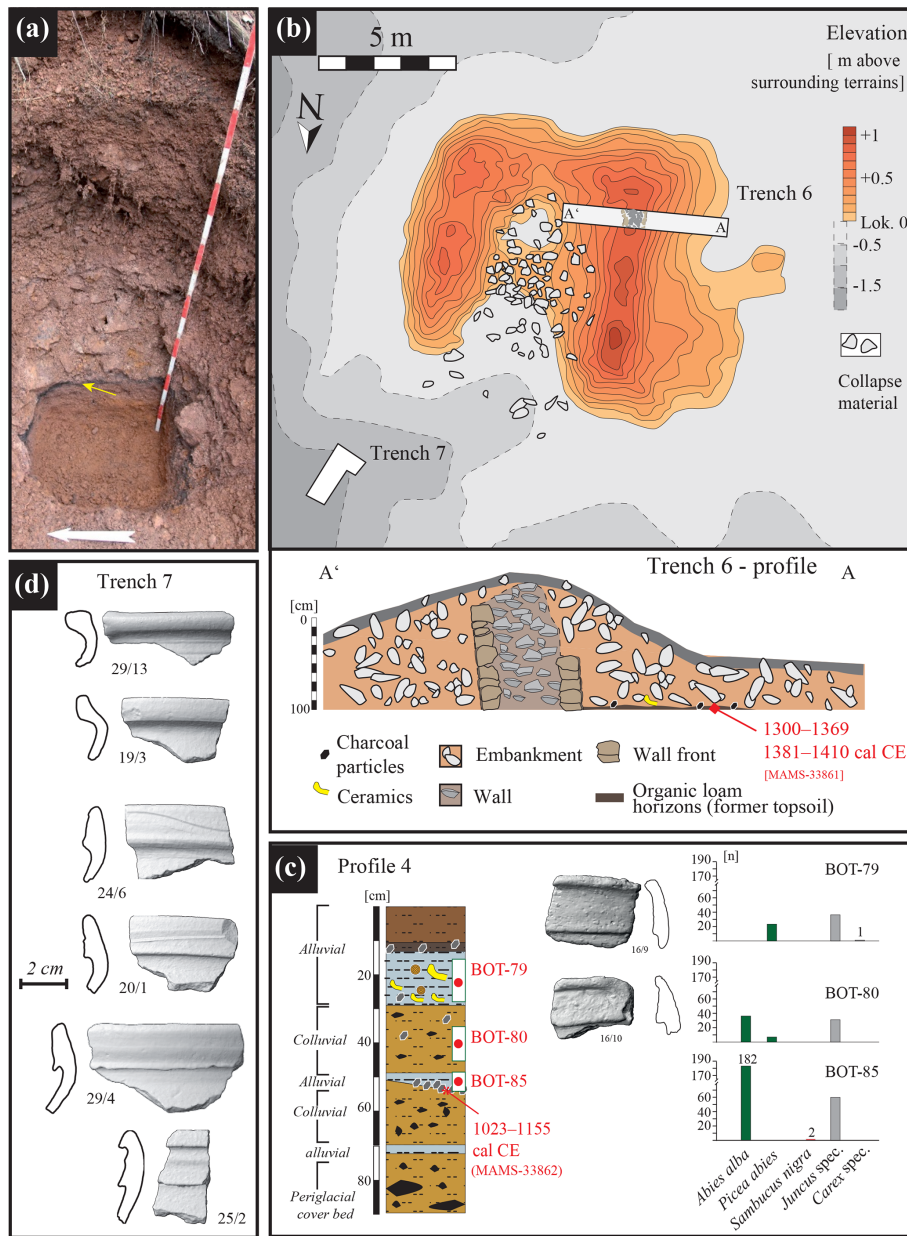
Figure 5. (a) Layer of burnt material (yellow arrow) below mining heap; **(b)** topography of the fortified building with profile recorded in profile 6; **(c)** profile 4 with macro-botanical analyses and chronological results; **(d)** selected artefacts from the site dating to the 14th century.

the road or been related to the protection of older mining facilities as discussed for other regions of the Ore Mountains (Schwabenicky, 1996; Kenzler, 2009). However, no historical record from this area ever refers to a fortification or mining activities, highlighting the incompleteness of this type of source. Botanical spectra from the settlement period derive from the burnt material below the mining heap (BOT-36) with abundant charred *Abies alba* needles and the upper part of profile 4 (BOT-79), where the dominance of *Picea abies* probably mirrors the local vegetation on the wet valley floor.

No cultivated plants or weeds have been detected in any sample.

The abandonment of the settlement can be narrowed down by combining the historical sources mentioning an abandoned village in 1492 CE and the ^{14}C time depth model in profile 1. Here the beginning of the ecological succession is dated to the mid 15th century (Fig. 6, phase 2), marked by a high share of pioneer taxa like *Corylus avellana* (hazel) and the absence of settlement indicators. During later decades, *Abies*, followed by *Picea* and *Pinus*, established in the area. Layers dated to the mid 16th century in profile 1 reveal a de-
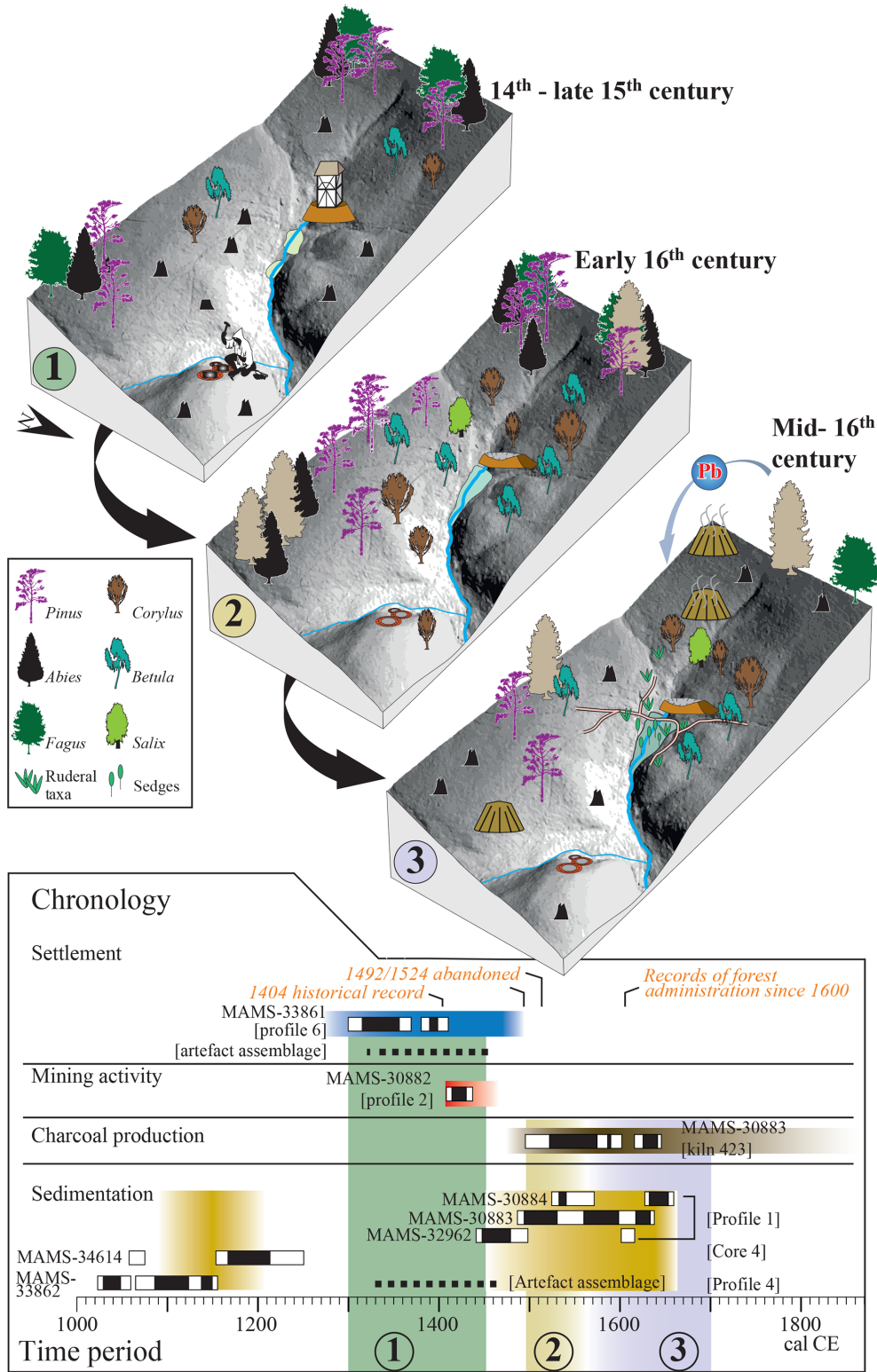
Figure 6. Reconstruction of land-use history at the site. Phase 1: settlement and mining activities during the 14th and early 15th centuries; phase 2: recovering forest vegetation after the settlement was abandoned in the mid 15th century; phase 3: metallurgical plants in Schmiedeberg since the mid 16th century prompt charcoal production and cause increased lead pollution.

clining share of arboreal pollen and rising contents of charcoal particles (Fig. 6, phase 3). This suggests resuming land use in this area, probably for the purpose of charcoal production. It is supported by a ^{14}C date of 1495–1602 or 1616–1646 cal CE (MAMS-32530) from charcoal kiln 423 and historical sources from the late 16th century (Reinhold, 1942). Rising lead concentrations in the upper part of profile 1 probably result from intensified metallurgical activities in nearby Schmiedeberg (2 km E) where smelting works were established during this period (Müller, 1964). While the pollen spectra capture a rising percentage of spruce in this area, the spectra from the charcoal kilns are more diverse, with pioneer taxa like *Betula* on the one hand and forest taxa like *Fagus sylvatica* and *Abies alba* on the other hand, and may simply reflect the natural local vegetation variety. The use of this area for logging and charcoal production continued until modern times; today the area is mainly covered by *Picea* plantations.

6   Conclusions

Our results indicate local settlement activities at least since 14th century CE and the existence of a strong building in this settlement may point towards the need to secure the area and its resources during this time period. It is likely that this area was affected by political reorganization following a feud in 1402 CE, and mining activities dating to the early 15th century may relate to a changed political and organizational background of the settlement that must have failed since the mid 15th century as indicated by reforestation and historical sources. Land use shifted to charcoal production to supply the striving metallurgical activities in the nearby Schmiedeberg area since the 16th century CE.

Author contributions. Fieldwork was performed by JFT, MS, FS, and MB under the project supervision of CH. Pollen analysis was done by LP, anthracological analyses by PK, and analysis of botanical remains by CH. JFT prepared the manuscript and figures.

References

Beug, H.-J.: Leitfaden der Pollenbestimmung für Mitteleuropa und angrenzende Gebiete, Pfeil, München, 2004.

Billig, G. and Geupel, V.: Entwicklung, Form und Datierungen der Siedlungen in der Kammregion des Erzgebirges, Siedlungsforschung, Archäologie, Geschichte, Geographie, 10, 173–194, 1992.

Cappers, R. T. J., Bekker, R. M., and Jans, J. E. A.: Digital zadenatlas van Nederland/Digital seed atlas of the Netherlands, Eelde: Barkhuis, 2012.

Ermisch, H.: Dohna und die Dohnaische Fehde, Die Grenzboten, 61, 77–86, 1902.

GK 25: Geologische Karte von Sachsen, 1:25000, Blatt 101 Dippoldiswalde-Glashütte, 1915.

Göhler, M. and Wehmeyer M.: Montanarchäologisch Kartierungen, in: ArchaeoMontan 2012, edited by: Smolnik, R., Erkunden – Erfassen – Erforschen, Arbeits- und Forschungsberichte zur sächsischen Bodendenkmalpflege, Beiheft 26, LfA Sachsen, Dresden, 197–203, 2013.

Hoffmann, Y.: Die Geschichte von Dippoldiswalde bis zum Ende der ersten Bergbauperiode um 1400. Arbeits- und Forschungsberichte zur sächsischen Bodendenkmalpflege, 51/52, 391–421, 2011.

Hrubý, P., Hejhal, P., Malý, K., Kočár, P., and Petr, L.: Centrální Českomoravská vrchovina na prahu vrcholného středověku: archeologie, geochemie a rozbory sedimentárních výplní niv [Central Bohemian-Moravian highlands on the threshold of the high middle ages: archaeology, geochemistry and the analyses of alluvial sediments] Opera Universitatis Masarykianae Brunensis, Facultas Philosophica, 422, Masaryk Univ., Brno, 2014.

Hürkamp, K., Raab, T., and Völkel, J.: Two and three-dimensional quantification of lead contamination in alluvial soils of a historic mining area using field portable X-ray fluorescence (FPXRF) analysis, Geomorphology, 110, 28–36, 2009.

Kenzler, H.: The medieval settlement of the Ore Mountains, The development of the settlement structure, in: Medieval Rural Settlement in Marginal Landscapes, edited by: Klápště, J. and Sommer, P., Brepolis, Turnhout, 379–392, 2009.

Kenzler, H.: Bergbau und Kolonisation, Die Rolle des Montanwesens innerhalb der mittelalterlichen Besiedlungsgeschichte des Erzgebirges, in: ArchaeoMontan 201, edited by: Smolnik, R., Erkunden – Erfassen – Erforschen, LfA Sachsen, Dresden, 157–163, 2013.

Knapp, H., Nelle, O., and Kirleis, W.: Charcoal usage in medieval and modern times in the Harz Mountains Area, Central Germany: Wood selection and fast overexploitation of the woodlands, Quatern. Int., 366, 51–69, 2015.

Mechelk, H.: Zur Frühgeschichte der Stadt Dresden und zur Herausbildung einer spätmittelalterlichen Keramikproduktion im säch-

sischen Elbgebiet aufgrund archäologischer Befunde, Dt. Verl. Wissenschaft, Berlin, 1981.

Müller, G.: Zwischen Müglitz und Weißeritz. Ergebnisse der heimatkundlichen Bestandsaufnahme im Gebiet Dippoldiswalde/Glashütte, Akademie-Verlag, Berlin, 1964.

Oberdorfer, E.: Pflanzensoziologische Exkursionsflora für Deutschland und angrenzende Gebiete, Ulmer, Stuttgart, 2001.

Reinhold, F.: Die Bestockung der kursächsischen Wälder im 16. Jahrhundert, Baensch, Dresden, 1942.

Reinisch, R.: Erläuterungen zur Geologischen Karte von Sachsen 1:25000. Nr. 101 Blatt Dippoldiswalde-Glashütte, Kauffmanns, Leipzig, 1915.

Schlöffel, M.: Die postglaziale Waldgeschichte der Lehmhaide. Rekonstruktion spät- und postglazialer Umweltbedingungen an einem Torfprofil aus dem Erzgebirge, Arbeits- und Forschungsberichte zur sächsischen Bodendenkmalpflege, 51/52, 9–27, 2010.

Schmidt-Wygasch, C., Schamuhn, S., Meurers-Balke, J., Lehmkuhl, F., and Gerlach, R.: Indirect dating of historical land use through mining: Linking heavy metal analyses of fluvial deposits to archaeobotanical data and written accounts, Geoarchaeology, 25, 837–856, 2010.

Schröder, F.: Die montanarchäologischen Ausgrabungen in Niederpöbel (2011–2013) – Befunde und Ergebnisse, in: ArchaeoMontan 2015, edited by: Smolnik, R., Montanarchäologie im Erzgebirge, LfA Sachsen, Dresden, 23–166, 2015.

Schwabenicky, W.: Beziehungen zwischen Burgen und Bergbau im sächsischen Erzgebirge, Burgenforschung in Sachsen, 9, 9–29, 1996.

Schweingruber, F. H.: Anatomie europäischer Hölzer, Haupt, Bern, 1990.

Shakesby, R. A. and Doerr, S. H.: Wildfire as a hydrological and geomorphological agent, Earth-Sci. Rev., 74, 269–307, 2006.

Stebich, M.: Beiträge zur Vegetationsgeschichte des Georgenfelder Hochmoores, Dissertation Universität Leipzig, Leipzig, 1995.

Stolz, C. and Grunert, J.: Late Pleistocene and Holocene landscape history of the central Palatinate forest (Pfälzerwald, southwestern Germany), Quatern. Int., 222, 129–142, 2010.

Tolksdorf, J. F., Elburg, R., Schröder, F., Knapp, H., Herbig, C., Westphal, T., Schneider, B., Fülling, A., and Hemker, C.: Forest exploitation for charcoal production and timber since the 12th century in an intact medieval mining site in the Niederpöbel Valley (Erzgebirge, Eastern Germany), J. Archaeol. Sci., 4, 487–500, 2015.

Tolksdorf, J. F., Petr, L., Schubert, M., Herbig, C., Kaltofen, A., Matson, S., and Hemker, C.: Palaeoenvironmental reconstruction in the mining town of Freiberg (Lkr. Mittelsachsen) in Saxony, from the 12th century onwards, Archaol. Korresponden., 48, 281–296, 2018.

Wagenbreth, O.: Bergbau im Erzgebirge: technische Denkmale und Geschichte, Dt. Verl. für Grundstoffindustrie, Leipzig, 1990.

Westphal, T., Heußner, K.-U., and Herbig, C.: Holz am Berg – Holz im Bergwerk, in: ArchaeoMontan 2014, edited by: Smolnik, R., Ergebnisse und Perspektiven, LfA Sachsen, Dresden, 243–256, 2014.

CONTENTS